2013-07-05

Susceptibility of Apoptotic Cells to Hydrolysis by sPLA2: Molecular Basis and Mechanisms Defined

Elizabeth Gibbons

Brigham Young University - Provo

Susceptibility of Apoptotic Cells to Hydrolysis by sPLA$_2$:

Molecular Basis and Mechanisms Defined

Elizabeth Gibbons

A dissertation submitted to the faculty of
Brigham Young University
in partial fulfillment of the requirements for the degree of

Doctor of Philosophy

John D. Bell, Chair
Allan M. Judd
Sandra H. Burnett
Michael R. Stark
Laura C. Bridgewater

Department of Physiology and Developmental Biology

Brigham Young University

July 2013

ABSTRACT

Susceptibility of Apoptotic Cells to Hydrolysis by sPLA$_2$:
Molecular Basis and Mechanisms Defined

Elizabeth Gibbons
Department of Physiology and Developmental Biology, BYU
Doctor of Philosophy

Secretory phospholipase A$_2$ hydrolyzes phospholipids at a lipid-water interface, resulting in pro-inflammatory products being released from cell membranes. Healthy cells are resistant to cleavage by this enzyme, but apoptotic cells become susceptible to its activity. Only bilayers with certain characteristics are able to be hydrolyzed. Most recently, studies in this lab have emphasized the idea that the biophysical state of the bilayer (in terms of lipid order, spacing, and fluidity) is relevant in determining the probability of one phospholipid escaping the membrane to be hydrolyzed. Prior to this study, it had been shown that apoptotic cells undergo biophysical alterations that weaken inter-lipid interactions early in apoptosis. The purpose of this dissertation was to examine these changes in more detail, define them more clearly on the molecular level, and suggest possible mechanisms responsible for their occurrence.

First, the role of increased membrane permeability in susceptibility to the phospholipase was investigated. S49 cells were treated with ionomycin or apoptotic agents and assayed for merocyanine 540 staining of the membrane and membrane permeability to a vital dye. Human group X and snake venom isoforms were active towards all treated cells, but human groups V and IIa only hydrolyzed cells that were moderately permeable to the vital dye. Different isoforms must then be sensitive to different membrane properties.

Second, the role of membrane oxidation in cell membrane vulnerability to the phospholipase (specifically human group IIa) was tested. The temporal onset of lipid peroxidation was assayed during apoptosis. This correlated with the onset of susceptibility to the IIa isoform. Direct oxidizers were then used to verify this result in isolation from other apoptotic membrane changes.

Third, biophysical alterations during thapsigargin-induced apoptosis were examined using TMA-DPH and Patman. Data from these probes in artificial bilayers undergoing phase transitions were used to quantify the decrease in interlipid interactions and predict a 50 – 100-fold increase in the probability of phospholipid protrusions. Patman equilibration kinetics also revealed more molecular detail about the biophysical changes related to susceptibility.

Finally, temperature- and ionomyin-induced alterations in membrane properties were compared. Both increased fluidity, but only ionomycin caused susceptibility. Patman equilibration kinetic analysis could distinguish responsible membrane properties. Actin fragmentation during apoptosis or calcium loading is proposed as the mechanism.

Keywords: secretory phospholipase A$_2$, fluorescence spectroscopy, confocal microscopy, flow cytometry, membrane biophysics, apoptosis, actin, cytoskeleton

ACKNOWLEDGEMENTS

First, I am so grateful to my family and friends for supporting me and cheering me on throughout my educational career. My parents especially are my biggest fans. I would like to thank them for believing that I could do anything and always encouraging me to develop my talents to the greatest degree possible without ever making me feel pressured to do anything. I loved it when they read my papers and acted impressed, even if they didn't completely understand them.

I don't know if I have the words to express my gratitude to my mentor, John Bell. I am so glad I took my freshman biology class from him at age 18 and that he took a chance and let me into his lab even though it was full. Since then, he has taught me how to think, how to write, and how to teach. I will miss our brainstorming sessions, writing parties, team-teaching, talks about life, and inside jokes. He and his wife, Rhonda, are like family to me, and I have loved spending time in their home.

I would like to thank my amazing graduate committee, Allan Judd, Michael Stark, Sandra Burnett, and Laura Bridgewater, for investing their time into helping me develop as a scientist. Dr. Judd especially has been so helpful with both my coursework and research and has become a dear friend. I will miss his advice and teasing.

I am also grateful for the many people that have worked with me in the lab for the past 7 years. I can't mention them all by name, but they truly were my second family during my time at BYU. I am grateful for Anne Heiner and Rachel Bailey for mentoring me as an undergraduate. As a graduate student, so many lab members contributed to my dissertation: Hannabeth Franchino, Lauryl Campbell, Mike Streeter, Ashley Warcup, Katalyn Pickett, Celestine Yeung, Kelly Brewer, Lynn Anderson, Stephanie Melchor, Mike Murri, Eric Moss, and Amy Hamaker.

In particular, Jen Nelson has been both a cherished friend and an invaluable collaborator. Our conversations about science and life will always be some of my fondest memories in the lab.

TABLE OF CONTENTS

LIST OF TABLES

LIST OF FIGURES

CHAPTER 1: REVIEW OF LITERATURE

Secretory Phospholipase A$_2$

Secretory phospholipase A$_2$ (sPLA$_2$) is a hydrolytic enzyme which cleaves the sn-2 ester bond of phospholipids, yielding lysophospholipids and free fatty acids. It is found in the venom of various species of snake and bee and there are many human isoforms. It is an excellent model for an enzyme acting at a lipid-water interface (Scott and Sigler, 1994).

This enzyme is relevant to many pathophysiological conditions. Hydrolysis by certain isoforms of sPLA$_2$ releases arachidonic acid, an important precursor of pro-inflammatory lipid mediators (Triggiani et al., 2005), so sPLA$_2$ activity is often associated with inflammatory, autoimmune, and allergic diseases (Bidgood et al., 2000; Cunningham et al., 2006; Hurt-Camejo et al., 2001; Ivandic et al., 1999; Pinto et al., 2003; Triggiani et al., 2006; Triggiani et al., 2005). Secretory PLA$_2$ is also known to be overexpressed in some cancers (Belinsky et al., 2007; Dong et al., 2010; Kupert et al., 2011). Therefore, targeted chemotherapy is being developed to utilize the ability of this enzyme to hydrolyze drug-encasing liposomes, releasing drug specifically near the tumor itself (Andresen et al., 2004; Mock et al., 2013).

Studies aimed at elucidating the regulation of sPLA$_2$ activity began in artificial vesicles. Early on it was observed that the enzyme exhibited low levels of activity toward liposomes initially but would eventually undergo rapid activation (Bell and Biltonen, 1989). This lag time has since been studied extensively and is now known to be due to accumulation of hydrolysis products in the membrane (Bell et al., 1995; Bell et al., 1996; Halperin and Mouritsen, 2005; Hoyrup et al., 2004). This latency period can vary based on the fluidity of the membrane, the organization of lipids in the bilayer, and the presence of certain molecules (such as diacylglycerol or cholesterol) in the membrane (Bell et al., 1996; Liu and Chong, 1999). The

accumulation of fatty acids and lysophospholipids influences both the binding of the phospholipase and the membrane's susceptibility to hydrolysis (Henshaw et al., 1998). Studies with red blood cells or erythrocyte ghosts showed that generally the same properties that govern membrane vulnerability to hydrolytic attack in artificial systems applies to more complex membranes (Best et al., 2002; Harris et al., 2001; Heiner et al., 2008).

Work with nucleated cells has proven more complex as expected. In regards to apoptosis, an interesting phenomenon is observed: healthy cells are naturally resistant to attack by sPLA$_2$, but membranes of dying cells become susceptible to the enzyme (Atsumi et al., 1997; Nielson et al., 2000). Bilayer properties must be perturbed enough to allow a single phospholipid to migrate into the enzyme's active site and become cleaved (Bailey et al., 2007; Wilson et al., 1999). Many studies have investigated membrane alterations that could account for this increase in enzyme activity toward apoptotic cells.

The most well-defined change is PS translocation to the outer leaflet of the membrane. This alteration of the surface of the cell could provide a more appealing substrate to the enzyme. Studies in artificial bilayers suggest that various sPLA$_2$ isoforms show increased activity toward vesicles containing anionic lipids (Bezzine et al., 2002; Jain et al., 1989; Yu et al., 2000). Annexin V has also been shown to inhibit sPLA$_2$ activity in vesicles containing PS by competing for the anionic phospholipid interface (Buckland and Wilton, 1998). In addition, exposure of PS would logically create greater interlipid spacing due to charge repulsion of the head groups. This reduction in lipid-lipid interactions would lower the energy required for a phospholipid to migrate from the bilayer.

Another alteration investigated by our lab has been described as an ill-defined change in the biophysical properties of the plasma membrane. This membrane alteration has been

suggested in studies utilizing fluorescent membrane probes such as merocyanine 540 (MC540), Laurdan, and diphenylhexatriene (DPH). These modifications appear to correlate temporally with susceptibility to sPLA$_2$, but they are vaguely defined as increases in lipid spacing and fluidity, corresponding with a decrease in membrane order. In addition, it is uncertain whether the probes used report on the plasma membrane alone or all internal membranes as well (Bailey et al., 2009; Bailey et al., 2007).

The extent of these characteristics and rate at which they appear differs during various modes of cell death (Bailey et al., 2009; Bailey et al., 2007; Nielson et al., 2000). In addition, different sPLA$_2$ isoforms respond to these different changes to varying degrees. For example, reduction in lipid order is sufficient to render membranes vulnerable to snake venom and the human group X isozymes, and PS exposure increases that activity (Olson et al., 2010). However, the human group IIa isoform of sPLA$_2$ showed minimal activity even when PS externalization and increased membrane fluidity were maximized (Olson et al., 2010). This was surprising because human group IIa showed preference for negatively-charged lipids in experiments with artificial bilayers (Singer et al., 2002).

No direct mechanistic explanation for this biophysical change has been elucidated to date. However, because death induced by calcium ionophore, glucocorticoid, and dibutyryl cyclic AMP all cause this change, it seems probable a common mechanism shared by all three inducers is responsible (Bailey et al., 2009; Bailey et al., 2007).

Apoptosis

Apoptosis, or programmed cell death, is a highly regulated and complex process in nucleated cells. This elegant method of cell destruction plays a critical role in embryonic development, tissue homeostasis, and immune system development and function (Brill et al.,

3

1999; Budtz and Spies, 1989; Eizirik and Mandrup-Poulsen, 2001; Elmore, 2007; Gressner, 2001; Griffith et al., 1995; Lenardo et al., 1999; Metzstein et al., 1998). Research in this field has increased exponentially in the past thirty years as malfunctions in the regulation of apoptosis have proven to be relevant to many different diseases (Diamantis et al., 2008). Some disorders exhibit inappropriate cell survival (e.g. autoimmunity diseases and cancer) whereas others include unwanted cell death (e.g. neurodegeneration and heart failure) (Eguchi, 2001; Fadeel and Orrenius, 2005; Hanahan and Weinberg, 2000; Nagata, 2010; Narula et al., 2006; Okouchi et al., 2007).

In order to understand apoptosis and thus relevant diseases, much effort has been put into elucidating the complex signaling pathways involved with this biochemical process. In contrast with necrosis, unnatural cell death due to injury or trauma, apoptosis is a carefully orchestrated series of biochemical events designed to shut down and eliminate unhealthy cells without eliciting an immune or inflammatory response. The line between classical programmed cell death and necrosis has been blurred as different pathways and mechanisms have been discovered. Different terms such as necroptosis, caspase-independent cell death, autophagy, and anoikis have been coined to describe such pathways (Cuny et al., 2008; Grossmann, 2002; Jaattela and Tschopp, 2003; Leist and Jaattela, 2001).

Two main pathways of classical apoptosis have been described: the extrinsic, initiated by death receptors on the cell surface; and the intrinsic, characterized by the release of cytochrome c from the mitochondrial membrane (Elmore, 2007). Recent investigations have also suggested an additional intrinsic pathway by which apoptosis can be initiated. This third pathway originates with the unfolded protein response and endoplasmic reticulum (ER) stress (Elmore, 2007; Rao et al., 2002; Rao et al., 2001). Each of these pathways leads to the activation of a family of

proteolytic enzymes called caspases (Alnemri et al., 1996). These proteases are synthesized as inactive proenzymes that become functional upon cleavage. Initiator caspases (including caspase-8 and -9) cleave and activate effector caspases, the most important being caspase-3, thus creating a cascade of activation (Elmore, 2007; Vaculova and Zhivotovsky, 2008). In the execution phase, these effector proteases cleave as many as 400 substrates, including cytoskeletal proteins, to cause the distinct morphological changes characteristic of programmed cell death (Benz et al., 2008; Janicke et al., 1998). Caspase-8 is usually associated with the extrinsic pathway while caspase-9 is activated after mitochondrial alterations. These two pathways converge on caspase-3 activation, beginning the "execution" phase of programmed cell death (Elmore, 2007; Hengartner, 2000; Vaculova and Zhivotovsky, 2008). Nakagawa et al. reported that caspase-12 is localized to the ER and specifically mediates ER stress-induced apoptosis in murine cell species (Nakagawa et al., 2000). Caspase-12 has been shown to activate caspase-9, converging with the intrinsic pathway independent of cytochrome c release (Morishima et al., 2002). Human cell lines do not express caspase-12, but similarly, human caspase-4 is located at the ER and is activated during ER stress-induced apoptosis (Hitomi et al., 2004).

Calpain, a calcium-activated protease originally associated only with necrotic cell death, has also been reported to be activated during apoptosis (Squier et al., 1994). Like caspases, calpains cleave many proteins included cytoskeletal components (Wang, 2000). There is even evidence for crosstalk between the two cysteine protease families: Nakagawa et al. reported that calpains can activate caspase-12 at the ER (Nakagawa and Yuan, 2000). Receptor-interacting protein kinases have been identified as the orchestrators of necroptosis when caspases are inhibited, as caspases cleave these kinases and inactivate them. These kinases act on

mitochondrial components, increasing generation of reactive oxygen species (Galluzzi et al., 2009).

Classic Apoptotic Membrane Changes

Although not as commonly studied, the clearance of cell corpses is just as critical as the signaling pathways that kill them. Apoptotic cells must be engulfed before harmful substances leak from the cytosol and cause inflammation. Changes in the plasma membrane during the dying process are critical to tag the cell for phagocytosis (Fadeel et al., 2010; Witasp et al., 2008).

Plasma membrane blebbing is one of the main morphological features of apoptosis. Late in apoptosis, the lipid bilayer buds off to form membrane blebs which become apoptotic bodies (Elmore, 2007). These bodies contain contents of the nucleus and cytosol and are engulfed by phagocytes cleanly to reduce inflammation (Coleman et al., 2001). Studies have suggested that blebbing requires a reduction in cytosolic volume, plasma membrane detachment from the cytoskeleton, actin reorganization, and myosin activation (Coleman et al., 2001; Mitran and Young, 2011; Nunez et al., 2010). Caspases cleave rho-associated protein kinase (ROCK I) which promotes coupling of actin-myosin filaments, causing membrane blebbing (Coleman et al., 2001).

Since it was first reported in 1992, the exposure of phosphatidylserine (PS) on the cell surface has become recognized as one of the characteristic features that identifies apoptotic cells (Fadok et al., 1992). Anionic PS is normally sequestered in the inner leaflet of the plasma membrane in healthy cells. During cell death, this asymmetry is lost as the phospholipids are scrambled and PS is externalized (Raggers et al., 2000; Verkleij and Post, 2000). This negatively-charged lipid exposed to the surface of the cell triggers the elimination of the cell by

6

macrophages (Fadeel and Orrenius, 2005; Fadok et al., 1998; Fadok et al., 2000; Fadok et al., 1992). Multiple proteins have been discovered that are involved in phospholipid translocation across the membrane. Flippase (aminophospholipid translocase) is ATP-dependent and specific to the negatively-charged phospholipids PS and phosphatidylethanolamine. Flippase is responsible for transporting these lipids to the inner leaflet and is inhibited during apoptosis (Devaux et al., 2008; Seigneuret and Devaux, 1984; Zachowski et al., 1986). Floppase is also an ATP-dependent protein, but it is outward-directed and primarily nonspecific (Daleke, 2003; Dekkers et al., 1998; Serra et al., 1996). A third protein, scramblase, is not ATP-dependent and facilitates bidirectional movement to disrupt membrane asymmetry. It is normally inactive in healthy cells but is activated by calcium during cell death (Basse et al., 1996; Raggers et al., 2000; Zhou et al., 1997). Additional mechanisms such as lipid peroxidation could also contribute to PS exposure (Raggers et al., 2000; Tyurina et al., 2004; Verkleij and Post, 2000). Some propose that oxidized PS could possibly form hydrophilic transbilayer pores in the membrane, making the diffusion of phospholipids across leaflets more energetically favorable (Tyurina et al., 2004).

CHAPTER 2: MATERIALS AND METHODS

Reagents

Secretory phospholipase A_2 isoforms were isolated and prepared as described: monomeric aspartate-49 $sPLA_2$ from the venom of Agkistrodon piscivorus piscivorus (AppD49) (Maraganore et al., 1984), hGIIa (Baker et al., 1998; Markova et al., 2005), hGV (Cho et al., 1999), and hGX (Pan et al., 2002). Snake venom $sPLA_2$ was generally used because of its availability and sensitivity to biophysical changes in the plasma membrane.

Ionomycin, 1,6-diphenyl-1,3,5-hexatriene (DPH), 1-(4-trimethylammoniumphenyl)-6-phenyl-1,3,5-hexatriene (TMA-DPH), acrylodan-labeled fatty acid-binding protein (ADIFAB), propidium iodide, 6-dodecanoyl-2-dimethylaminonaphthalene (Laurdan), 6-palmitoyl-2-[[2-(trimethylammonio)ethyl]-methylamino]naphthalene chloride (Patman), 4,4-difluoro-5-(4-phenyl-1,3-butadienyl)-4-bora-3a,4a-diaza-s-indacene-3-undecanoic acid (C11-BODIPY$^{581/591}$), MC540, Alexa Fluor® 488 Phalloidin Conjugate, and annexin V Alexa Fluor® 488 conjugate were all purchased from subsidiaries of Life Technologies (Grand Island, NY). The carboxyfluorescein-labeled peptide (Val-Ala-Asp) fluoromethylketone caspase inhibitor (FAM-VAD-fmk) was acquired from Cell Technology (Mountain View, CA). Thapsigarin (TG), NecroX-5™, and Z-Val-Ala-Asp(OMe)-Fluoromethylketone (Z-VAD-fmk) were both acquired from Enzo Life Sciences (Plymouth Meeting, PA). Dexamethasone (DEX) and tert-Butyl hydroperoxide (TBHP) were purchased from Sigma-Aldrich (St. Louis, MO). 2,2'-azobis-2-methyl-propanimidamide, dihydrochloride (AAPH) and 6-hydroxy-2,5,7,8-tetramethylchroman-2-carboxylic acid (Trolox) were purchased from Cayman Chemical (Ann Arbor, MI). These agents were dissolved in N,N-dimethylformamide (DMF), dimethylsulfoxide (DMSO), or aqueous buffer as appropriate. Formaldehyde (16%, no methanol) was obtained from Thermo

Fisher Scientific (Rockford, IL). Lipids were purchased from Avanti Polar Lipids (Birmingham, AL). All other reagents were obtained from standard suppliers.

Cell Culture and Treatment with Agents

S49 mouse lymphoma cells were grown in suspension in Dulbecco's Modified Eagle Medium at 37 °C (10% CO_2) as explained (Wilson et al., 1997). Cells were treated in culture with TG (5 µM), DEX (100 nM), AAPH (3 mM, dissolved in culture medium fresh immediately prior to each experiment), or equivalent volumes of the associated vehicles (parallel incubation times, DMSO ≤ 0.1% v/v). When applicable, Z-VAD-fmk (50 µM) was added in culture 30 min before TG or DMSO. For experiments, cells were collected by centrifugation, washed, and suspended (0.25–3.5 x 10^6 cells/ml) in a balanced salt medium (NaCl = 134 mM, KCl = 6.2 mM, $CaCl_2$ = 1.6 mM, $MgCl_2$ = 1.2 mM, Hepes = 18.0 mM, and glucose = 13.6 mM, pH 7.4, 37 °C). Treatments with ionomycin (300 nM) or TBHP (0.4 mM) were done in the balanced salt medium after cell harvesting. All experiments, treatments, and incubations were conducted at 37 °C unless otherwise specified. Sample viability was assessed by trypan blue exclusion. Unless stated otherwise, all error representations are SE.

Vesicle Prep

Multilamellar vesicles were made using 1,2-dipalmitoyl-sn-glycero-3-phosphocholine (DPPC), 1,2-dimyristoyl-sn-glycero-3-phosphocholine (DMPC), or 1,2-distearoyl-sn-glycero-3-phosphocholine (DSPC). Samples (0.1 µmole phospholipid dissolved in chloroform) were dispersed with TMA-DPH (1:200 probe:lipid), dried under a N_2 gas stream, and suspended in 2 mL citrate buffer (20 mM sodium citrate/citric acid, 150 mM KCl, pH 7). Suspensions were

incubated 1 h in a shaking water bath at ≥ 50 °C (or ≥ 60 °C for all samples containing DSPC) with intermittent vortex mixing at 10-min intervals.

For experiments in which PS was added exogenously to S49 cells, vesicles containing 50% L-α-phosphatidylserine (PS; brain, porcine) and 50% L-α-phosphatidylcholine (PC; egg, chicken) were used. Lipids were dried under nitrogen and resuspended in PBS (1 mM final). In order to make unilamellar liposomes, samples were sonicated in a Misonex Sonicator 3000 (20 kHz) at 2 watts for 3 min.

Addition of Exogenous PS

For assays in which PS was added exogenously to the cell membrane, cells were harvested as described above and resuspended to a volume of 0.5 – 1.5 million cells/mL. Cells were then incubated with 50% PS, 50% PC liposomes (50 μM final) for 30 min at 37 °C. Samples were then washed via centrifugation and resuspended in a balanced salt buffer for experimentation.

Fluorescence Spectroscopy

Time-based fluorescence intensities and emission spectra were collected with a Fluoromax (Horiba Jobin Yvon, Edison, NJ) photon-counting spectrofluorometer. Anisotropy measurements were taken with a PC-1 (ISS, Champaign, IL) photon-counting spectrofluorometer. Continuous gentle stirring with a magnetic stir bar ensured sample homogeneity, and temperature was maintained by a jacketed sample chamber fed by a circulating water bath. Bandpass was set at 16 nm for anisotropy measurements and 4 nm for all other experiments. When necessary, fluorescence emission at multiple wavelengths was acquired by rapid sluing of monochromator mirrors. Cell samples were treated and prepared as described

above and equilibrated in the fluorometer sample chamber for at least 5 min before initiating data

acquisition. Vesicles were equilibrated at each temperature for 10 min before collecting data

unless indicated otherwise.

Membrane Susceptibility Assays

Cell membrane hydrolysis catalyzed by various sPLA$_2$ isozymes (35–70 nM) was

measured by assaying fatty acid release using ADIFAB (65 nM final) as described (Olson et al.,

2010). Most experiments were conducted using the AppD49 isozyme as a standard for

comparison to previous studies and because it mimics many general behaviors of the human

enzymes (Olson et al., 2010). Key results were then repeated with hGIIA, hGV, and hGX.

The amount of fatty acid released was quantified by comparing ADIFAB fluorescence

emission (65 nM final; excitation = 390 nm) at 432 and 505 nm (I_{432} and I_{505}) and calculating the

generalized polarization (GP_{ADIFAB}) as described (Richieri and Kleinfeld, 1995; Wilson et al.,

1997):

Eq. 1
$$GP_{ADIFAB} = \frac{I_{505} - I_{432}}{I_{505} + I_{432}}$$

Cells treated with DMSO, TG, or DEX were incubated for 600 s with the enzyme. The

maximum displacement in ADIFAB GP during this incubation period was calculated to quantify

the amount of hydrolysis by sPLA$_2$. In some instances, this displacement was then divided by the

equivalent value obtained from parallel experiments with cells treated 10 min with 300 nM

ionomycin. Ionomycin renders 100% of S49 cells vulnerable to hydrolysis by AppD49 sPLA$_2$

(Bailey et al., 2007) and was therefore used as a standard to establish the maximum for

normalization. For experiments involving human isoforms of sPLA$_2$, the total amount of

hydrolysis possible under the various experimental conditions was estimated using AppD49 sPLA$_2$.

The initial hydrolysis rate was quantified for each isozyme by measuring the displacement in ADIFAB GP during the initial 5 s (AppD49), 20 s (hGX), or 50 s (hGV or hGIIa) of the hydrolysis time courses and then dividing that value by the length of the incubation. The specific activity of each enzyme preparation was assayed by likewise assessing the initial hydrolysis rate using DPPG liposomes (25 μM lipid) as substrate. The maximal hydrolysis rate was estimated by fitting the data to an arbitrary function (sum of exponentials) by nonlinear regression and calculating the first derivative of the resulting curve.

Plasma membrane susceptibility to sPLA$_2$ was also indirectly assayed using a vital dye. Propidium iodide fluorescence was collected over time (excitation = 537 nm, emission = 617 nm) as propidium iodide (37 μM final), sPLA$_2$ (70 nM final), and triton X-100 were added sequentially. Triton X-100 permeabilizes all cells and provides the maximal fluorescence. The proportional rise in propidium iodide fluorescence after the addition of both propidium iodide and sPLA$_2$ was quantified by fitting fluorescence intensity time courses with an arbitrary function by nonlinear regression. The subpopulation of cells that were alive but susceptible to sPLA$_2$ was quantified as the fraction of total propidium uptake that occurred after sPLA$_2$ addition. The data were adjusted to account for cells with degraded DNA (invisible in this assay) using data obtained from flow cytometery (see below). Details of these calculations have been reported previously (Olson et al., 2010).

Merocyanine 540

Merocyanine 540 (170 nM final) spectra (excitation: 540 nm, emission: 550 to 700 nm) were collected before probe addition (to assess stray light background), after 5 min equilibration

with MC540, and after 10 min treatment with 300 nM ionomycin (a calcium ionophore which quickly initiates a maximal MC540 response (Bailey et al., 2007)). Intensity values from 565 to 615 nm were summed to quantify the overall intensity for each spectrum. The intensity of the first spectrum was subtracted from the second, and the difference was divided by the intensity of the third spectrum (also corrected for background) to standardize for cell number. To quantify shifts in the spectral peak, spectra were fit by nonlinear regression to an arbitrary function (sum of Gaussian curves). The peak wavelength was then calculated as the point at which the first derivative of the generated curve was equal to zero. The magnitude of spectral shifts was calculated by subtracting the peak wavelength of the second spectrum from the third (ionomycin). The data are expressed as the average change in peak wavelength after ionomycin addition for the control group minus the change observed for each individual sample. The intensity of MC540 fluorescence (170 nM final) was assayed at 585 nm (excitation = 540 nm) as described (Bailey et al., 2009; Bailey et al., 2007).

DPH and TMA-DPH

Measurements of DPH and TMA-DPH (2.5 µM final) fluorescence were collected with different configurations of excitation (350 nm) and emission (452 nm) polarizers in the vertical and horizontal positions after 10 min equilibration of cells with the probe. The anisotropy (r) was then calculated from the fluorescence intensity when both polarizers were vertical ($I_{//}$) and when the excitation was vertical and the emission horizontal ($I_{\perp}$). Correction for differential transmission and detection at the two polarizer positions was included (G) according to convention:

Eq. 2
$$r = \frac{I_{//} - GI_{\perp}}{I_{//} + 2GI_{\perp}}$$

Anisotropy measurements were also made with DMPC, DPPC, or DSPC multilamellar vesicles equilibrated with TMA-DPH during vesicle preparation as described above. Samples were equilibrated first with the probe and then 5 min at each temperature in 1–2 °C increments spanning the main phase transition for each lipid (DMPC: 15–35 °C; DPPC: 18–50 °C; DSPC: 18–60 °C). The change in anisotropy associated with the phase transition was calculated as the difference in limiting anisotropy values at the two ends of the transition (r_{low} and r_{high}) obtained by nonlinear regression using the following:

Eq. 3
$$r = r_{low} + \frac{r_{high} - r_{low}}{1 + e^{n(T_m - T)}}$$

where n is the cooperativity of the transition, and T_m is the melting temperature.

Laurdan and Patman

Both Laurdan and Patman (250 nM final) fluorescence intensity measurements were acquired as a function of time with excitation at 350 nm and emission collected at 435 and 500 nm (I_{435} and I_{500}). Spectral changes were quantified by calculating the generalized polarization (GP) as follows (Parasassi et al., 1991):

Eq. 4
$$GP = \frac{I_{435} - I_{500}}{I_{435} + I_{500}}$$

For Patman equilibration analyses for TG and temperature studies, time courses of probe intensity were smoothed by nonlinear regression to an arbitrary function (analogous to Eq. 5) and normalized to the intensity at 435 nm at 400 s to aggregate data from multiple replicate samples. These pooled data were then fit by nonlinear regression to the following:

Eq. 5
$$I = A(1 - e^{-bt}) + C(1 - e^{-dt}) + F$$

where A and C are arbitrary scalars, b and d are rate constants, and F is the intercept intensity. Intensities at both wavelengths were fit together with b and d constrained as shared parameters. These fitting parameters were then used to calculate model parameter values (fraction of probe in each configuration, polarity of each configuration, and rate of probe entering each configuration) according to Eqs. 11–14 in Franchino's 2013 study (Franchino et al., 2013). Error was estimated by using the extreme values of the 95% confidence intervals for each fitting parameter generated by nonlinear regression. Every permutation of these fitting parameters was inputted into Eqs. 11–14 (Franchino et al., 2013) to determine the range of possible model parameter values. This range is illustrated as error bars in the relevant figure.

For Patman equilibration studies with ionomycin, the ionophore was added after probe. These intensity profiles were fit according to an arbitrary function similar to Eq. 5 with a third exponential term applied after the time of ionomycin addition. The rate of this third exponential term was constrained to be shared among the 435 nm and 500 nm curves.

Flow cytometry

All flow cytometry samples were immediately processed (without fixation) in a BD FACSCanto flow cytometer (BD Biosciences, San Jose, CA) with an argon excitation laser (488 nm). Emission was assessed using a bandpass filter at 515–545 nm (FAM-VAD-fmk, annexin V, or C11-BODIPY[581/591]) or 564–606 nm (propidium iodide and MC540).

FAM-VAD-fmk

For caspase assays, FAM-VAD-fmk was added in culture 30 min before cell harvesting according to instructions provided with the vendor's kit. Because peaks were not easily distinguishable for analysis by gating, histograms of FAM-VAD-fmk intensity were fit with a

sum of Gaussian curves. The area under the curves composing the more positive peak was used to represent the percent of the population staining positive for caspase activation.

Merocyanine 540 and Annexin V

Merocyanine 540 (250 nM) was added after cells were resuspended in buffer and samples were processed after a 10 min incubation. Merocyanine 540 data were analyzed in the same way as for the caspase assay. The annexin V Alexa Fluor® 488 conjugate was used to assay PS externalization according to manufacturer's instructions (Life Technologies, Grand Island, NY). A gate representing positive staining was determined from either samples containing no probe or from stained control cells as specified in figure legends.

Propidium Iodide

After harvesting, cells were stained with propidium iodide (10 μM) for 10 min. Where indicated, 70 nM sPLA$_2$ was also included. To quantify the number of cells cdontaining hypodiploid-staining DNA due to fragmentation, propidium iodide and Triton X-100 were used in conjunction as described (Riccardi and Nicoletti, 2006). This proportion was determined by setting a gate below the peak representing G1-phase DNA staining.

C11-BODIPY$^{581/591}$

When assaying oxidative potential, cells were incubated with C11-BODIPY$^{581/591}$ (2 μM final) for at least 1 h in culture prior to treatment with TG or an oxidizer. Fluorescence histograms of control sample fluorescence were fit to a Gaussian curve. Fluorescence histograms of treated samples were then fit with two Gaussian curves with one constrained to the mean and standard deviation of the corresponding control. The area under the second Gaussian curve

normalized to the total fluorescence was reported as the percent of the population staining positive for oxidized C11-BODIPY[581/591].

Two-Photon Microscopy

Two-photon excitation microscopy was performed at the Laboratory for Fluorescence Dynamics (Irvine, CA) using an Axiovert 35 inverted microscope (Zeiss, Thornwood, NY). S49 cells were prepared for experiments as described above, treated with Laurdan, Patman, DPH, or TMA-DPH (250 nM final), and equilibrated for 10 min before data acquisition. Excitation was usually set at 753 nm, but when experiments involved only Laurdan or Patman, 780 nm was used because of more efficient excitation. Using software obtained from the Laboratory for Fluorescence Dynamics, histograms of Laurdan GP were created for both the whole cell and the middle of each cell ($54 \pm 5\%$ (SD) of image pixels). The average GP for the perimeter of the cell was calculated as the difference between the average GP of the whole cell and its middle.

Confocal Microscopy

Images were collected on an Olympus FluoView FV 300 confocal laser scanning microscope using a 60x oil immersion objective lens.

C11-BODIPY[581/591]

Cells were stained with C11-BODIPY[581/591] (2 μM final) for at least 1 h in culture prior to treatment with TG or an oxidizer. Two different lasers and emission filter sets were used concurrently to excite and collect fluorescence from both oxidized (488 nm argon laser, 505–525 nm bandpass emission filter, green color in images) and non-oxidized probes (543 nm helium-neon laser, 560–660 nm bandpass emission filter, red color in images). Experimental temperature was maintained throughout imaging using a heated stage.

<u>Phalloidin</u>

For actin studies, cells were simultaneously fixed, permeabilized, and stained with fluorescent phalloidin (Alexa Fluor© 488) according to the manufacturer's protocol (Life Technologies). After being mounted onto slides, cells were stained with a solution containing 165 nM phalloidin, 3.7% formaldehyde, 1% bovine serum albumin, and 0.1 mg/mL lyso-PC (1-palmitoyl-2-hydroxy-sn-glycero-3-phosphocholine) for 20 min at 4 °C. Slides were then washed with buffer before coverslips were mounted. The 488 nm argon excitation laser was used.

ImageJ software was used to quantify the circularity index of all particles in each image (Schneider et al., 2012). Color images were converted to 8-bit greyscale images and inverted so particles were dark against a white background. After subtracting background, the images were converted to 1-bit black and white images before the particles were analyzed. The data are represented as the percentage of total pixels that appear in particles of highest circularity index (0.75 – 1).

CHAPTER 3: RELATIONSHIP BETWEEN MEMBRANE PERMEABILITY AND

SPECIFICITY OF HUMAN SECRETORY PHOSPHOLIPASE A$_2$

ISOFORMS DURING CELL DEATH

Introduction

Early attempts at distinguishing apoptotic and necrotic cells often focused on

permeability of the cells to vital stains such as propidium iodide (reviewed in (Darzynkiewicz et

al., 1997). The original paradigm was that necrotic cells are immediately permeable to the dye

while apoptotic cells display a significant temporal delay before they become stained. It was

soon discovered that the latent permeability to propidium iodide during apoptosis is not an "all or

none" phenomenon. Instead, there is a gradual acceleration of probe uptake that initially

produces faint cellular fluorescence quantifiable only by flow cytometry but eventually

culminating in complete staining of the cells (Vitale et al., 1993; Zamai et al., 1996).

Presumably, this gradual acceleration represents alterations to the structure and dynamics of the

cell membrane that progressively become more pronounced. Although these observations have

been substantiated by several investigators, the focus has been confined to development of assay

methods; determinations of mechanisms and physiological/pathological consequences have

lagged.

Another membrane event that occurs during early apoptosis is an increase in the ability of

secretory phospholipase A$_2$ (sPLA$_2$) to hydrolyze phospholipids and release fatty acids and

lysophospholipids from the outer face of the plasma membrane (Atsumi et al., 1997; Bailey et

al., 2009; Bailey et al., 2007; Nielson et al., 2000; Olson et al., 2010). This interesting

relationship between sPLA$_2$ and apoptosis is an extension of a broader paradigm that healthy

cells resist hydrolysis by the enzyme whereas membranes of damaged or dying cells are

vulnerable (Atsumi et al., 1997; Bailey et al., 2009; Bailey et al., 2007; Jensen et al., 2005; Nielson et al., 2000; Olson et al., 2010; Wilson et al., 1999). At least some of this enhanced vulnerability to hydrolytic attack is observed in apoptotic cells that have not yet become fully stained by propidium iodide (Bailey et al., 2009; Bailey et al., 2007; Nielson et al., 2000; Olson et al., 2010). Apparently, the increased susceptibility to hydrolysis also represents alterations to the structure and dynamics of the cell membrane (Bailey et al., 2009; Bailey et al., 2007; Best et al., 2002; Bezzine et al., 2002; Harris et al., 2001; Jensen et al., 2005; Singer et al., 2002; Smith et al., 2001). Biophysical studies of this phenomenon have yielded some clues as to what these alterations might involve. Possible candidates include increased lipid spacing, decreased lipid order, and increased exposure of phosphatidylserine on the outer face of the cell membrane (Bailey et al., 2009; Bailey et al., 2007; Olson et al., 2010). Nevertheless, a complete understanding of the nature of relevant membrane changes during early apoptosis has not yet been achieved. These observations raise the question of whether the alterations that permit hydrolysis by $sPLA_2$ might correspond to those that allow modest permeability to propidium iodide. Answering that question could clarify mechanisms involved in controlling $sPLA_2$ activity as well as a possible novel biological significance for subtle changes in membrane permeability to vital stains during apoptosis.

To address this question, we examined responses to various death stimuli using flow cytometry to classify populations of cells based on their intensity of staining with fluorescent probes that detect specific membrane properties. The objective was to identify which populations were most susceptible to enzymatic attack and determine how those populations related to permeability to propidium iodide and other physical properties. We included agents that initiated death through endoplasmic reticulum stress, glucocorticoid receptor stimulation, and calcium

loading. Although we compared results using each of these stimuli, we focused most of our

attention on endoplasmic reticulum stress caused by the calcium ATPase inhibitor TG (Bian et

al., 1997; Kass and Orrenius, 1999; Nielson et al., 2000; Yoshida et al., 2006). Thapsigargin was

emphasized because it induces apoptosis rapidly in S49 cells thereby augmenting the size of

relevant populations by maintaining high synchrony of cells as they proceed through the death

process. In addition to propidium iodide, MC540 was used as a marker of increases in interlipid

spacing and membrane lipid disorder that have been reported to enable hydrolysis by $sPLA_2$

(Ashman et al., 1995; Bailey et al., 2009; Bailey et al., 2007; Mower et al., 1994; Olson et al.,

2010; Stillwell et al., 1993). Exposure of phosphatidylserine was eliminated as a variable by

including death stimuli and incubation times known to result in optimal exposure of the anionic

phospholipid on the extracellular membrane surface (Ahn et al., 2004; Diaz et al., 1999; Martin

et al., 1995; Mazur et al., 2009; Nielson et al., 2000).

Results

Susceptibility to $sPLA_2$ of moderately-permeable cells

S49 lymphoma cells were treated for 3 h with TG or control vehicle (DMSO), stained

with propidium iodide, and classified based on staining intensity by flow cytometry. Figure 3-1

illustrates contour plots of the flow cytometry results. As shown in Fig. 3-1A, three distinct

populations were identified in control samples based on their level of propidium iodide

fluorescence intensity (ordinate axis). The designation "P" refers to those cells staining positive

for propidium iodide. This population was indistinguishable from cells that had been

permeabilized by the detergent Triton-X 100 (not shown). Therefore, it is assumed to represent

cells with permeable membranes. The negative population ("N") did not stain with propidium

iodide since the apparent fluorescence intensity was comparable to the background observed with cells that had never been exposed to the dye. A third population was labeled "I" for intermediate. The average staining intensity of this population was about 10 times that of the negative population but only1/30 that of the positive population. Cells in the negative and positive populations exhibited stable fluorescent intensities over time. However, for the intermediate population, the degree of staining increased incrementally over time. The cells shown in Fig. 3-1A were representative of typical control samples (84.3% negative, 11.3% intermediate, 4.4% positive).

A likely interpretation of the intermediate population was suggested in a study by Vitale (Vitale et al., 1993). The researchers proposed that it represents a trait inherent to apoptotic cells—slightly compromised membranes that have therefore become modestly permeable to propidium iodide. To examine the applicability of this idea to apoptotic S49 cells, we monitored the distribution of propidium iodide staining at different times after introduction of the dye to a TG-treated sample. We assumed that if the intermediate population represented cells with modest permeability, the population would gradually migrate along the fluorescence intensity axis of the contour plot while the negative and positive populations would remain stable. As shown in Panels B–D, the positive population was clearly defined, contained a greater number of cells than in the control sample (12% compared to 4%), and remained stable in intensity over time. Initially, cells staining with low intensity were distributed across both the negative and intermediate regions (Panel B). As time progressed, a population with higher intensity staining emerged and migrated along the ordinate indicating that the amount of staining per cell was increasing. By 10 min, the two populations had resolved into the negative and intermediate regions.

Figure 3-2 shows histograms of fluorescence intensity from an experiment like that of Fig. 3-1 for cells incubated without (black curves) or with (red curves) sPLA$_2$. In control samples (Panel A), 10-min treatment with sPLA$_2$ produced only minor alterations. With TG-treated cells (Panel B), the effects of hydrolysis by sPLA$_2$ were obvious. The proportion of cells found in the positive peak tripled. These were accounted for quantitatively by a comparable reduction in the number occupying the intermediate peak. The proportion of cells found in the negative population stayed about the same with a small increase in staining intensity, suggesting a minor perturbation to those cells, perhaps from modest hydrolysis. This result suggested that cells in the intermediate peak are a prominent target of sPLA$_2$.

Figure 3-3A represents the evolution of the various populations of apoptotic cells over time after addition of propidium iodide. Consistent with the results in Fig. 3-1, the main change was a time-dependent migration of cells from the negative region (black lines and symbols) to the intermediate region (red). A moderate rise in the number of cells staining positive was also observed (blue). Panels B and C demonstrate the effect of sPLA$_2$ on the distribution of populations over time. The main effect was conversion of the intermediate population to positive cells, presumably due to membrane damage during hydrolysis. As expected, very little hydrolysis was detected in untreated control samples.

As indicated by the relative areas under the black and red curves in Fig. 3-3D, only about 40% of the cells in the intermediate population was hydrolyzed by sPLA$_2$ (i.e. 22–29% of the total sample). There were at least two reasons that cells remained in the intermediate population after addition sPLA$_2$. First, a subpopulation of the intermediate group was already fully permeable to propidium iodide but stained with low intensity because of DNA fragmentation. The existence of this subpopulation was verified by addition of Triton X-100 (Riccardi and

23

Nicoletti, 2006). Obviously, hydrolysis would have had no impact on the intensity of propidium iodide staining of this subpopulation. We performed parallel control experiments to quantify the contribution of these hypodiploid cells to the result. We found that about 10% of the sample contained fragmented DNA under the conditions of Fig. 3-3, which would account for about a fourth of the intermediate cells that did not change staining intensity after sPLA$_2$ treatment (not shown).

The second reason why the remaining cells in this population did not appear to be hydrolyzed is not clear; however, one clue may come from close examination of the histograms shown in Fig. 3-2. The average staining intensity for the intermediate population was reduced by an average of 0.15 log units after hydrolysis by sPLA$_2$. This effect is shown in Fig. 3-3D comparing the residual intermediate subpopulation (red) with that apparently removed by hydrolysis (blue). This difference between the vulnerable and resistant subpopulations in the intermediate cohort was reproducible; the lack of overlap between the 95% confidence intervals for the respective histogram means shown in Fig. 3-3D was true for all of the replicate samples in Fig. 3-3. This result indicates that the vulnerable subpopulation has a slightly greater permeability to propidium iodide (about 41% greater) compared to those that remain resistant. If the intermediate population represents cells with membranes perturbed in a way that makes them susceptible to hydrolysis, then the data presented here would suggest that the enzyme is quite sensitive to the magnitude of that perturbation, and only those cells with sufficient permeability above a narrow threshold are attacked. This result is reasonable for sPLA$_2$ given the extreme sensitivity of the enzyme to subtle changes in artificial membranes (Bell and Biltonen, 1989; Honger et al., 1996; Lichtenberg et al., 1986).

Quantification of hydrolysis

Experiments parallel to those in Fig. 3-3 were conducted spectroscopically on bulk samples using the fluorescent fatty acid binding protein ADIFAB to assess the total amount of hydrolysis occurring during incubation with sPLA$_2$ (Fig. 3-4A). Consistent with previous reports, the control cells displayed transient hydrolysis detected by ADIFAB indicative of a small subset of cells (10–15% of the sample based on Figs.3- 2 and 3-3) that were compromised in culture or during sample preparation and therefore became vulnerable to the enzyme (Olson et al., 2010). After treatment with TG, the amount of lipid hydrolyzed was 52% of the total achieved when 100% of the cells are susceptible to the enzyme (Fig. 3-4C, green bar).

Previous reports have indicated that the total number of cells vulnerable to sPLA$_2$ can also be quantified by counting the number stained by MC540 (Bailey et al., 2009; Bailey et al., 2007). Accordingly, we also assessed MC540 staining by flow cytometry (Fig. 3-4B). Quantitatively, the number of cells staining brightly for MC540 in control and TG samples (violet bars, Fig. 3-4C) matched the percentage hydrolyzed (green; see statistical details in the legend to Fig. 3-4).

Comparison between hydrolysis and propidium iodide uptake for various inducers of cell death

The purpose for obtaining these two estimates of the number of cells vulnerable to enzymatic attack was to compare to the propidium iodide flow cytometry results and identify those populations of cells likely to be targets for sPLA$_2$. For control samples and those treated with TG, the positive (blue) and intermediate (red) populations were adequate to account for the amount of hydrolysis and the apparent numbers of susceptible cells (Fig. 3-4C). As predicted by the data in Fig. 3-3D (red curve), the amount of hydrolysis was less than the sum of the intermediate and positive populations (p < 0.001). In contrast, cells treated with DEX exhibited a

25

greater amount of hydrolysis than could be explained by flow cytometry assessments of MC540 fluorescence or PI permeability ($p < 0.01$). This result implies that either there is a greater amount of lipid hydrolyzed per cell, or some of the negative propidium iodide population (gray) is hydrolyzed at a rate low enough that it does not produce enhanced permeability to propidium iodide. One way in which the first of these possibilities could be realized is that cells treated with DEX, but not TG or ionomycin, may break into fragments during hydrolysis that exposes additional intracellular membranes to sPLA$_2$. Further experiments will be required to resolve this difference and to identify the extent to which it is a common feature among various apoptotic stimuli.

Cells induced to die by brief treatment (10 min) with a calcium ionophore, ionomycin, also behaved differently. In this case, all the cells were vulnerable to the enzyme and stained brightly for MC540 as reported previously (Bailey et al., 2007). However, only about 30% of the cells sorted into the positive or intermediate propidium iodide populations by flow cytometry, indicating that most of the hydrolysis observed with ionomycin-treated samples originates from cells that exclude propidium iodide completely.

Comparisons among sPLA$_2$ isoforms

To test the potential physiological relevance of these findings, we compared the relative abilities of three human isoforms of sPLA$_2$ to hydrolyze samples using data obtained with the AppD49 enzyme as a standard. We compared initial rates rather than total hydrolysis amounts because they more readily resolve quantitative differences related to enzyme activity. Figure 3-5 summarizes the initial rate of hydrolysis for all four isozymes under various experimental conditions. As suggested by Fig. 3-4A, the initial rate catalyzed by AppD49 toward TG-treated cells was similar to that observed for unhealthy cells in the control sample ($p > 0.05$) even

though the total available substrate was very different (Fig. 3-5A). Dexamethasone induced susceptibility to sPLA$_2$ at a slightly higher initial rate that was distinguishable from that observed toward damaged cells in the control sample ($p < 0.05$). As shown in prior studies, the rate toward ionomycin-treated samples was much greater than with any of the other conditions ($p < 0.01$ compared to DMSO) (Bailey et al., 2007; Olson et al., 2010). A similar pattern was obtained with the hGX isoform toward the weakened population in control samples and toward cells treated with the various inducers of cell death (Fig. 3-5B). In this case, only the ionomycin group was statistically different from the control group ($p < 0.01$). In contrast to the results with the AppD49 and hGX isozymes, the hGIIa and hGV isozymes generally showed a different pattern with more obvious differences in the rate of hydrolysis between control and apoptotic samples (TG and DEX) but diminution of the rate toward samples incubated briefly with ionomycin (Figs. 3-5C and D; see legend for statistical details). As explained for the AppD49 isoform, the amount of lipid hydrolyzed in the various treatment groups was always much greater than observed in the control sample (reflecting the larger number of cells participating in biochemically-programmed death) even though the initial rate was sometimes comparable (Bailey et al., 2007).

The lower activity of hGIIa toward mammalian cell membranes has been reported previously (Beers et al., 2002; Bezzine et al., 2002; Birts et al., 2010; Boyanovsky and Webb, 2009) and probably relates to the absence of tryptophan at its interfacial binding surface (Baker et al., 1998; Beers et al., 2003; Bezzine et al., 2002). This difference was not due to low activity of the enzyme preparation since hGIIa was the most active of the four toward the DPPG liposomes used as a positive control (AppD49 = 0.05 GP units·s^{-1}, hGIIa = 0.08 GP units·s^{-1}, hGV = 0.005 GP units·s^{-1}, hGX = 0.01 GP units·s^{-1}). This dichotomy between hGIIa activities

toward liposomes versus apoptotic cells probably reflects the much higher density of negative charge on the liposome compared to that achievable in S49 cells (Wilson et al., 1999).

Discussion

The data in this study argue strongly that one consequence of the modest increase in membrane permeability detected by propidium iodide as an intermediate-staining population is enhanced susceptibility to hydrolysis by sPLA$_2$. Moreover, this enhanced susceptibility is likely to have physiological significance because several sPLA$_2$ isoforms present in human plasma responded to these early apoptotic cells (Fig. 3-5). In contrast, cells dying by ionophore treatment showed two important deviations from this pattern. First, the cells did not display a sizeable intermediate-staining propidium iodide population even though they stained brightly with MC540 and were aggressively attacked by AppD49 and hGX sPLA$_2$. Second, the ionophore-treated cells were hydrolyzed at a much lower rate by hGV and hGIIa sPLA$_2$. This second observation was reported previously and raised the question of whether there might be differences in physical properties of the membranes of apoptotic and ionophore-treated cells that explain this apparent specificity of the isozymes (Olson et al., 2010). The presence of anionic lipids such as phosphatidylserine on the membrane surface and enhanced spacing of bilayer lipids, two properties known to be relevant to the activity of these enzymes, were excluded as candidates since both are expressed more completely in ionophore-treated cells than in those undergoing apoptosis (Fig.3-4 and (Olson et al., 2010)). However, the relationship between hydrolysis and the intermediate-staining propidium iodide population discovered here (Figs. 3-4 and 3-5) is a match with the prior observations and may explain the specificity of hGV and hGIIa sPLA$_2$ isoforms toward apoptotic cells.

This result begs the interesting question: what is the molecular source of the intermediate-staining population, and why does it appear to relate to enhanced enzymatic activity of hGIIa and hGV sPLA$_2$ isoforms? An attractive possibility is that both events are produced by lipid oxidation. This idea stems from three published observations. First, lipid peroxidation appears to occur during apoptosis, perhaps catalyzed by cytochrome c oxidase released from mitochondria (Greenberg et al., 2008; Tyurin et al., 2009; Tyurin et al., 2008b; Tyurina et al., 2000). Second, studies with artificial bilayers suggest that lipid oxidation can perturb the physical properties of membranes in ways that enhance their permeability (Greenberg et al., 2008; Howland and Parikh, 2010; Smith et al., 2009; Yajima et al., 2009). Third, membranes containing oxidized lipids are more vulnerable to hydrolysis by sPLA$_2$, especially the hGIIa isozyme (Akiba et al., 1997; Korotaeva et al., 2010; Korotaeva et al., 2009a; Korotaeva et al., 2009b; McLean et al., 1993).

A second possibility relates to studies with artificial membranes demonstrating that fluctuations caused by changes in membrane order and fluidity can permit charged molecules like propidium iodide to temporarily traverse the bilayer (Apellaniz et al., 2010; Deamer and Bramhall, 1986; Freire and Biltonen, 1978; Marsh et al., 1976; Wilson-Ashworth et al., 2004). The increased staining of the membrane by MC540 (Fig.3- 4 and Ref. (Bailey et al., 2009; Bailey et al., 2007)) probably also represents changes of that nature (Ashman et al., 1995; Mower et al., 1994; Stillwell et al., 1993; Stott et al., 2008; Wilson-Ashworth et al., 2006). Thus, it may be that the intermediate propidium iodide population does not represent emergence of an additional membrane physical trait but instead, greater magnitude of the same perturbations detected by MC540. In other words, perhaps MC540 is sensitive to low levels of perturbation as perhaps occurs with ionomycin. When the perturbation escalates to also become detectable by propidium

iodide, such as during apoptosis, there is no additional staining by MC540 because the intensity was already maximal at a weaker perturbation. If this is true, then the differences among isoforms with respect to membrane physical properties would be quantitative rather than qualitative and could be summarized as follows.

1. Cells that are negative for both MC540 and propidium iodide were not attacked by any of the $sPLA_2$ isoforms studied here.

2. Cells that are weakly perturbed, as during ionomycin treatment, stain brightly by MC540 but are still negative for propidium iodide. These cells were good substrates only for the AppD49 and hGX isoforms.

3. Cells that are more strongly perturbed stain brightly by MC540 and at an intermediate level with propidium iodide. These cells were observed during apoptosis and were susceptible to all four isoforms.

4. The cells that are most heavily perturbed are positive for both propidium iodide and MC540. A previous study demonstrates these cells are also hydrolyzed by the various isozymes, at least during mid-apoptosis (Olson et al., 2010).

Finally, there is evidence that membrane permeability is enhanced in a more specific fashion early during apoptosis via pannexin 1 channels (Chekeni et al., 2010). This rise in permeability allows release of nucleotides such as ATP and UTP from apoptotic cells. These nucleotides function as signals to attract macrophages in preparation for clearance of apoptotic remnants (Chekeni et al., 2010; Chekeni and Ravichandran, 2011). Whether activation of these channels accounts for the modest rise in permeability to propidium iodide is unknown. Other vital stains such as YO-PRO-1 and TO-PRO-3 appear to be conducted by pannexin channels, but propidium iodide was reported not to stain cells at a stage of apoptosis when pannexin channels

are open (Chekeni et al., 2010). Unfortunately, the experimental data were not reported in sufficient detail to allow one to ascertain whether the more moderate propidium iodide diffusion characteristic of early apoptotic cells could be explained by pannexin channel activation. Moreover, it is unclear how pannexin channel activation might relate directly to increased vulnerability of the membrane to hydrolysis by sPLA$_2$.

The data in this study suggest the possibility that the temporary moderate increase in membrane permeability during apoptosis could have significant consequences because these cells can be hydrolyzed by pro-inflammatory enzymes present in the plasma. In general, it is thought that this kind of problem would be avoided through elimination of apoptotic cells by macrophages (Peter et al., 2010a; Peter et al., 2010b, c). The issue, then, becomes one of timing. Recent studies have suggested that macrophage participation involves two signals: a recognition or "find-me" signal followed by an "eat-me" signal (Chekeni et al., 2010). The first appears to involve increases in membrane permeability via the pannexin 1 channel mentioned above (Chekeni et al., 2010). The second is the exposure of phosphatidylserine on the external face of the cell membrane (Callahan et al., 2000; Fadeel, 2004; Krahling et al., 1999; Verhoven et al., 1995). Since the hGV and hGIIa isoforms require the presence of phosphatidylserine in addition to enhanced membrane permeability, they would not be capable of generating inflammatory precursors until the "eat-me" signal and the resulting protection by phagocytosis. Therefore, these isoforms are unlikely to produce an untoward inflammatory response. However, as recently demonstrated, the hGX isozyme actively hydrolyzes the cell membrane during apoptosis prior to the exposure of phosphatidylserine (Olson et al., 2010). Accordingly, the potential exists for production and release of inflammatory fatty acids and lysophospholipids during apoptosis before the dying cells can be cleared by macrophages. This scenario may not be

disadvantageous, however. Although pannexin channel activation has been proposed as one

mechanism for releasing certain "find-me" signals, additional molecules that fulfill the same

function have also been reported to be released during early apoptosis through undetermined

means (Peter et al., 2010a; Peter et al., 2010b, c). Among those other signals is

lysophosphatidylcholine (Lauber et al., 2003; Mueller et al., 2007; Peter et al., 2008). It is thus

tempting to speculate that hGX sPLA$_2$ may play a major role in releasing

lysophosphatidylcholine as a "find-me" signal through mechanisms described in this study.
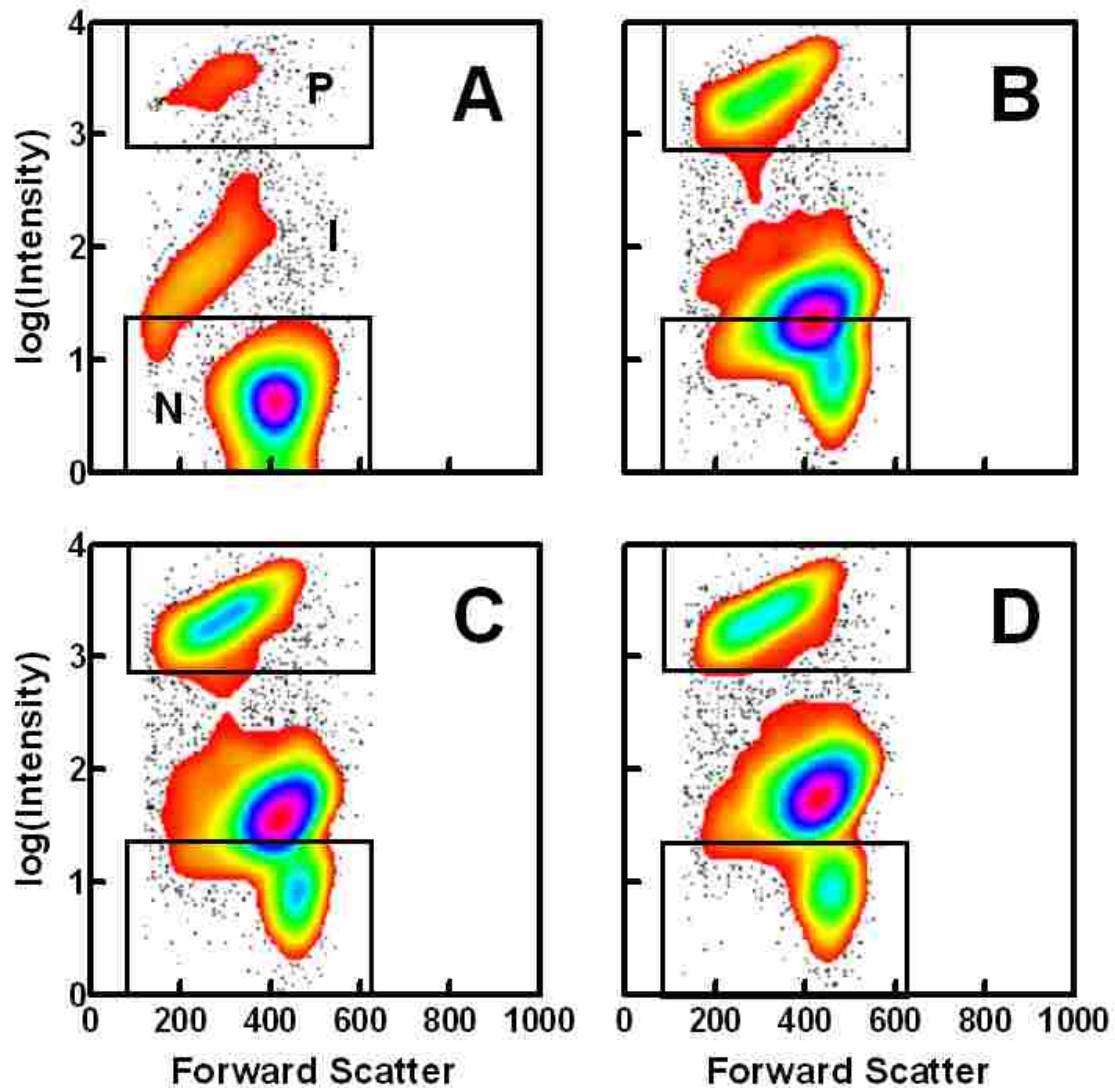
Figure 3-1: Contour plots of propidium iodide fluorescence and forward light scatter.

Samples were stained for 10 min with propidium iodide in Panel A and fluorescence intensity and forward light scatter were assessed for individual cells by flow cytometry. In Panels B–D, cells were stained for 1 min (B), 5 min (C), or 10 min (D) with propidium iodide prior to immediate flow cytometry. Labels: "N", negative (same as background); "I", intermediate propidium iodide staining; "P", positive or complete propidium iodide staining.
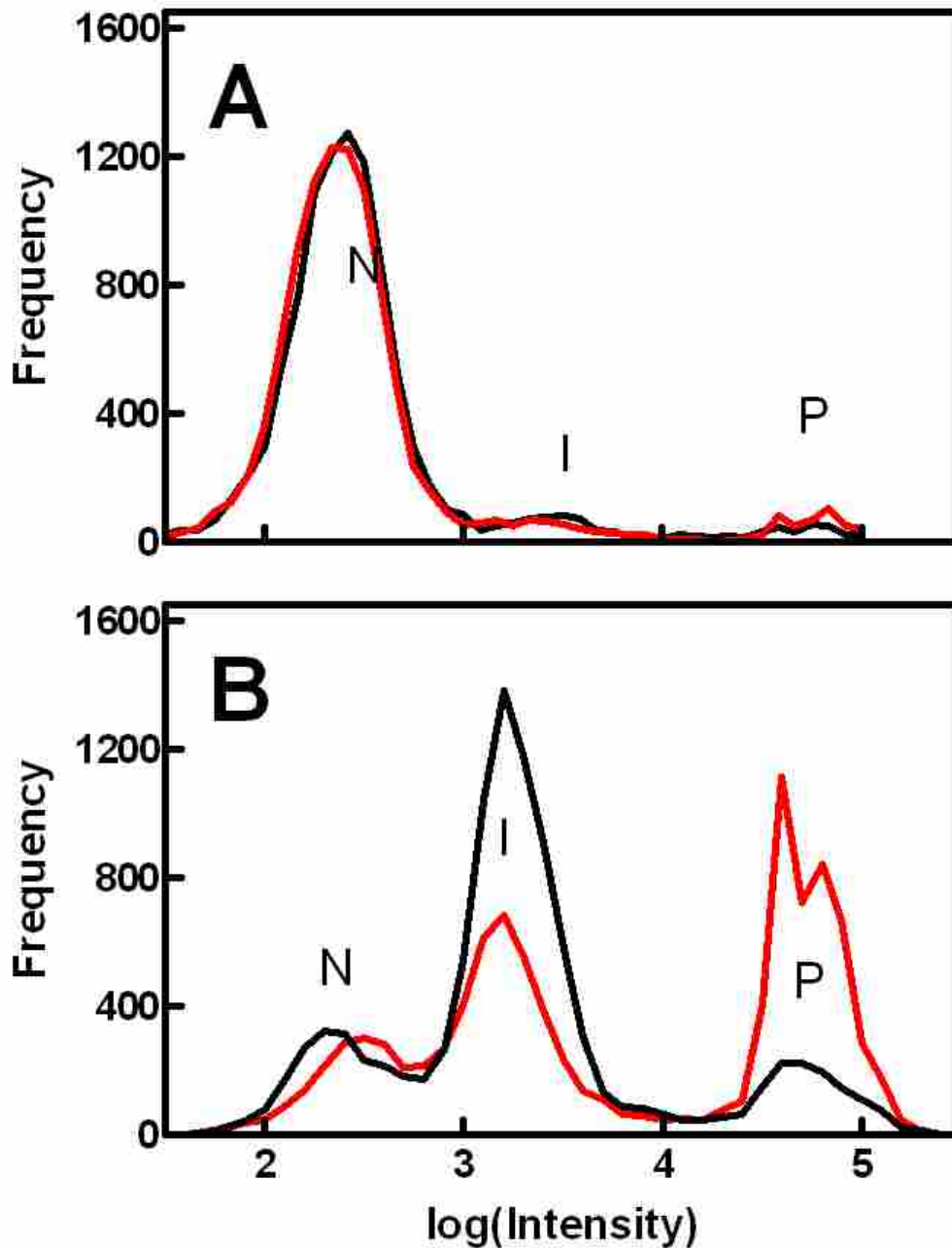
Figure 3-2: Histograms of propidium iodide fluorescence intensity before and after hydrolysis by sPLA$_2$.

Cells were treated with DMSO (Panel A) or TG (Panel B). Samples were stained for at least 10 min with propidium iodide without (black curves) or with (red curves) AppD49 sPLA$_2$. Fluorescence intensity per cell was assessed by flow cytometry. Histograms were smoothed by nonlinear regression using multiple Gaussian functions. Labels: "N", negative (same as background); "I", intermediate propidium iodide staining; "P", positive or complete propidium iodide staining.
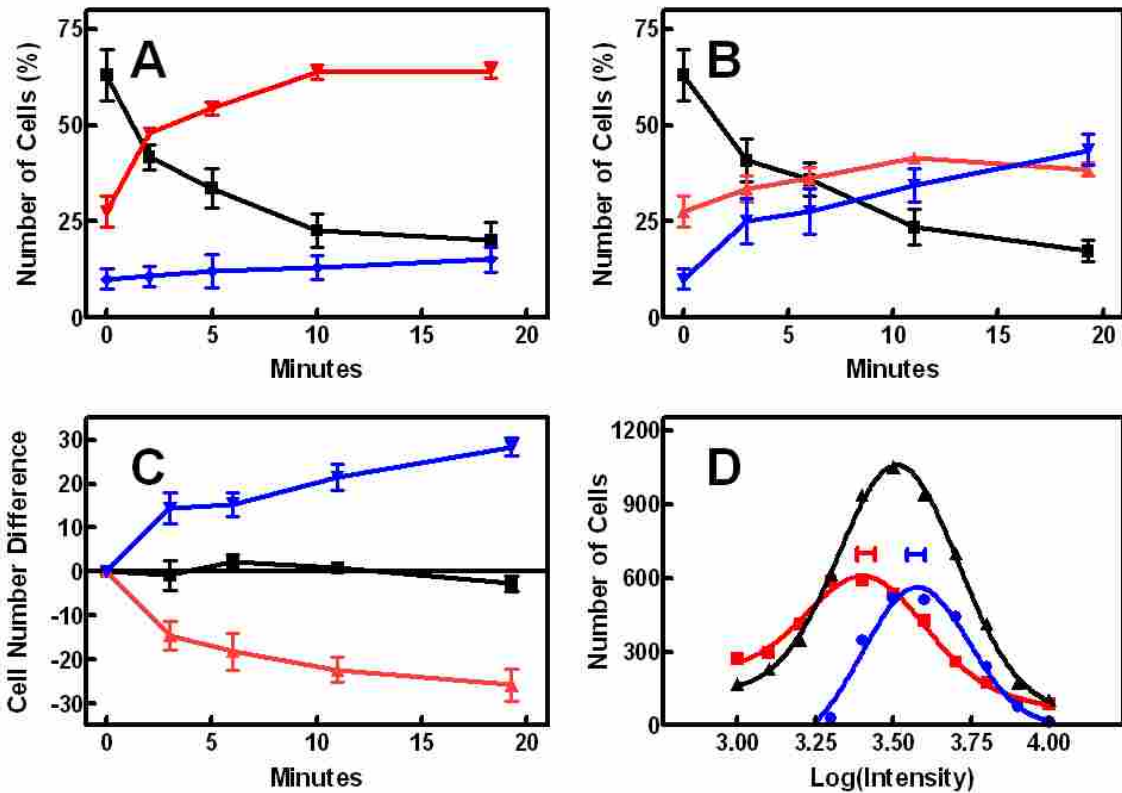
Figure 3-3: Time course of distribution of cells among populations defined by propidium iodide fluorescence intensity before and after hydrolysis by sPLA$_2$.

Panel A: data from three independent experiments such as that shown in Fig. 2 were quantified at the indicted time points following mixing with propidium iodide—black, percentage of the cell sample staining negative for propidium iodide intensity (see field marked "N" on Fig. 2); red, intermediate for propidium iodide ("I" on Fig. 2); blue, propidium iodide positive ("P" on Fig. 2). Panel B: The experiments and analysis of Panel A were repeated for samples incubated with sPLA$_2$ simultaneously during the propidium iodide staining. Panel C: The data represent the differences between Panels A and B. Panel D: Histograms of the intermediate peak corresponding to the last time point from one of the samples in Panels A–C for cells without sPLA$_2$ (black), with sPLA$_2$ (red), and the arithmetic difference between the two (blue). Data were fit by nonlinear regression to a Gaussian function. The brackets represent the 95% confidence intervals for the fitting parameter corresponding to the mean values.

35
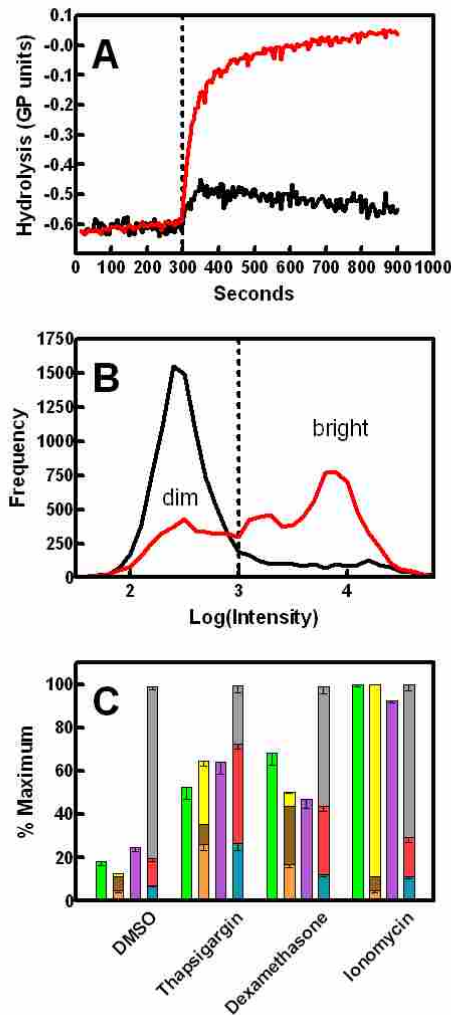
Figure 3-4: Comparison of compartment sizes assessed by various methods for cells treated with TG, DEX and ionomycin.

Panel A: Time profile of membrane hydrolysis by AppD49 sPLA$_2$ (dotted line) assayed with ADIFAB as explained in Materials and Methods (DMSO: black, TG: red). Panel B: Flow cytometry histograms of MC540 staining for cells treated with DMSO (black) or TG (red). Panel C: Cell compartment sizes were estimated by spectroscopy or flow cytometry and normalized to maxima. Green bars: total amount of lipid lipid hydrolyzed by sPLA$_2$ in 300 s (as in Panel A). Orange bars: number of cells permeable to propidium iodide prior to addition of sPLA2 (spectroscopy). Brown bars: number of cells staining hypodiploid for propidium iodide due to fragmented DNA (flow cytometry). Yellow bars: number of cells excluding propidium iodide but permeabilized within 300 s by sPLA2 (spectroscopy). Violet bars: number of cells staining positive for MC540 (flow cytometry, as in Panel B). Blue, red, and gray bars: number of cells staining positive, intermediate, and negative for propidium iodide (flow cytometry as in Figs. 1–3). Error bars represent SEM (n = 3–42). The four sets of observations representing hypothesized sPLA$_2$-susceptible cohorts (green, orange + brown + yellow, violet, and blue + red) were compared to each other by one-way analysis of variance separately for DMSO, TG, and DEX treatments. All three analyses were significant ($p < 0.02$). Dunnett's post test comparing each cohort to the corresponding hydrolysis group (green) was conducted. For DMSO, none of the cohorts was different from hydrolysis. For TG, the flow cytometry (blue + red) cohort was statistically different ($p < 0.01$). For DEX, all cohorts except MC540 (violet) were statistically significant compared to hydrolysis ($p < 0.05$).

36
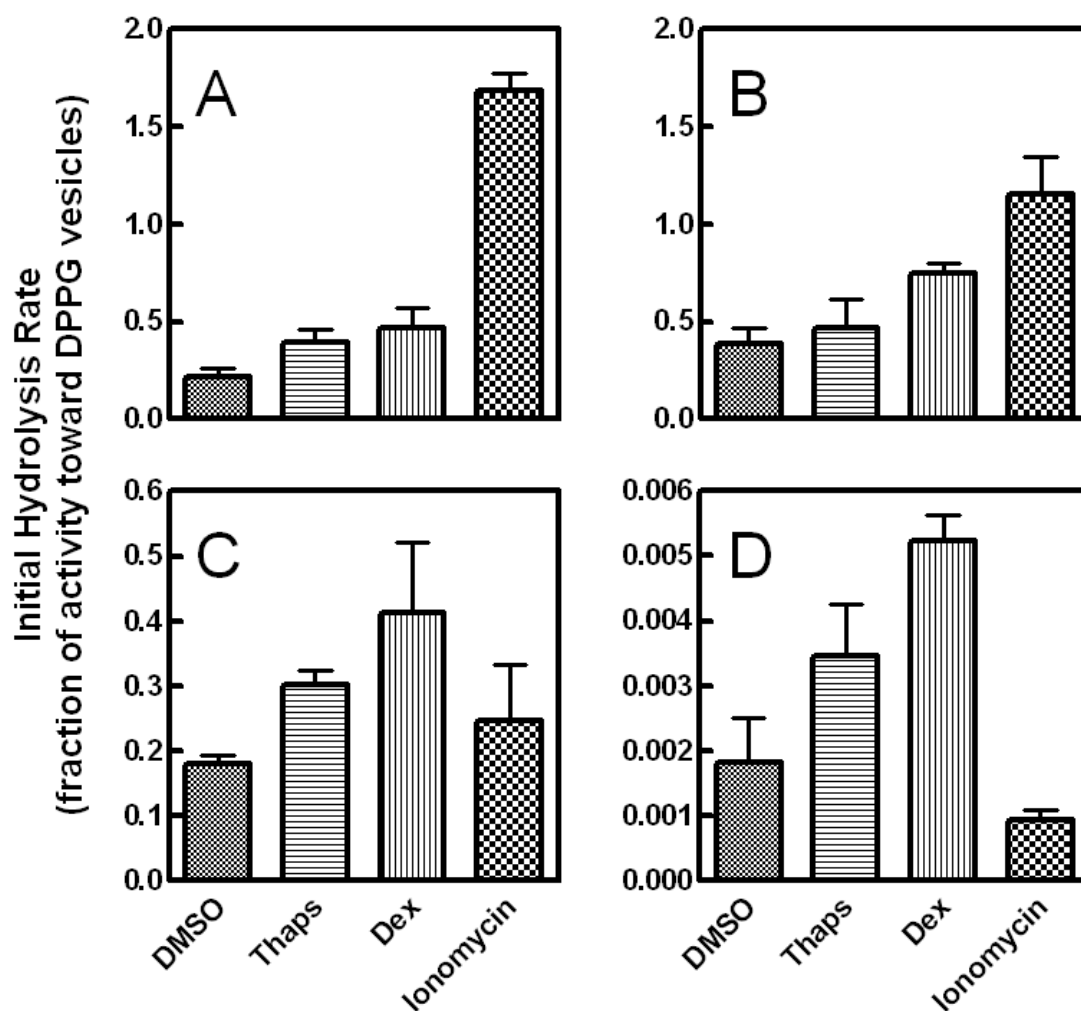
Figure 3-5: Comparison of initial hydrolysis rates catalyzed by snake venom and human sPLA$_2$ isoforms among cells treated with DMSO, TG, DEX, or ionomycin.

Hydrolysis was measured by ADIFAB fluorescence as in Fig. 4A for cells treated as indicated. The initial rate was quantified as described in Materials and Methods. Panel A: AppD49; Panel B: hGX; Panel C: hGV; Panel D: hGIIa. For the AppD49, hGX, and hGIIa isozymes, the results were significant by one-way analysis of variance ($p < 0.008$). As indicated by Dunnett's post-test, the following treatments were statistically different from the corresponding DMSO controls ($p < 0.05$): AppD49—DEX and ionomycin, hGX—ionomycin, hGIIa—DEX.

CHAPTER 4: ROLE OF MEMBRANE OXIDATION IN CONTROLLING THE ACTIVITY

OF HUMAN GROUP IIA SECRETORY PHOSPHOLIPASE A$_2$ TOWARD

APOPTOTIC LYMPHOMA CELLS

Introduction

Recently, we have focused on the relationship between apoptosis and the activity of

various isoforms of sPLA$_2$. Numerous studies have identified two physical changes as being

relevant to the action of sPLA$_2$ during cell death: 1) an increase in the presence of anionic

phospholipids (generally phosphatidylserine, PS) in the outer leaflet of the membrane (Bezzine

et al., 2002; Harris et al., 2001; Koduri et al., 1998; Murakami et al., 1999; Olson et al., 2010;

Singer et al., 2002; Smith et al., 2001) and 2) a decrease in membrane lipid order reflecting

diminished strength of interactions among adjacent phospholipids (Best et al., 2002; Harris et al.,

2001; Heiner et al., 2008; Jensen et al., 2005; Olson et al., 2010). In addition, studies with

calcium ionophore-stimulated death indicated that a third membrane alteration must be essential

for the human group IIa isoform (hGIIa) of the enzyme (Nelson et al., 2011; Olson et al., 2010).

Even though ionophore-stimulated calcium uptake caused immediate full exposure of PS and

maximal reduction in lipid order, hGIIa sPLA$_2$ did not hydrolyze the cell membrane. These

observations strongly contrasted the response of the enzyme to artificial membranes composed

entirely of anionic phospholipids (Bezzine et al., 2002; Buckland and Wilton, 1998; Kinkaid and

Wilton, 1995; Nelson et al., 2011; Olson et al., 2010; Singer et al., 2002). Furthermore, a

different isoform, hGX, hydrolyzed ionophore-treated cells at a greater rate than apoptotic cells

and appeared not to require a third factor (Olson et al., 2010).

A recent publication reported that some apoptotic inducers produce a subpopulation of cells with

slight permeability to propidium iodide (Nelson et al., 2011). This modest permeability

correlated with increased susceptibility to the hGIIa isozyme. That study suggested that plasma membrane oxidation could be a candidate for the third membrane alteration mentioned above (Nelson et al., 2011). This hypothesis is supported by three observations. First, cytochrome c release during apoptosis causes lipid oxidation (Fabisiak et al., 1998; Greenberg et al., 2008; Jiang et al., 2004; Tyurin et al., 2009; Tyurin et al., 2008a; Tyurina et al., 2000). Second, lipid oxidation enhances the permeability of artificial bilayers (Greenberg et al., 2008; Howland and Parikh, 2010; Smith et al., 2009; Yajima et al., 2009). Third, membranes containing oxidized lipids are more susceptible to hydrolysis by the hGIIa isoform of sPLA$_2$ (Akiba et al., 1997; Korotaeva et al., 2010; Korotaeva et al., 2009a; Korotaeva et al., 2009b; McLean et al., 1993). We have therefore tested the hypothesis that membrane oxidation is the third factor required for a membrane to become susceptible to hydrolysis by hGIIa sPLA$_2$. Accordingly, we assayed lipid oxidation potential of S49 lymphoma cells during death triggered by TG, an inhibitor of the endoplasmic reticulum Ca^{2+} ATPase that causes ER stress (Feng et al., 2006; Kass and Orrenius, 1999; Yoshida et al., 2006). Activity of hGIIa sPLA$_2$ was then assayed to determine if susceptibility correlated with membrane oxidation. Cell membranes were then directly oxidized using *tert*-butyl hydroperoxide (TBHP) or 2,2'-azobis-2-methyl-propanimidamide, dihydrochloride (AAPH, a hydrophilic radical initiator), and hydrolytic activity of hGIIa sPLA$_2$ was determined. Externalization of PS and lipid order were also assessed to establish which of these membrane changes is necessary for hGIIa sPLA$_2$ activity.

Results

A fluorescent lipid analog, C11-BODIPY$^{581/591}$, was used to assess the lipid oxidative potential of cell membranes after treatment with TG (Drummen et al., 2002). As shown in Fig. 4-1, confocal microscopy revealed that C11-BODIPY$^{581/591}$ became oxidized (green) after TG

treatment (Panel B) compared to control cells (Panel A). The percentage of the cell population that contained oxidized C11-BODIPY$^{581/591}$ was quantified using flow cytometry after different lengths of incubation with TG to determine the temporal onset of lipid oxidation (Panel C). Maximum oxidation did not occur until after 4.5 h with TG.

Previous reports demonstrated that the activity of the hGIIa isozyme is enhanced during apoptosis, including that stimulated by TG (Nelson et al., 2011; Olson et al., 2010). However, even though the enhancement was significant compared to the undetectable hydrolysis of quiescent cells, it was dwarfed by that catalyzed by other sPLA$_2$ isozymes (Nelson et al., 2011; Olson et al., 2010). Compared to a standard for full activity (hydrolysis of dipalmitoylphosphatidylglycerol liposomes), human groups V and X isozymes were 31 ± 2 and $58 \pm 7\%$ of that maximum when hGIIa was only $0.46 \pm 0.09\%$ (Nelson et al., 2011; Olson et al., 2010). In the case of TG-induced apoptosis, these measurements were obtained at 3-h treatment with TG, a time point at which the activity of the other sPLA$_2$ isozymes toward apoptotic cells is maximal (Nelson et al., 2011). However, Fig. 4-1 shows that oxidation is a later event in TG-induced death. Therefore, to explore the possible role of oxidation, hGIIa sPLA$_2$ activity was compared between 3 and 5 h incubation with TG (Fig. 4-2A). The initial hydrolysis rates from multiple replicates are represented as gray bars in Fig. 4-2B and overlaid with PS externalization (dashed curve; data from) and C11-BODIPY$^{581/591}$ oxidation (solid curve; data from Fig. 4-1C). Although significant activity was detectable at 3 h, it increased 30-fold at 5 h.

To further validate the possibility that membrane oxidation is the key factor required for this isozyme, chemical oxidizing agents were used to directly cause lipid oxidation (Fig. 4-3). Confocal microscopy with C11-BODIPY$^{581/591}$ was used to verify that the plasma membrane becomes oxidized after treatment with TBHP (60 min; Panel B compared to Panel A) and AAPH

(15 h; Panel D compared to Panel C). In both cases, oxidation was widespread among the cells. In contrast, treatment of the cells with ionomycin, which renders them fully susceptible to some sPLA$_2$ isozymes, such as human group X, but not hGIIa (Olson et al., 2010), did not result in appreciable oxidation (Panels E and F). Figure 4-4A demonstrates that the two agents that caused membrane oxidation also stimulated hydrolysis by hGIIa. In fact, the rates were substantially higher than that observed with 5 h TG (2.5–3-fold greater). Control experiments with TBHP in the presence of antioxidants (trolox or NecroX-5™) demonstrated that the results depended on oxidation rather than artifactual effects of the agent.

As mentioned above, decreased lipid order and exposure of phosphatidylserine have been linked to high sPLA$_2$ activity. Therefore, these two membrane changes were assayed after treatment with TBHP and AAPH. Lipid order was assessed with three different fluorescent probes: MC540, TMA-DPH, and Patman. As shown in Fig. 4-4B, TBHP treatment caused an increase in MC540 fluorescence comparable to that caused by TG (Chapter 5). This effect has been shown previously to reflect a decrease in lipid packing density in the plasma membrane pursuant to a reduction in bilayer order (Bailey et al., 2009; Bailey et al., 2007; Stillwell et al., 1993). Likewise, TBHP caused a decrease in the value of TMA-DPH anisotropy similar to the result with TG (Fig. 4-4C). In contrast, effects of TBHP on Patman fluorescence were less than half that observed with 5 h TG treatment (Fig. 4-4D). The results with AAPH differed substantially from those with TBHP. Although it was equal or better at promoting hydrolysis compared to TBHP, it was much weaker at promoting changes in membrane order detected by Patman or MC540 (black bars, Figs. 4-4B and D). Interestingly, TMA-DPH anisotropy was altered by AAPH to a level comparable to that induced by the other agents (Fig. 4-4C). Externalization of PS (annexin V binding) was assayed by flow cytometry. Both TBHP and

41

AAPH induced PS exposure, as expected (Piga et al., 2007; Sardao et al., 2007), although the effects tended to be smaller and more variable than experienced in S49 cells with apoptotic agents such as TG or glucocorticoid (TBHP: $37.7 \pm 9.6\%$ increase in annexin-positive cells, AAPH: $39.0 \pm 13.2\%$ increase, TG: $85.6 \pm 0.7\%$ increase , glucocorticoid: 83.7% increase (Bailey et al., 2009)).

Discussion

We concluded, based on these results, that oxidation is likely to be the source of the "third membrane alteration" postulated previously (Nelson et al., 2011) as described in the Introduction. However, the data of Figs. 4-4B–D indicate that all three alterations are not simultaneously required for the membrane to experience a high level of hydrolysis. Specifically, the reduction in membrane order, thought previously to be critical, was not necessary when oxidation had occurred. To test whether this effect was confined to hGIIa, we repeated the hydrolysis experiments of Fig. 4-4A toward AAPH-treated cells with a generic snake venom sPLA$_2$ for which the role of membrane order is prominent and well established (Bailey et al., 2009; Bailey et al., 2007; Bell and Biltonen, 1989; Bell et al., 1996; Henshaw et al., 1998; Olson et al., 2010). Treatment with AAPH stimulated hydrolysis by the snake venom isozyme to an extent similar to that observed when membrane order changes and PS exposure have occurred in the absence of oxidation ($110 \pm 23\%$ of the activity observed at 3, 5 h TG treatment, n = 4). This result suggests that oxidation of the membrane can replace the need for alterations of membrane order by promoting the same step in the hydrolysis reaction scheme. In fact, the data for hGIIa argue that oxidation is more effective. Chapter 5 demonstrates quantitatively that the change in membrane order is likely to enhance hydrolysis by increasing the probability that individual phospholipids in the bilayer can spontaneously protrude to an extent sufficient to enter

42

the active site of adsorbed sPLA$_2$. Although oxidation of membrane lipids does not necessarily alter overall membrane physical properties in the same way as observed during apoptosis (compare patterns of TBHP and AAPH with TG results in Figs. 4-4B–D), other structural analyses have identified an alternative hypothesis that may explain how this chemical alteration could increase phospholipase activity (Catala, 2012; Greenberg et al., 2008; Khandelia and Mouritsen, 2009). This "lipid whisker hypothesis" describes a dominant conformation of oxidized phospholipids in which the altered fatty acid tail extends out from the membrane surface into the aqueous phase. Thus, the lipid is positioned in the bilayer with one tail immersed normally and the other extended in the opposite direction. This altered conformation might allow entry of the extended acyl chain into the enzyme active site without need for vertical protrusion of the phospholipid (Greenberg et al., 2008; Hazen, 2008). Although the data of this paper do not prove that idea, they are consistent with it. Future experiments identifying directly the specific substrates for sPLA$_2$ during apoptosis will be needed to validate this idea further.

The ability of oxidation to replace the need for a change in membrane order begs the question of whether exposure of anionic lipids such as PS on the exterior of the cell is still necessary for hGIIa after oxidation. This question cannot be answered definitively with the data obtained here since all treatments that produced oxidation also caused exposure of PS. This result may corroborate earlier findings that oxidation of phospholipids creates a means of both enzymatic and non-enzymatic transfer of PS to the outer leaflet of the cell membrane (Tyurina et al., 2004; Volinsky et al., 2011). Nevertheless, it is well established that the residence time of hGIIa on a membrane surface is extremely short unless anionic lipids are also present. Measurements of adsorption of hGIIa sPLA$_2$ to artificial membranes by a centrifugation assay revealed that the apparent association constant increased from undetectable for a 10%

43

PS/phosphatidylcholine mixture to 5000 M^{-1} in a 30% mixture (Singer et al., 2002). Likewise, the rate of hydrolysis of a pure anionic membrane is 300-fold greater than that observed toward a zwitterionic bilayer (Singer et al., 2002). The reason for this significant effect is clear upon considering the structure of the interfacial binding surface of hGIIa. It is highly enriched in cationic residues and devoid of trp residues present on the interfacial adsorption surface of other sPLA$_2$ isozymes that act more effectively on zwitterionic membranes (Baker et al., 1998; Beers et al., 2003; Diraviyam and Murray, 2006; Han et al., 1999; Snitko et al., 1997).

Some of the products of phospholipid oxidation are also anionic, with carboxylic acids on fatty acid chains broken by the introduction of peroxides. Based on the lipid whisker hypothesis, these carboxylic acids would be exposed on the membrane surface where they could interact with sPLA$_2$. Thus, it seems plausible that oxidation would assist adsorption of the enzyme directly in addition to its effect to enhance the ability of affected phospholipids to enter the active site of sPLA$_2$. Nonetheless, it is likely that this contribution of lipid oxidation would be relatively small since many oxidation products are not charged. Thus far, to the authors' knowledge, no evidence for improved adsorption of hGIIa to bilayers composed of oxidized lipids has been reported, and experiments to test that idea are therefore needed. Regardless, the adsorption potential of hGIIa is still not fully realized with mammalian cells even with the combined effects of PS exposure and lipid oxidation. For example, we found that hGIIa hydrolyzes liposomes of pure anionic phospholipid (dipalmitoylphosphatidylglycerol) analogous to bacterial membranes at a 4-fold higher rate than oxidized mammalian cell membranes (comparing average of TBHP and AAPH data of this paper to standards reported by us in previous studies (Nelson et al., 2011; Olson et al., 2010)).

Much of what is known about phospholipid oxidation and sPLA$_2$ comes from studies of lipoproteins. The heightened action of hGIIa toward oxidized lipoproteins has been proposed as a major action of the isozyme with significant implications for the pathology of atherosclerosis (Korotaeva et al., 2009a; Leitinger et al., 1999; Pruzanski et al., 1998). The potential for similar responsiveness of hGIIa toward cell membranes that have become oxidized during apoptosis or other traumatic events had not received comparable attention. Here we show that that potential is real and merits further investigation. Although the focus here was on the hGIIa isozyme, preliminary results with snake venom sPLA$_2$ raise the possibility that other isozymes may respond similarly to oxidation. At least some of these other isozymes, such as group X and group V, respond to other membrane changes such as decreased lipid order and PS exposure to a greater extent than hGIIa in the absence of oxidation (Olson et al., 2010). Thus, different forms of cell damage as well as different moments along the time course of programmed cell death will capacitate different sPLA$_2$ isozymes depending on the types and relative amounts of membrane changes occurring. For example, early in some forms of apoptosis, the membrane becomes susceptible to group X sPLA$_2$ prior to significant PS exposure and oxidation (Nelson et al., 2011; Olson et al., 2010). As shown in this study, hGIIa will attack those cells later in the process when oxidation initiated in the mitochondria has spread to the plasma membrane. Physiologically, this secondary attack by hGIIa should be forestalled by phagocytosis of apoptotic cells activated by exposure of oxidized PS (Greenberg et al., 2006; Kagan et al., 2002). Nevertheless, in other conditions in which membrane oxidation is prevalent, such as certain neurodegenerative diseases (Lee et al., 2011; Sun et al., 2005), the action of hGIIa and other sPLA$_2$ isozymes may be substantial, leading to death of affected cells and untoward release of proinflammatory fatty acids and lysophospholipids.
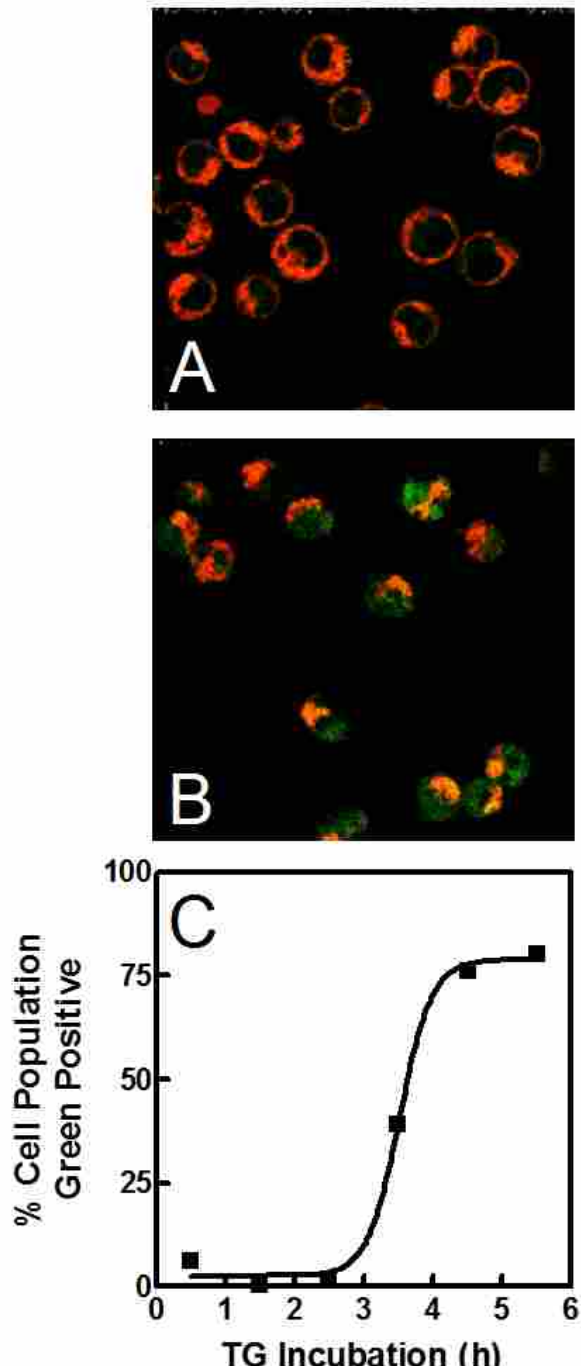
Figure 4-1: Plasma membrane oxidation during TG-induced apoptosis.

Lipid oxidative potential of the membrane was assessed by confocal microscopy (Panels A, B) and flow cytometry (Panel C) using C11-BODIPY[581/591]. Probes fluorescing green represent those that have been oxidized. Panel A: control cells. Panel B: cells treated with TG for 4.5 h.
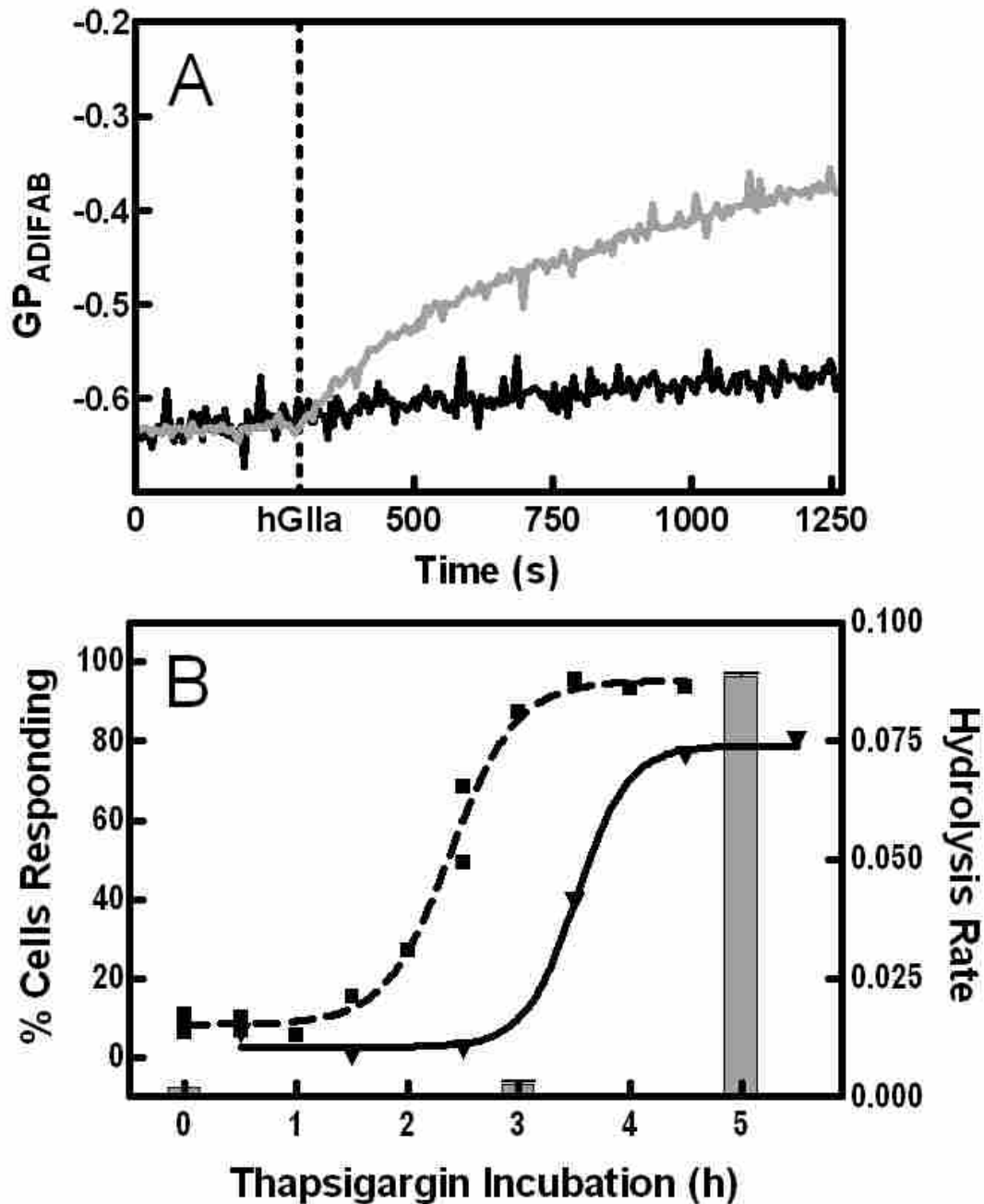
Figure 4-2: Membrane hydrolysis by hGIIa sPLA$_2$ during TG-stimulated apoptosis.
Panel A: Time profile of membrane hydrolysis after addition of hGIIa sPLA$_2$ (dotted line) in cell samples treated 3 h (black) or 5 h (gray) with TG. Panel B: Initial rates of hydrolysis (gray bars) were calculated from data like those in Panel A. The error was ≤ 0.0001 GP$_{ADIFAB}$ units (n = 2–4), which is difficult to discern visually in the graph. Overlays show timing of PS exposure (dashed curve) and membrane oxidation (solid curve) assayed by flow cytometry (AlexaFluor-labeled annexin V and C11-BODIPY[581/591], respectively).
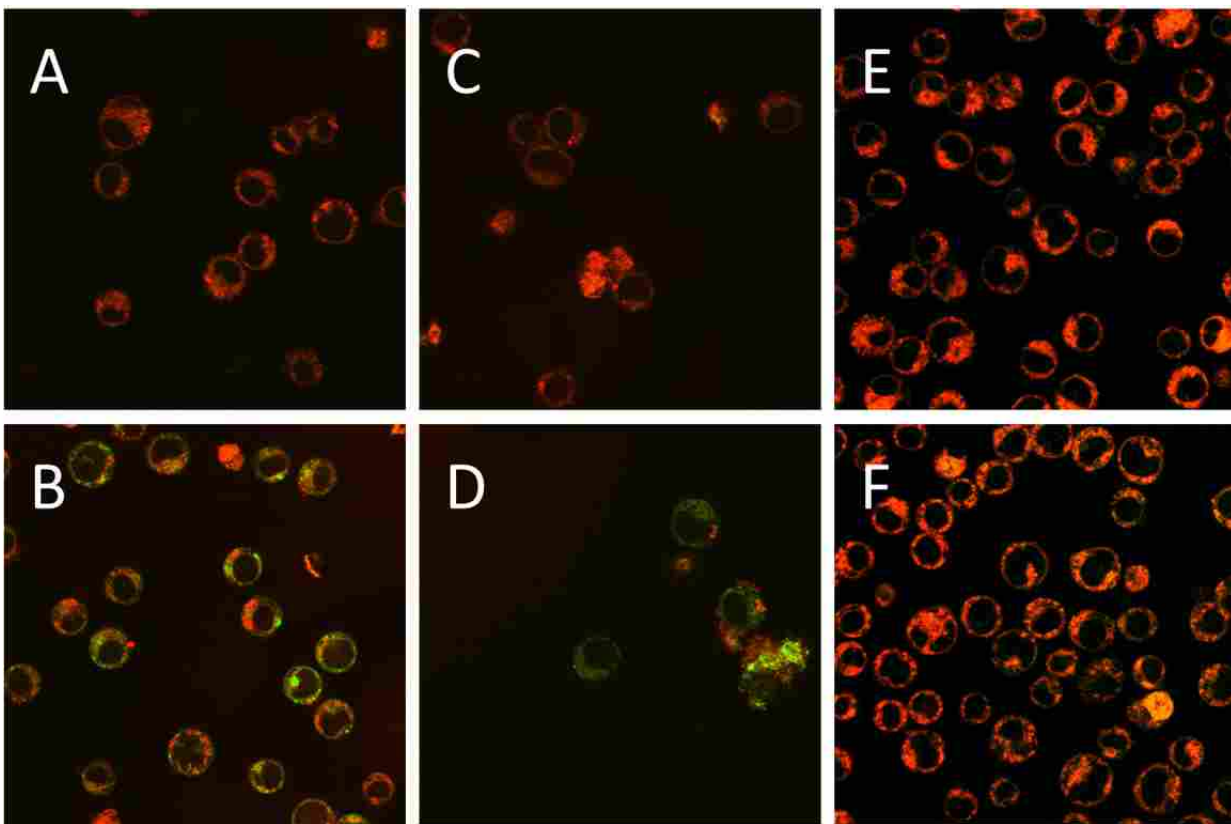
Figure 4-3: Confocal microscopy images of membrane oxidation in cells treated with TBHP, AAPH, or ionomycin.

See Fig. 1 for fluorescence details. Panels A, C, E: Relevant vehicle controls matched with the treatment samples in Panels B, D, and F. Panel B: 60 min TBHP; Panel D: 15 h AAPH; Panel F: 9 min ionomycin.
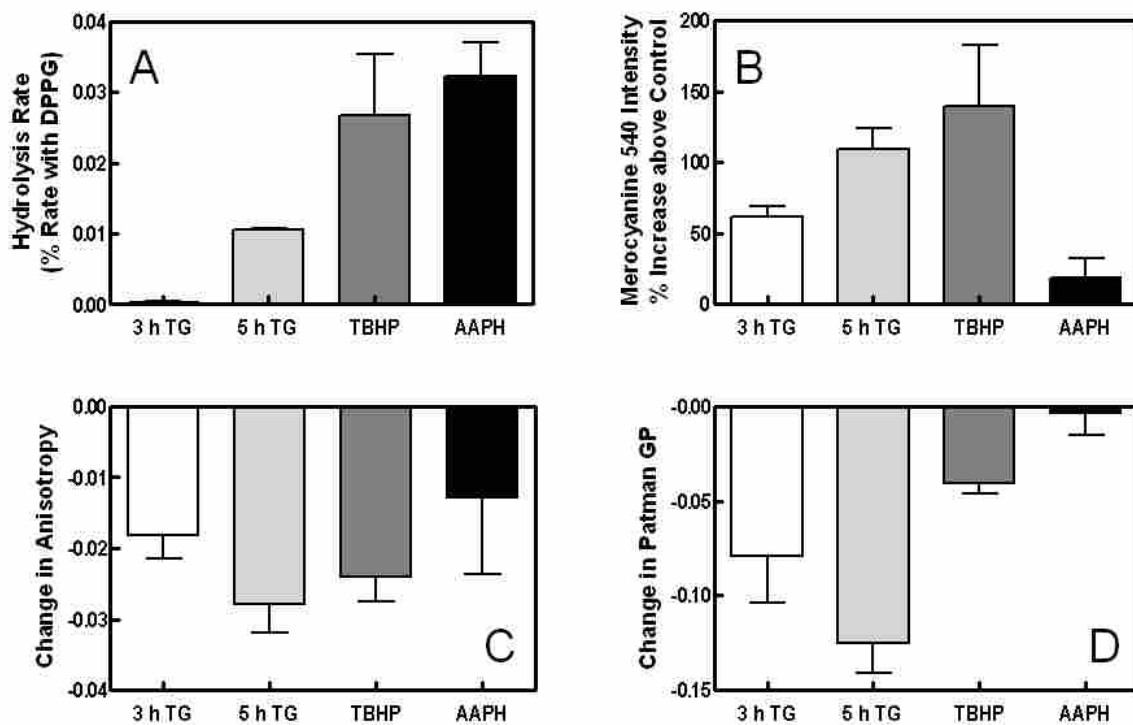
Figure 4-4: Effects of TBHP and AAPH on hydrolysis by sPLA$_2$ and on membrane order.

Panel A: Initial hydrolysis rates were calculated from data like those in Fig. 2A for samples treated 3 or 5 h with TG, at least 21 min with TBHP, or at least 14 h with AAPH. Parallel samples were assessed for MC540 fluorescence (Panel B), TMA-DPH anisotropy (Panel C), or Patman GP (Panel D). Differences among treatment groups were significant by one-way analysis of variance ($p < 0.016$) for Panels A, B, and D (n = 2–8 per group).

CHAPTER 5: MOLECULAR DETAILS OF MEMBRANE FLUIDITY CHANGES

DURING APOPTOSIS AND RELATIONSHIP TO

PHOSPHOLIPASE A_2 ACTIVITY

Introduction

Secretory phospholipase A_2 ($sPLA_2$) is an enzyme which adsorbs to the cell surface and

hydrolyzes phospholipid acyl chains in the sn-2 position, yielding lysophospholipid and fatty

acid (often arachidonic acid). Moreover, $sPLA_2$ is a model protein for studying enzymatic

activity at a lipid-water interface. Interestingly, all cell membranes are not equally susceptible to

hydrolysis by $sPLA_2$. Healthy cells resist hydrolysis by this enzyme whereas apoptotic or

damaged cells become susceptible (Atsumi et al., 1997; Bailey et al., 2007; Nielson et al., 2000;

Wilson et al., 1999). Studies have suggested that perturbations to the bilayer cause changes in the

physical properties of the membrane, allowing individual lipids to migrate into the enzyme's

active site and become hydrolyzed (Bailey et al., 2009; Bailey et al., 2007; Best et al., 2002;

Harris et al., 2001; Jensen et al., 2005; Smith et al., 2001).

Attempts to understand this differential susceptibility have emphasized changes that

occur in the plasma membrane during apoptosis. Three relevant changes have been described,

but all are not equally understood. The most well-defined change is externalization of

phosphatidylserine (PS), which is sequestered in the inner leaflet of the lipid bilayer in healthy

cells. The thought is that the negative charge of exposed PS facilitates adsorption of $sPLA_2$ to the

membrane surface (Harris et al., 2001; Murakami et al., 1999; Olson et al., 2010). Accordingly,

many studies have demonstrated that $sPLA_2$ has higher activity toward anionic compared to

zwitterionic synthetic membranes (Bezzine et al., 2002; Diraviyam and Murray, 2006; Jain et al.,

1989; Kinkaid and Wilton, 1995; Scott et al., 1990; Yu et al., 2000). A second property

correlating with sPLA$_2$ activity is increased membrane permeability (Nelson et al., 2011). The mechanistic basis of this relationship is not yet understood and will not be addressed in this paper. The third alteration has been suggested by studies utilizing fluorescent membrane probes such as MC540, Laurdan, and diphenylhexatriene (DPH) (Bailey et al., 2009; Bailey et al., 2007; Harris et al., 2001). These modifications appear necessary for membrane susceptibility to sPLA$_2$, but they are vaguely defined as changes in "membrane fluidity" and "order." In addition, there have been challenges in interpreting the results to focus solely on the plasma membrane because Laurdan and DPH freely enter the cell and interact with intracellular membranes.

These biophysical changes are more specifically defined in this study by assaying Patman spectral shifts and equilibration kinetics as well as trimethylammonium-DPH (TMA-DPH) anisotropy during TG-induced apoptosis. Thapsigargin produces endoplasmic reticulum stress by inhibiting the Ca^{2+} ATPase, and was chosen because it initiates synchronized cell death on a time scale amenable to the experiments required for this study. Patman and TMA-DPH are cationic versions of Laurdan and DPH that have been reported to reside primarily in the plasma membrane (Kuhry et al., 1983; Williams and Webb, 2000; Zipfel et al., 2003) and therefore eliminate the ambiguities of probe entering the cell. The experiments with Patman apply work done in model membranes by Franchino et al. (Franchino et al., 2013). Using vesicles of different compositions and a quantitative model, they determined that the pattern of equilibration of Patman reflects different configurations of the probe in the bilayer. They also concluded that the kinetics reveal dynamic changes in the molecular environment around the probe and can be used to infer additional biophysical detail beyond what can be gleaned from steady-state observations. Additionally, another model developed in artificial membranes is utilized here to estimate the change in phospholipid protrusion density. Patman and TMA-DPH data collected

51

during the main phase transition of artificial bilayers with different compositions are also used to correlate fluorescence observations with the interaction energy among adjacent phospholipids. The resulting calibration coefficients are then applied to data from living cells to estimate increases in the probability of lipid protrusions that promote hydrolysis during apoptosis (Halperin and Mouritsen, 2005; Hoyrup et al., 2004).

Results

Death

A timeline of major apoptotic markers during TG-induced death is shown in Fig. 5-1. Caspase activation was assessed using the fluorescent pan-caspase inhibitor FAM-VAD-fmk which enters the cell and irreversibly binds activated caspases. The caspase cascade was activated in half of the cells (*triangles, dashed curve, left panel*) and preceded externalization of PS (*circles, solid curve, left panel*), trypan blue uptake (*inverted triangles, solid curve, right panel*; note the different time scale on the right panel), and DNA fragmentation (*squares, dashed curve, right panel*). Likewise, DNA fragmentation was observed in 50% of the cells, although it was not complete until 7 h after addition of TG. In contrast, 100% of the cells exposed PS in the outer leaflet of the cell membrane. This exposure was complete after 3 h with TG. However, only half of the gain in PS exposed in response to TG was preventable by the general caspase inhibitor, Z-VAD-fmk ($42.3 \pm 9.2\%$ reduction; $p < 0.05$; effect of Z-VAD-fmk on control cells was insignificant; analysis of variance with Bonferroni post-test, n = 5 for all groups). The proportion of the cell population that was permeable to trypan blue gradually increased, reaching ~85% at 12 h of TG treatment. These results suggested that about half of the cells died by classical apoptosis although the rest eventually died by another mechanism.

Figure 5-2 illustrates that treatment with TG rendered S49 cells susceptible to hydrolysis by sPLA$_2$. Fig. 5-2A is a summary of the total amount of membrane hydrolysis after different incubation times with the apoptotic inducer. Maximal hydrolysis was observed after 3 h with TG. When the vital stain propidium iodide is included to assess viability concurrently, it is possible to quantify the subpopulation of cells that is still alive but has progressed far enough into the death process to be susceptible to sPLA$_2$. As demonstrated previously, these cells exclude the dye until their membranes are damaged by hydrolysis (Bailey et al., 2009; Nielson et al., 2000). Figure 5-2B shows that this alive and susceptible subpopulation reached a maximum of about 30% of the total cell population around 3.5 h. As shown in Fig. 5-2C, about half of this subpopulation was apoptotic (based on inhibition by Z-VAD-fmk). This proportion of alive but susceptible cells was large compared to the ~5–8% seen previously with DEX (Bailey et al., 2009; Nielson et al., 2000), indicating that TG-induced apoptosis is a good model for exploring membrane changes responsible for susceptibility. At longer time points, this alive but susceptible subpopulation diminished in size because a larger proportion of the cells were now already permeable to propidium iodide in the absence of sPLA$_2$. Comparing the shapes of the time profiles in Figs.5-2A and B demonstrates that the cells continued to be good substrates for sPLA$_2$ after they become permeable to propidium iodide. Interestingly, the subpopulation of alive and susceptible cells never reached zero at long incubation times even though all other markers of apoptotic progression indicate completion of the process for vulnerable cells by ~7 h. This result suggests that about 10% of the cells progress far enough to become susceptible to hydrolysis but remain static in that state without completing the death process. The ~10% discrepancy between PS

exposure and trypan blue uptake shown in Fig. 5-1 supports this conclusion as it illustrates that there are cells with altered membranes that remain alive up to 12 h.

Probes of membrane biophysics

The strategy we employed to identify the nature of biophysical changes in the cell membrane associated with enhanced hydrolysis by sPLA$_2$ was to use information from several membrane probes sensitive to the level of lipid order in the membrane (MC540, Laurdan, Patman, TMA-DPH and DPH). Figure 5-3 illustrates that TG treatment caused both an increase in the intensity (Panel A) and red-shift in the peak (Panel B) of the MC540 emission spectrum compared to vehicle controls (DMSO). These two effects appeared to follow a similar time course and were maximal by about 5 h. Figure 5-3C indicates that about half of the response was prevented by treatment with Z-VAD-fmk. Therefore, the cells displaying changes in membrane physical properties included both apoptotic and non-apoptotic subpopulations, as was observed in Fig. 5-2C for sPLA$_2$ vulnerability.

Figure 5-4A illustrates that DPH anisotropy increased gradually with TG treatment. As shown by two-photon microscopy in Fig. 5-4B, DPH distributes rapidly among all membranes in the cell, thus reporting an average for probe mobility throughout the cell. To isolate effects at the plasma membrane, we repeated the experiment of Fig. 5-4A with a charged analog of DPH, TMA-DPH. The trimethylammonium moiety on TMA-DPH is reported to retard diffusion of the probe into the cells so that it is enriched in the plasma membrane (Kuhry et al., 1983). This assertion was verified for S49 cells by two-photon microscopy as shown in Fig. 5-4D. Figure 5-4C demonstrates two major differences between TMA-DPH and DPH anisotropy. First, the baseline anisotropy differed by 0.16 anisotropy units suggesting a very different mobility in the plasma membrane compared to the cell interior, a result reminiscent of the higher GP value

reported for Laurdan at the plasma membrane compared to internal membranes (Bailey et al., 2009). Second, the temporal trend during TG treatment was sharper and in the opposite direction compared to DPH. The time scale for the changes in TMA-DPH anisotropy was comparable to that observed for MC540.

Figure 5-5A illustrates the absence of any distinct pattern in Laurdan fluorescence assessed spectroscopically in bulk samples with increasing TG incubation time. As explained previously, interpretation of Laurdan data with cells is confounded by the fact that the probe rapidly penetrates the plasma membrane and stains the interior as well as the exterior of the cell (Fig. 5-5B). The problem is mitigated by analyzing images of the fluorescence staining. Two-photon images (Fig. 5-5D) suggested that the average Laurdan GP of the cell perimeter was different from that of the interior. Figure 5-5C is a quantification of this observation, confirming the difference between plasma membrane and internal membrane staining and that this difference changes with TG treatment. Nevertheless, these images cannot distinguish fluorescence originating from the internal leaflet of the cell membrane versus the external, which is the site of action of sPLA$_2$.

Patman has essentially the same structure as Laurdan except for a charged moiety attached to its head (Lakowicz et al., 1983). This modification appears to provide the same advantage as TMA-DPH, i.e., retaining the probe in the outer leaflet of the cell membrane (Williams and Webb, 2000; Zipfel et al., 2003). We verified this expectation for S49 cells with two-photon microscopy as shown in Fig. 5-6A. Figure 5-6B illustrates that Patman GP decreased with increasing TG incubation time, starting between 1 and 2 h, similar to the time scale observed with MC540 and TMA-DPH. The data suggest that the maximum response may occur sooner with Patman compared to the other probes, raising the possibility that the details sensed

by this probe are especially early in the time course of TG-induced apoptosis. In any case, the

Patman result suggests greater water penetration into the plasma membrane (Parasassi et al.,

1991). At later time points, when the membranes begin to become permeable, the reduction in

Patman GP appeared to partially reverse, perhaps due to probe entering the cell interior.

During Patman data acquisition, an interesting phenomenon was observed; the probe

appeared to equilibrate at different rates when emission was measured at 435 nm compared to

500 nm. These differences are most easily seen by normalizing the data at the two wavelengths

to their own values at 400 s (Fig. 5-7A). As shown in the accompanying paper (Franchino et al.,

2013), this phenomenon also occurs in artificial membranes and may provide additional

information regarding the properties of the bilayer beyond that revealed by the GP alone.

Extraction of that information requires analysis with a quantitative model such as the one

developed in the companion paper (Franchino et al., 2013). That model is employed here.

Accordingly, Patman time courses were smoothed by nonlinear regression using Eq. 5.

The regression curves at 435 (*solid*) and 500 nm (*dashed*) were normalized to the intensity of the

435 nm curve at 400 s. This normalization made it possible to aggregate results from multiple

experiments to examine general patterns in shape. Averages of controls, samples treated for 2–5

h with TG, and those treated for 6.5–8 h are shown in Figs. 5-7B, C, and D respectively. The

pattern of Patman equilibration in living cells resembles that observed with vesicles in that they

both represent a sum of two kinetic processes distinguished by rate constants that differ by at

least a factor of 10 (Franchino et al., 2013). Figure 5-8 displays the effects of TG treatment on

the parameters associated with the model (discussed below).

Discussion

As expected, TG induced apoptosis in S49 cells as seen by caspase activation, PS exposure, DNA fragmentation, and cell death. These classical events were accompanied by a previously reported biophysical change in the plasma membrane that correlates with susceptibility to sPLA$_2$ and precedes cell death. Consistent with other studies of apoptosis, MC540 emission spectra became red shifted and increased in intensity during TG treatment, suggesting a reduction in lipid packing (Bailey et al., 2009; Williamson et al., 1983).

DPH and Laurdan have previously been used to investigate changes in membrane fluidity and order. As a lipid bilayer becomes less fluid and more ordered, movement of DPH becomes more restricted and its anisotropy increases (Dale et al., 1977; Veatch and Stryer, 1977). Laurdan is sensitive to the presence and mobility of water molecules near the phospholipid glycerol backbone (Parasassi et al., 1991). Alignment of water dipoles with that of the excited probe shifts the emission spectrum (quantified by calculating the GP) to longer wavelengths indicating greater water penetration into the membrane, presumably allowed by a reduction in phospholipid order and packing (Harris et al., 2002). As shown in Figs. 5-4B and 5-5B, these two probes quickly cross the plasma membrane to stain the cell interior, making interpretation difficult. In addition, their fluorescence properties did not change in a pattern reproducible enough to defend statistically during the time range when membranes became susceptible to hydrolysis. When the cell perimeter and interior of two-photon Laurdan images were examined separately, however, an early trend of decreasing GP was observed. This trend suggested that alterations of the plasma membrane detected by Laurdan on a time scale relevant to sPLA$_2$ activity do occur (Fig. 5-5C).

To more fully define this biophysical change in the membrane, charged analogues of DPH and Laurdan, TMA-DPH and Patman respectively, were utilized. As shown in Figs. 5-4D

and 5-6A, diffusion of these two probes into the cell interior is reduced, validating their direct use for assessment of plasma membrane properties. The trend in TMA-DPH anisotropy after TG treatment was substantially different from that of DPH, showing instead a decrease (Fig. 5-4C) at the same time that membranes were becoming vulnerable to $sPLA_2$ (Figs. 5-2A and B). This diminished anisotropy implied a reduction in stereo-constraints imposed by neighboring membrane lipids during early apoptosis, a result consistent with the MC540 data. The concurrent drop in Patman GP displayed in Fig. 5-6B substantiated this interpretation since a loosening of neighbor-neighbor interactions would allow increased water penetration into the membrane. The data at long time points (> 6 h) for Patman suggest that this reduction in lipid order is reversed as the apoptotic process progresses. The data with TMA-DPH hinted at the same effect, although the late trend was much smaller than observed with Patman. These results suggest that this phenomenon is either complex in nature or confounded by membrane blebbing and differential distribution of these probes during that late time frame. Therefore, at these later time points, Patman and, to a lesser degree, TMA-DPH could also be staining internal membranes and reflect the increased order seen with DPH and reported previously for glucocorticoid-induced apoptosis (Bailey et al., 2009). Moreover, the focus of this study is to understand the nature of membrane changes facilitating hydrolysis by $sPLA_2$ early in apoptosis before membrane integrity is compromised. Thus, the remainder of the discussion will focus on changes during the 2–5 h interval after TG addition.

Further information can be obtained from Patman if equilibration kinetics are examined in addition to the endpoint GP (Franchino et al., 2013). The same phenomenon shown in Fig. 5-7 was observed in artificial vesicles, and suggested that the probe exists in multiple configurations in the membrane. One possibility is that the configurations correspond to probe localized in

different bilayer domains. This possibility was considered and rejected in the accompanying study (Franchino et al., 2013) for artificial membranes. Molecular dynamics simulations of other probes with structure related to Patman suggest a second possibility that these configurations represent different stereo-conformations of the probe (Parisio et al., 2011). Experimental measurements of Patman fluorescence quenching indicate that they may refer to different depths in the membrane (Jurkiewicz et al., 2006). For parsimony, only two configurations were considered here (referred to as "fast" and "slow", see Ref. (Franchino et al., 2013)) even though data such as those shown in Ref. (Jurkiewicz et al., 2006) indicated a possible continuum of Patman locations. With the data gathered thus far, a continuous model cannot be distinguished from a two-state model in which the observable properties of the states overlap as a function of the independent variable, in this case wavelength. Regardless of the molecular details of the configurations, the data in Ref. (Franchino et al., 2013) argue that equilibration of Patman's fluorescence represents the local microenvironment relaxing around newly-inserted probe.

By applying the specific model described in the accompanying paper (Franchino et al., 2013), it was possible to determine which specific parameters were altered with TG treatment. Figure 5-8 illustrates that TG treatment produced three detectable effects. First, a smaller proportion of Patman molecules populated the "slow" configuration compared to control cells (66% compared to 85%, circles, Panel A). To the extent that the "slow" configuration represents a deeper location in the membrane, the vertical distribution of Patman molecules was skewed toward shallower depths after TG treatment. Second, the "fast" configuration became more polar, presumably reflecting the invasion of water molecules into the membrane (triangles, Panel A). Third, the rate of equilibration slowed for probes in this more polar microenvironment (diamonds, Panel B).

The positioning of Patman in the membrane is probably determined by two factors: the ability to form a salt bridge between its trimethylammonium and the phosphate of a neighboring lipid, and the strength of the interactions between Patman's 16-carbon chain and the surrounding fatty-acid tails. In the accompanying paper, it was proposed that the "fast" configuration applies to Patman molecules bonded electrostatically to phospholipid heads and the "slow" configuration connotes Patman molecules with weaker interactions with the heads and therefore anchored predominately through the 16-carbon tail (Franchino et al., 2013). The increase of Patman molecules in the "fast" configuration, then, suggests a weakening of the interactions between the probe's hydrophobic tail and neighboring lipids with, perhaps, a net movement of the probe toward shallower depths.

It was interesting that only the "fast" configuration experienced a change in polarity after TG treatment. We assume that this polarity increase reflected enhanced water penetration, an assumption that is well supported (Parasassi et al., 1991). If the two configurations represent different depths, then only the shallow configuration was influenced by this additional water penetration. However, fluorescence quenching measurements indicate that the expected difference in depth is less than an angstrom (Jurkiewicz et al., 2006), smaller than the size of a water molecule. Thus, if depth is the distinction of the configurations, then the change in polarity must be localized superficially to both depths so that water's influence on both configurations is long-range. The sub-angstrom distinction between configurations must then rely on the sensitive distance dependency of solvent dipole influences on the fluorophore's excited state (i.e., d^6), which would produce large changes in solvent effects with small adjustments to probe location.

The slower equilibration of the "fast" (presumably shallower) configuration implies a greater diversity of metastable conformations of Patman relative to the molecules comprising its

local microenvironment such that fluctuations among these conformations delays achievement of steady state. The presence of that diversity further suggests a lessening of constraints imposed on the probe by neighboring molecules, allowing greater freedom to sample conformations as equilibrium is approached. This interpretation is also consistent with the idea that the anchoring of Patman's tail among the phospholipid chains has been weakened.

Taken together, the TMA-DPH and Patman results complement the findings with MC540 and suggest that early events in apoptosis produce a membrane that now possesses three new characteristics. Lipid headgroups are more spaced. The amount and/or depth of water located among the heads has/have increased. Interactions among lipids in the phospholipid tail region are reduced so that molecules such as Patman are less tightly anchored to the deep part of the bilayer and constraints on TMA-DPH motion are lessened.

Based on these interpretations, we are able to explain the increase in phospholipase activity on the molecular level quantitatively. In order for hydrolysis to occur, a single lipid must protrude 1.5 nm from the lipid bilayer up into the active site of sPLA$_2$ adsorbed to the membrane surface (Berg et al., 2001). Normally the frequency of such phospholipid protrusions is very low because of the "friction" opposing this movement created by favorable interactions between neighboring fatty acid tails. Hence, healthy cells show minimal susceptibility to hydrolysis by sPLA$_2$. A reduction of these associations between carbon chains, and thus a decrease in that "friction," will increase the likelihood of a single lipid migrating from the membrane to be cleaved. Here we assume that this reduction in lipid interactions is analogous to the phase transition of artificial membranes, which is known to greatly enhance sPLA$_2$ activity (Bell et al., 1995; Bell and Biltonen, 1989; Honger et al., 1996; Lichtenberg et al., 1986; Menashe et al., 1981). Therefore, data from vesicles were used to estimate the magnitude of energy reduction

61

between neighboring lipids during apoptosis and the consequential change in the density of lipid protrusions. Patman GP and TMA-DPH anisotropy were measured across the main phase transition of vesicles (pure DMPC, DPPC, or DSPC) to obtain the total change in anisotropy or GP in each system. The average change in enthalpy for these phase transitions was used to determine a coefficient relating TMA-DPH and Patman measurements to energy changes (Table 1). Linear regression of the enthalpy and probe fluorescence in Table 1 yielded coefficients of 3.00×10^{-6} TMA-DPH anisotropy units/J and 1.12×10^{-5} Patman GP units/J. These coefficients were then applied to the change in TMA-DPH anisotropy and Patman GP after about 3 h of TG treatment (Figs. 5-4C and 5-6B), the time at which the alive and susceptible subpopulation was the largest (Fig. 5-2B). As shown in Table 2, TMA-DPH and Patman measurements predicted a -1.31×10^{-20} J and -1.11×10^{-20} J change in interaction energy per phospholipid after TG treatment respectively. The change in density of lipid protrusions after TG treatment was calculated from an adaptation of the theory presented by Mouritsen and co-workers (Halperin and Mouritsen, 2005; Hoyrup et al., 2004).

Eq. 6
$$p_{(z)} = p_{(0)} \exp\left(\frac{-yz}{k_B T}\right)$$

where $p_{(z)}$ is the probability or frequency of protrusions of distance z and y is the energy cost of a protrusion of distance z. Some of the parameters, $p_{(z)}$, $p_{(0)}$ and y, are not known for a cell membrane. However, the proportional change in protrusion frequency ($\Delta p_{(z)}$) upon discounting the energy cost due to reduced lipid-lipid interactions can be calculated without explicit knowledge of the basal condition as follows:

Eq. 7
$$\Delta p_{(z)} = \frac{p_{(z,TG)}}{p_{(z,control)}} = \frac{p_{(0)} \exp[-(y + \Delta y_{app})z / k_B T]}{p_{(0)} \exp(-yz / k_B T)} = \exp\left(\frac{-\Delta y_{app} z}{k_B T}\right)$$

where Δy_{app} is the apparent change in interaction energy estimated from the TMA-DPH or Patman data and $z = 1.5$ nm. As indicated in Table 2, TMA-DPH and Patman predicted a 50–100-fold increase in the protrusion frequency after 3 h treatment with TG. We note that this analysis assumes that the membrane environments detected by these probes are generally synonymous with those hydrolyzed by sPLA$_2$. The diversity of structure within cell membranes surely implies that the numbers calculated here are averages for the overall system. Our calculations also assume that all of the phospholipids "seen" by TMA-DPH and Patman have experienced similar physical alterations. If this assumption is not true, then a smaller proportion of lipids is experiencing a greater change in protrusion probability than we have estimated here.

One of the challenges of detailed biophysical studies on simple artificial membranes is applying the results and conclusions to complex biological systems. In this paper, we have demonstrated a combined application involving a membrane-binding enzyme (sPLA$_2$) and two fluorescent membrane probes. In one case, the supporting work with artificial bilayers included thermodynamic analysis relating kinetic and structural data for sPLA$_2$ to create a molecular model relating lipid dynamics (protrusion fluctuations) to enzyme activity (Halperin and Mouritsen, 2005; Hoyrup et al., 2004). In the other, we assessed the behavior of TMA-DPH and Patman with artificial membranes quantitatively to provide a frame of reference for interpretation of data with cells (Table 1 and Ref. (Franchino et al., 2013)). These quantitative approaches were then used together here to interpret biological phenomena at a level of detail greater than generally achieved in the discipline of cell membrane biology. In particular, this study demonstrates a new level of real time application of fluorescence spectroscopy to bulk samples of living cells.

Table 1: Changes in TMA-DPH anisotropy and Patman GP during main phase transitions of DMPC, DPPC, or DSPC vesicles.

	T_m (°C)[a]	ΔH (joules)[a]	ΔTMA-DPH r[b]	ΔPatman GP[c]
DMPC	23.7	2.43E+04	−0.0943	−0.43
DPPC	41.4	3.46E+04	−0.0916	−0.44
DSPC	54.4	4.18E+04	−0.1235	−0.51

a Obtained from averages of all relevant observations reported in LIPIDAT (Koynova and Caffrey, 1993).

b Assessed using Eq. 3 as described in Materials and Methods.

c Obtained by applying Eq. 3 to Patman spectral data as a function of temperature from Ref. (Franchino et al., 2013).

Table 2: Change in frequency of lipid protrusions during TG-induced apoptosis.

	Δr or ΔGP	Δy_{app} (joules)	fold-increase in $p_{(z)}$
TMA-DPH	−0.0237	−1.31E-20	99.2
Patman	−0.0931	−1.11E-20	48.9

[a] The changes in TMA-DPH anisotropy and Patman GP after 3.25 h TG treatment (the time at which the subpopulation of alive and susceptible cells is at a maximum) are from Figs. 5-4C and 5-6B respectively.
[b] The coefficients calculated from Table 1 were used to determine Δy_{app}, the apparent change in interaction energy estimated from the TMA-DPH or Patman data
[c] Calculated according to Eq. 7.
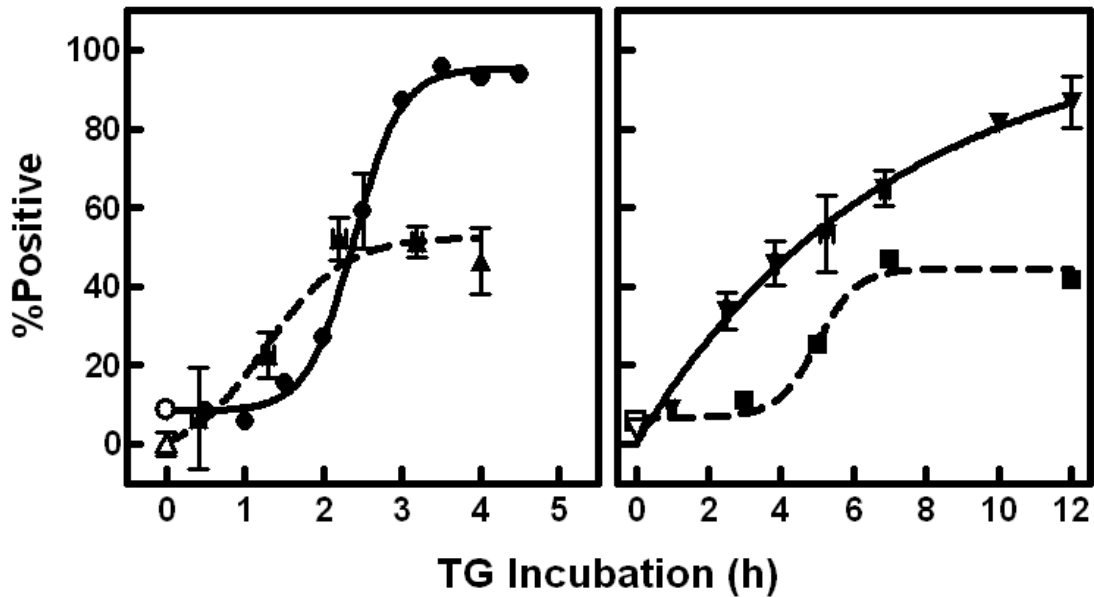
Figure 5-1: Timing of apoptotic events during TG-induced death.

Cells were treated in culture with either DMSO (vehicle control; open symbols) or TG (solid symbols) for various times as indicated on the x-axis. Caspase activation (triangles, n = 6–13 in TG groups, 47 in control group), PS externalization (circles, each time point is a separate experiment), and DNA degradation (squares, each time point is a separate experiment) were assessed via flow cytometry after incubation with FAM-VAD-fmk (30 min), AlexaFluor-labeled Annexin-V (15 min), or propidium iodide with Triton X-100 (10 min) respectively. Death (inverted triangles, n = 1–31 in TG groups, 72 in control group) was determined by cell permeability to trypan blue. Data are represented as the percentage of the population positive for each response. Nonspecific binding of FAM-VAD-fmk (Pozarowski et al., 2003) was subtracted from all time points.
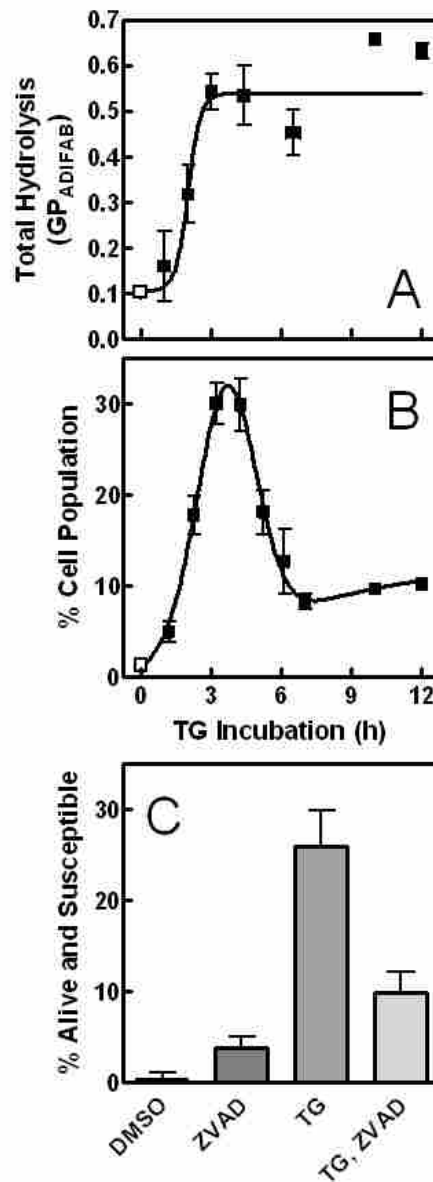
Figure 5-2: Susceptibility of TG-treated cells to sPLA$_2$.

Cells were treated for various times with DMSO (vehicle control; open squares) or TG (solid squares) in cell culture. (A) Fatty acid release was measured using ADIFAB. The total amount of hydrolysis was calculated as the maximal change in ADIFAB GP after addition of sPLA$_2$ (n = 1–6 in TG groups, 20 in control group). (B) The percentage of the cell population that was both alive and susceptible to sPLA$_2$ was assessed using propidium iodide (n = 1–18 in TG groups, 63 in control group) as described in Materials and Methods. (C) Cells were incubated with Z-VAD-fmk or control solvent (DMSO) for 30 min before TG or DMSO treatment. The percentage of cells alive and susceptible to hydrolysis by sPLA$_2$ was assayed as in Panel B. Groups differed significantly by one-way analysis of variance (p < 0.0001, n = 4–8 per group). A post-test (Bonferroni) demonstrated that the TG group differed from all others (p < 0.01) and that cells treated with Z-VAD-fmk alone or before TG were indistinguishable from control cells.

67
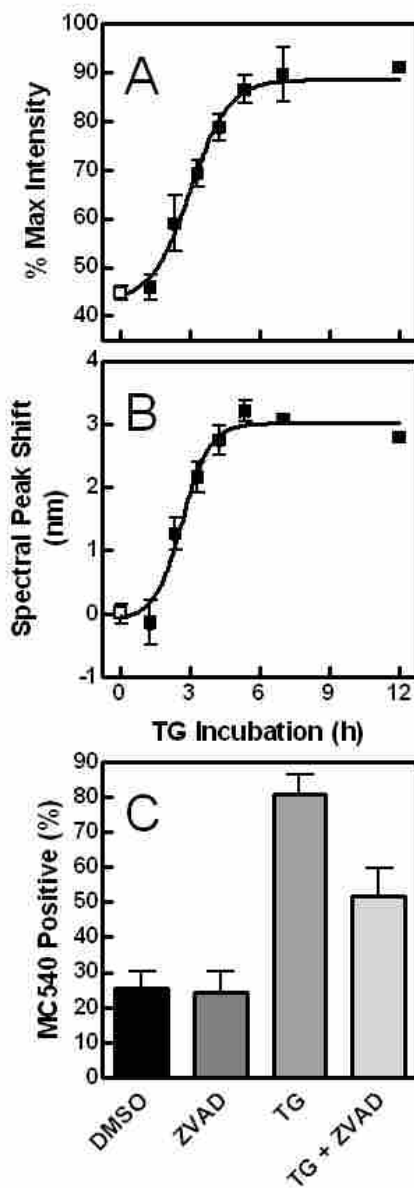
Figure 5-3: Effect of TG treatment on MC540 fluorescence.

The effect of DMSO (open squares) or TG (solid squares) on MC540 emission intensity (A) or spectral maximum (B, expressed as shift compared to that induced by ionomycin) was obtained and calculated as explained in Materials and Methods (n = 1–13 in TG groups, 45 in control group). (C) Cells were pretreated with Z-VAD-fmk or control solvent (DMSO), equilibrated with MC540, and analyzed by flow cytometry. Data represent the percentage of the cell population staining positive for MC540. Groups differed significantly by one-way analysis of variance ($p < 0.0001$, n = 5 per group). A Bonferroni post-test revealed that TG significantly increased MC540 fluorescence ($p < 0.001$). Treatment with Z-VAD-fmk alone was not distinguishable from control cells ($p > 0.05$). Addition of Z-VAD-fmk before TG treatment was significantly different from both control cells and cells incubated with TG alone ($p < 0.05$ in both cases).

68
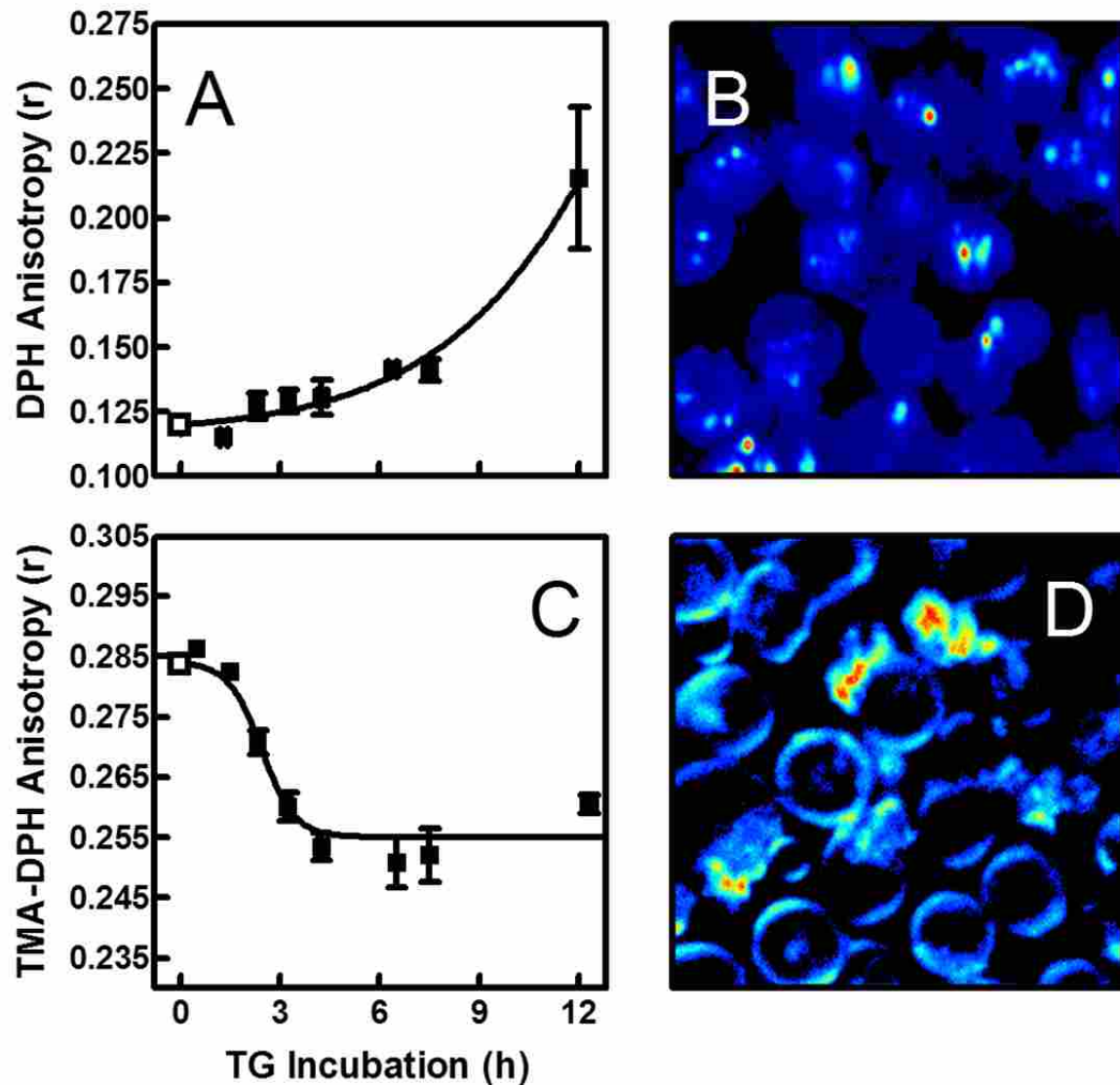
Figure 5-4: DPH and TMA-DPH anisotropy and localization in TG-treated cells.

After incubation with DMSO (open squares) or TG (solid squares) for the indicated times, DPH (A and B) or TMA-DPH (C and D) was added to cell samples. Panels A and C show anisotropy measurements (DPH: n = 2–5 in TG groups, 26 in control group; TMA-DPH: n = 2–6 in TG groups, 30 in control group). Panels B and D are representative two-photon images showing localization of probe intensity after 2 h TG treatment and 12 min equilibration with the probe. Fluorescence intensity is represented by a relative false color scale (blue, low; red, high).
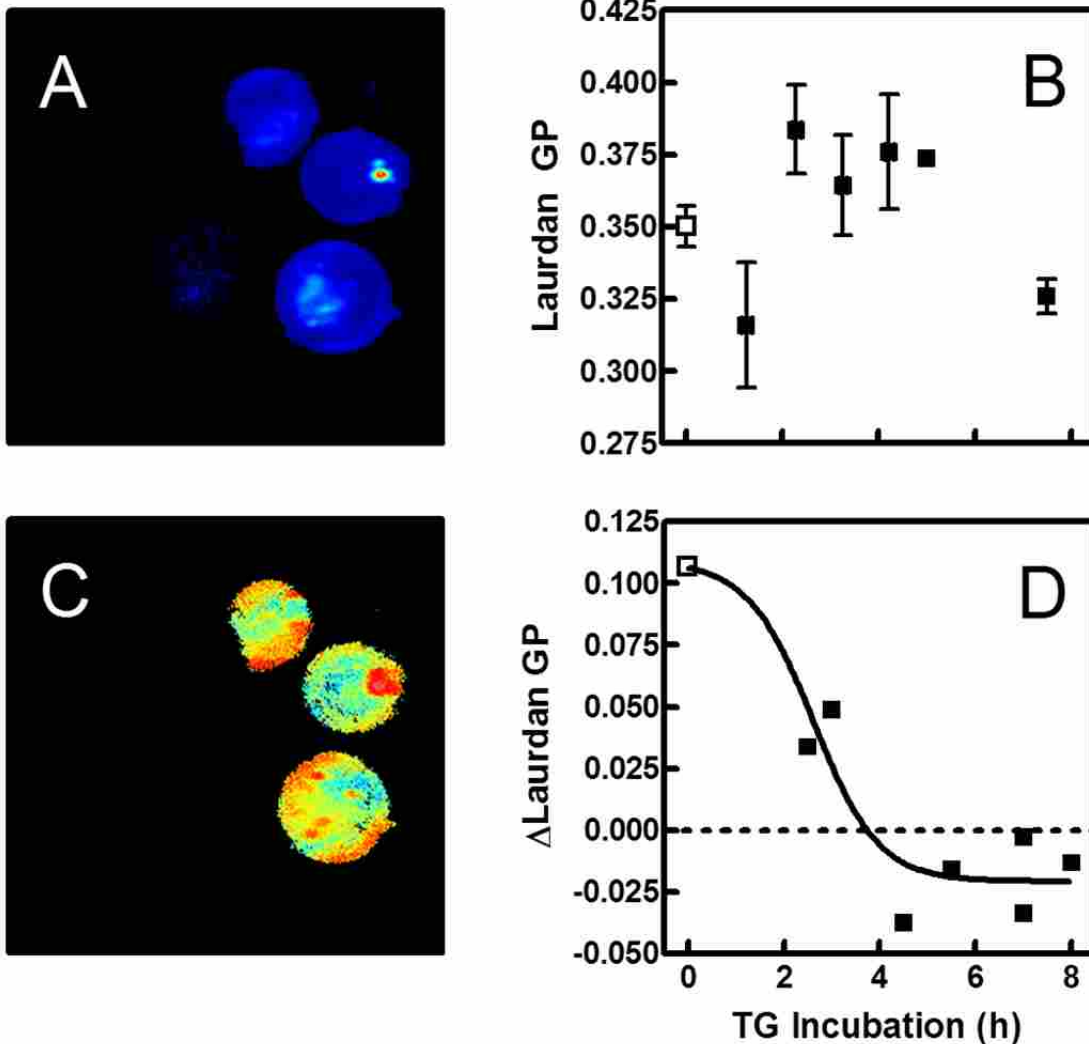
Figure 5-5: Effect of TG incubation on Laurdan intensity and GP.
(A) Laurdan GP of cells treated with DMSO (open squares) or TG (solid squares) for various times was assessed via fluorescence spectroscopy (n = 1–8 in TG groups, 31 in control group). Values of GP were calculated from the intensities measured 600 s after probe addition. (B) Laurdan intensity was visualized by two-photon microscopy after a 3 h incubation with TG and 12 min with probe. Fluorescence intensity is represented by a relative false color scale (blue, low; red, high). (C) Images such as that in Panel D were quantified (n = 151 cells) by calculating the difference in GP between pixels corresponding to the cell perimeter and those in the middle (see Materials and Methods) for control (open squares) and TG-treated cells (solid squares). (D) The image from Panel B is shown with false coloring representing Laurdan GP (blue = –0.25 GP units; red = 0.75 GP units).
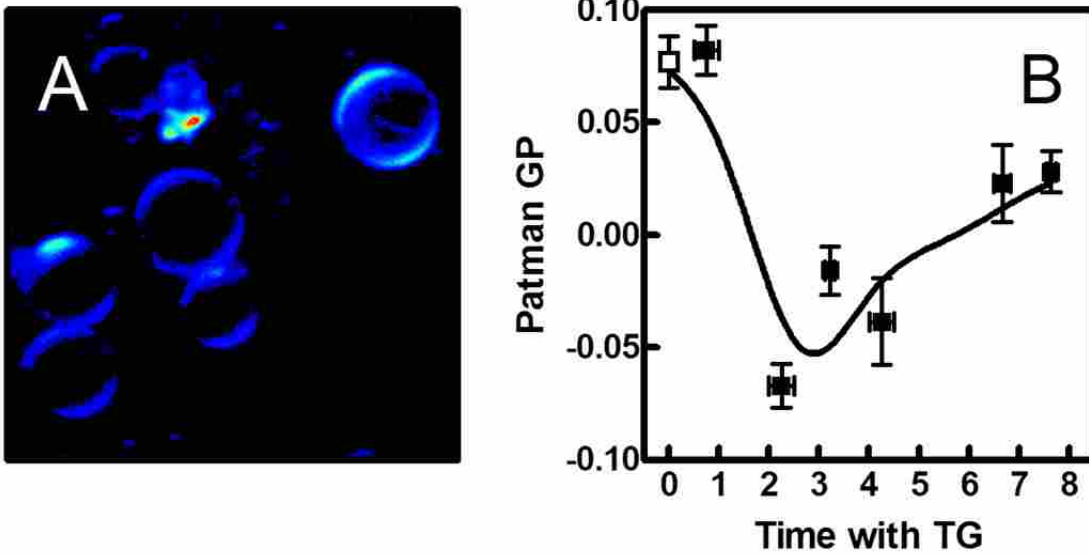
Figure 5-6: Patman localization and GP after TG treatment.

(A) Patman intensity was visualized by two-photon excitation microscopy after 3 h TG treatment plus 12 min with probe. Fluorescence intensity is represented by a relative false color scale (blue, low; red, high). (B) Patman GP of cell samples treated with DMSO (open square) or TG (solid squares) was assessed by fluorescence spectroscopy. GP was assessed 400 s after probe addition (n = 2–7 in TG groups, 24 in control group).
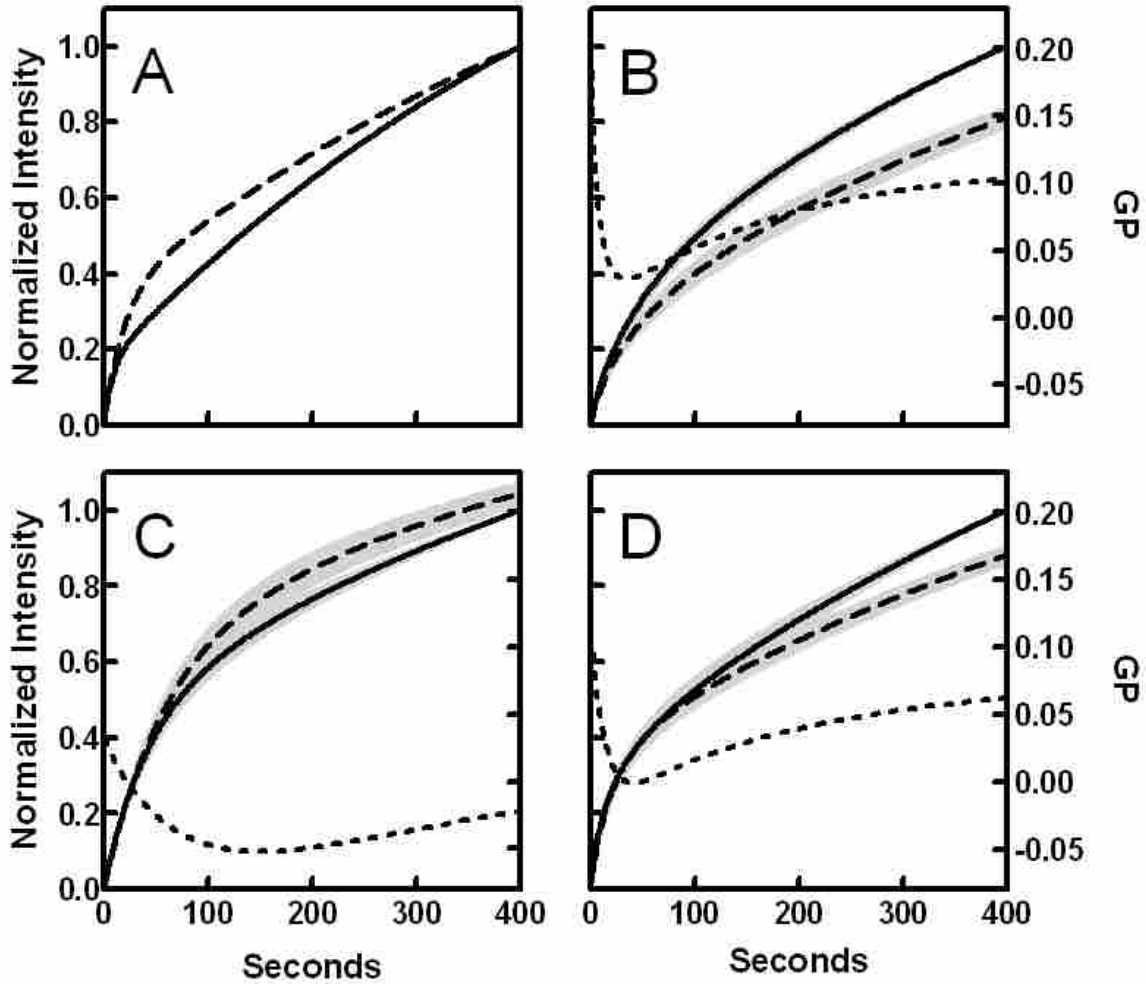
Figure 5-7: Effect of TG on Patman equilibration kinetics.

(A) Patman was added to control cells and intensity measured for 400 s. Normalized intensity at both 435 nm (solid curves) and 500 nm (dashed curves) is shown to illustrate differences in equilibration kinetics. (B, C, and D) Equilibration time profiles of intensity at 435 nm, intensity at 500 nm, and GP (dotted curves) from control samples (B), samples treated with TG from 2–5 h (C), and samples treated for over 6.5 h (D). Data from both wavelengths were normalized to that measured at 435 nm at 400 s and aggregated (n = 10–25 per group). Gray shading represents ± SE.
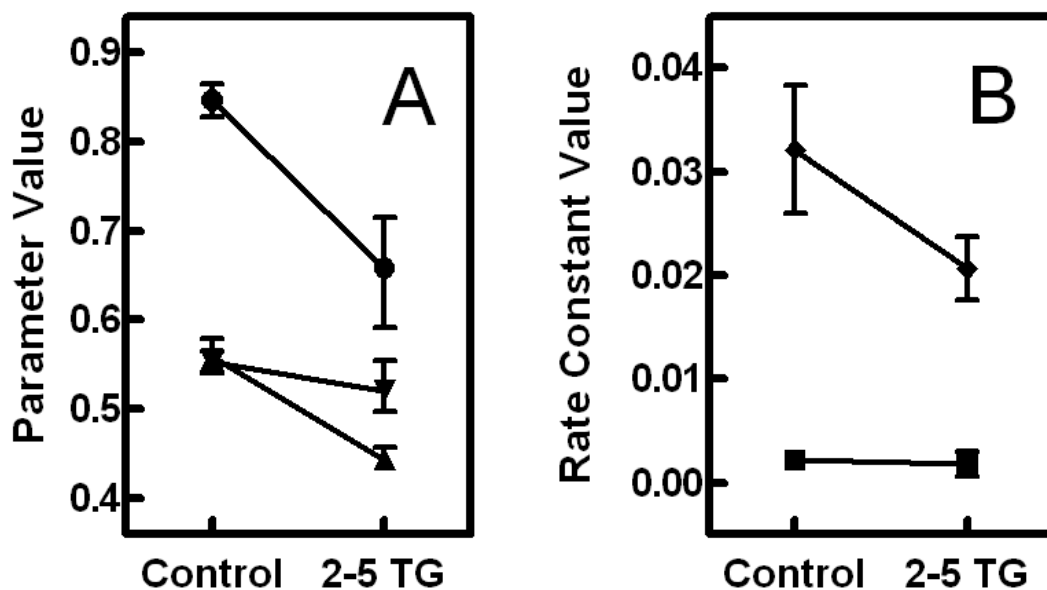
Figure 5-8: Effect of TG on membrane properties and Patman distribution.

(A) The effect of TG on the fraction of the probe in the "slow" environment (circles), the polarity of "slow" environment (inverted triangles), and the polarity of the "fast" environment (triangles) were estimated using the model developed in (Franchino et al., 2013). (B) The same model was used to estimate the change in the equilibrations rates of the "slow" environment (squares) and the "fast" environment (diamonds). Model parameters and error estimates were obtained from nonlinear regressions of the data shown in Figs. 7 B and C as explained in Materials and Methods.

CHAPTER 6: IONOMYCIN CAUSES SUSCEPTIBILITY TO PHOSPHOLIPASE A$_2$ WHILE

TEMPERATURE-INDUCED INCREASES IN MEMBRANE FLUIDITY FAIL:

POSSIBLE INVOLVEMENT OF ACTIN FRAGMENTATION

Introduction

Prior studies have investigated the role of biophysical alterations to the plasma membrane in its susceptibility to hydrolysis by sPLA$_2$. Fluorescent membrane probes such as MC540, Laurdan, DPH, TMA-DPH, and Patman have been used to detect increases in lipid spacing and fluidity that correlate with susceptibility (Bailey et al., 2009; Bailey et al., 2007; Best et al., 2002; Harris et al., 2001; Heiner et al., 2008). These biophysical alterations (as seen by MC540) preceded all other membrane changes during DEX-induced apoptosis in S49 cells (Bailey et al., 2009), so it is clearly important in availability of cell membranes to act as a substrate for the enzyme. However, other cases have been reported in which membrane fluidity is altered and does not result in hydrolysis by sPLA$_2$ such as vesicles of different compositions experiencing phase transitions (Bell et al., 1996).

This chapter attempts to more fully define biophysical changes in the plasma membrane that are directly responsible for susceptibility to hydrolytic attack by comparing temperature- and ionomycin-induced alterations of the plasma membrane. These two treatments result in similar changes in membrane fluidity as currently defined, yet have different impacts on membrane vulnerability to attack. In this study, susceptibility induced by ionomycin is used because of its fast-acting and synchronous effect on cell samples. The membrane probe Patman is used to define the difference between the membrane alterations caused by these two treatments.

Actin fragmentation is proposed as a possible mechanism for the extra alteration caused by ionomycin. This hypothesis is plausible because actin and actin-associated proteins are known

to be cleaved/altered during apoptosis (Franklin-Tong and Gourlay, 2008; Gourlay and Ayscough, 2005; Leadsham et al., 2010; Wang, 2000). Additionally, various studies have reported changes in membrane fluidity (assayed with fluorescent membrane probes) in conditions that involve cytoskeleton alterations. Examples include disorders of abnormal cell locomotion (Fiorini et al., 2000), T-cell activation (Gaus et al., 2005; Rajendran et al., 2009), detachment of cells from focal adhesion proteins (Gaus et al., 2006), membrane receptor clustering (Pato et al., 2008), diabetic nephropathy (Jones et al., 1998), and endocytosis (Wolkers et al., 2003). Magnetic field exposure (Santoro et al., 1997), hydrogen peroxide treatment (Zhu et al., 2005), and cytoskeleton-disrupting drugs (Huotari et al., 1996) also cause alterations in membrane order that correlate with changes in the cytoskeleton.

Results

Temperature-induced changes in membrane fluidity were assessed with the membrane probe TMA-DPH. Cells were incubated at temperatures ranging from 32 – 45 °C with and without ionomycin. As shown in Fig. 6-1, TMA-DPH anisotropy decreased as temperature was increased (black bars), and ionomycin caused an additional drop in anisotropy at all temperatures (striped bars). A two-way analysis of variance indicated that ionophore treatment was responsible for 30.98% of the variation within the data (p<0.0001), temperature caused 23.81% of the variation (p<0.0001), and the interaction between the two was insignificant (3.35% of total variation; p=0.0918). The TMA-DPH anisotropy of control cells at 45 °C was comparable to that of ionomycin-treated cells at 32 °C.

The solvation relaxation-sensitive probe Patman was also used to determine if altering temperature could induce biophysical membrane changes sufficient to mimic apoptotic systems. Again, S49 cells were incubated with Patman at a range of temperatures and the GP was

calculated. Linear regression of samples from $32 - 45$ °C revealed a slope of $-0.009249 \pm$ 0.003064 (p=0.0046), suggesting a -0.12026 GP unit drop across this temperature range. This result is comparable to data the -0.11533 Patman GP unit decrease during TG-induced apoptosis reported in Chapter 5.

Because ionomycin-treated cells at 32 °C and control cells at 45 °C had similar TMA-DPH anisotropies, the amount of hydrolysis resulting after incubating these samples with $sPLA_2$ was assayed using ADIFAB. Figure 6-2 shows example profiles of ADIFAB GP over time, with an increase suggesting fatty acid release from the plasma membrane. Regardless of temperature, there was a small rise in GP after addition of $sPLA_2$ (first dotted line) with a subsequent return to baseline levels as the product is re-acylated into the membrane as is characteristic of control cells (Wilson et al., 1999). Ionomycin was added at the second dotted line in the 32 °C sample (black curve), causing a large increase in ADIFAB GP, suggesting the ionophore rendered the cells susceptible to attack by $sPLA_2$. Incubating the sample at 45 °C (red curve) caused no such vulnerability to hydrolysis by the enzyme.

It is known that calcium influx causes externalization of PS on the cell surface (Bevers et al., 1983; Nielson et al., 2000; Zhou et al., 1997), so the effect of temperature on annexin V binding was measured via flow cytometry. As shown in Fig. 6-3, cells at 32, 37, and 45 °C exhibit low levels of PS on the cell surface (24.7, 18.6, and 34.7% of the cell population staining positive, respectively). The effect of temperature was not statistically significant by one-way analysis of variance (p = 0.5878, n = 3), and Bonferroni's multiple comparison post test showed that none of the pairs of columns were significantly different from each other (p > 0.05 in all cases).

To test whether larger amounts of externalized PS would cause the kind of susceptibility seen with ionomycin treatment, PS was added exogenously to the outer leaflet of the plasma membrane. This was accomplished by incubating cells with vesicles composed of 50% egg PC and 50% brain PS as described in Materials and Methods. Successful delivery was assessed by fluorescent annexin V binding, measured by flow cytometry. Fig. 6-4a shows an example set of histograms of PS exposure of control cells (black) and cells incubated with vesicles containing PS (green). Samples were fit by nonlinear regression (sum of Gaussian curves) to quantify the number of cells staining low, medium, or high levels of intensity as described in the figure legend. As summarized in Fig. 6-4b, incubating the cells with exogenous PS most obviously increased the fraction of cells staining at a medium intensity ($p < 0.001$, two-way analysis of variance with Bonferroni's post test, $n = 7$).

After incubation with these vesicles, samples were assayed for susceptibility to sPLA$_2$ by repeating the experiments of Fig. 6-2. Fig. 6-4c shows example time profiles of ADIFAB GP in cells at 37 °C after addition of the hydrolytic enzyme. There appeared to be no difference between control cells and cells loaded with PS. The maximum rise in GP was quantified for multiple replicates of these experiments at both 37 and 45 °C and is summarized in Fig.6- 4d. These data suggest a slight increase in fatty acid release from these samples both as temperature increases and PS is added, but neither of these effects (nor an interaction between the two) was significant as shown by a two-way analysis of variance ($p = 0.25$, 0.59, and 0.92, respectively).

Because Patman equilibration has been used to detect biophysical membrane changes that are indistinguishable by TMA-DPH or Patman GP alone, those kinetics were examined here. As before, intensity at both 435 and 500 nm was collected over time for 500 s after Patman was added to cell samples. These data were fit by nonlinear regression by an arbitrary function

analogous to Eq. 5 and normalized to the maximum intensity at 435 nm. These normalized data were then aggregated with others collected at the same temperature. Figure 6-5a is an example of this at 37 °C with error bars representing the SE. These aggregated curves were then fit by nonlinear regression (Eq. 5) and analyzed according to the model proposed and utilized previously (Franchino et al., 2013). In this way, it is possible to determine the fraction of Patman located in two different configurations in the membrane, the polarity of those configurations, and the rate at which the probe equilibrates with its environment in those two configurations. The temperature-dependence of all of these parameters was determined by linear regression. None correlated significantly with temperature except the polarity of the more slowly-equilibrating configuration (p=0.0001), which is shown in Fig. 6-5b. This configuration became more polar as temperature increased.

Ionomycin's effect on Patman equilibration was examined in a slightly different way because the ionophore acts quickly and on the entire population simultaneously. Computer simulations were performed to determine what the expected the curves would look like if certain parameters were altered by ionomycin addition midway through Patman's equilibration with the membrane. Figure 6-6a shows an expected intensity profile if the distribution of the probe among the two configurations was altered. The intensity at both wavelengths immediately increased and to different degrees. When only the polarity of one of the configurations was changed by ionomycin, a curve like that seen in Fig. 6-6b resulted, with the intensity at 435 and 500 nm changing in opposite directions but with the identical magnitude. If both the distribution of the probe and the polarity of its environment were altered after ionophore treatment, it was possible to get a curve such as that shown in Fig. 6-6c. In this case, the intensity at the two wavelengths changed trajectory in opposite directions and with uneven scalar values.

In order to quantify the actual effect of ionomycin, the intensity profiles were fit as described in Materials and Methods (example: Fig. 6-6d). In this way it was possible to obtain the amount (both magnitude and direction) and rate at which ionomycin altered the trajectory of the equilibration. The scalar values of the 435 and 500 nm curves (normalized to the total intensity at 435 nm) were summed to determine if they were mirror images of each other, or in other words, if that sum were equal to 0. The average sum of ionomycin at all temperatures was actually 0.2256 and significantly different from 0 ($p<0.0001$). This suggests that ionomycin treatment causes a change in probe distribution as well as the polarity of the probe's environment, a different result than that seen with temperature manipulation.

To investigate the possibility that ionomycin causes cytoskeletal alterations while temperature does not, F-actin was stained with fluorescent phalloidin and photographed via confocal microscopy. Fig. 6-7 shows example images of control cells, ionomycin-treated cells, and cells incubated at 45 °C (Panels A, B, and C, respectively). Control cells (Fig. 6-7A) contained more fibrous actin filaments while Fig. 6-7B shows smaller actin fragments after ionomycin treatment as if the fibers had been severed. Cells incubated at 45 °C for 10 min (Fig. 6-7C) appeared more fibrous than ionomycin-treated cells, but not quite like the corresponding controls. In order to quantify this effect, ImageJ software was used to calculate the circularity index of all particles in such images as explained in Materials and Methods. Figure 6-8 shows the average percentage of particles with the highest circularity index (0.75 – 1) of images of both control and ionomycin-treated cells at 32, 37, and 45 °C. Control cells at 45 °C contained more circular (and therefore shorter) actin filaments than those incubated at lower temperatures, but ionomycin treatment caused an increase in the percentage of particles of high circularity at every temperature. Two-way analysis of variance reported that ionomycin treatment was the main

79

source of variation (40.14%, p<0.001) with temperature contributing to 14.29% of the variation (p=0.0315) without significant interaction between the two (p=0.2751).

To further investigate the connection between actin severing and susceptibility to sPLA$_2$, changes in the actin cytoskeleton were investigated during TG-induced apoptosis. As shown in Fig. 6-9, 4 h TG treatment (Panel A) caused actin fragmentation compared to control cells (Panel B). Images of cells treated with TG for 1 – 4 h and corresponding vehicle controls were analyzed as described for Fig. 6-8 and the percentage of pixels of the highest circularity is summarized in Fig. 6-9C. The overlaid curve (from Fig. 5-2) is included to show the temporal correlation between actin alterations and susceptibility of TG-treated cells to sPLA$_2$. The data are fit by nonlinear regression (a sigmoid function) to estimate the time at which each effect has reached 50% of its maximum. The inflection point of actin fragmentation occurs at 1.256 h (95% confidence interval: 0.3351 – 2.177 h) while that of susceptibility does not occur until 2.006 h (95% confidence interval: 1.783 – 2.229 h).

Discussion

S49 cells were incubated at various temperatures in order to manipulate phospholipid fluidity independently of other common alterations to the plasma membrane that occur during calcium loading or apoptosis. The membrane probes Patman and TMA-DPH were used to determine if altering temperature could induce changes of sufficient magnitude to match those observed in previous studies. Heating the cells to 45 °C increased the fluidity of the membrane, allowing greater probe rotation within the bilayer (hence a decrease in TMA-DPH anisotropy), to the same degree that ionomycin treatment did at 32 °C (Fig. 6-1); however, increasing the temperature to 45 °C failed to induce susceptibility of the lipids to hydrolysis by sPLA$_2$ (Fig. 6-2). This clearly implies that the absolute value of TMA-DPH anisotropy in a membrane cannot

fully predict the availability of substrate for the enzyme. Because the anisotropy always drops

further when ionomycin is added (Fig. 6-1), it appears TMA-DPH is picking up an additional

alteration occurring in the membrane after calcium loading, but it cannot give us enough

information to understand that change.

A simple cause of this supplementary change detected by TMA-DPH could involve the

exposure of the negatively-charge PS to the outer leaflet of the plasma membrane, a well-

understood change known to correlate with membrane vulnerability to hydrolytic attack (Bailey

et al., 2009; Nielson et al., 2000). As demonstrated in Fig. 6-3, increasing the incubation

temperature to 45 °C did not produce a statistically significant increase in the population of cells

staining annexin V positive. While nearly a third of the cell population exhibited PS exposure,

this was not comparable to ionomycin treatment, which causes nearly 100% of a cell population

to flip PS to the outer leaflet (Nielson et al., 2000). If a negatively-charged outer leaflet fully

accounts for the difference between the susceptibility of the two samples in Fig. 6-2, it would be

probable that increasing the amount of PS on the surface would render the cells vulnerable to

$sPLA_2$. Figure 6-4b illustrates that loading the outer leaflet with exogenous PS was successful,

yet this did not cause a significant increase in susceptibility (Fig. 6-4D). It could be argued that

susceptibility was not affected because the bulk of the annexin V positive cells in Fig. 6-4A and

B stained with lower intensity than seen in ionomycin-treated samples (largely staining at the

"high" intensity). To investigate this possibility, parallel annexin V and susceptibility assays

were compared to determine if the percentage of cells with "high" intensity staining correlated

with the amount of fatty acid release from the membrane. Linear regression revealed that there

was no significant correlation between ADIFAB GP increase and cells with "high" intensity

annexin V staining in control cells or cells loaded with exogenous PS (p = 0.2793 and 0.3357

respectively). By manipulating exposure of PS and membrane fluidity independent of cell death, it was possible to investigate their individual roles in membrane susceptibility to hydrolysis. As demonstrated in Figs. 6-1 – 6- 4, both extensive PS exposure in the outer leaflet and temperature-induced increases in membrane fluidity (or even a combination of the two) were insufficient to cause S49 cells to become susceptible to hydrolysis by $sPLA_2$.

As published previously, the equilibration of Patman with the membrane can reveal more information about the biophysical properties of the phospholipid bilayer than its GP alone by applying a model in which Patman can exist in two different configurations in the membrane (Franchino et al., 2013). By examining time profiles of both 435 and 500 nm emission intensities after Patman addition, the polarity of these configurations, rates of equilibration of these two configurations, and proportion of probe in each configuration can be determined (Franchino et al., 2013). Aggregated intensity profiles at different temperatures were fit as explained in Materials and Methods (Fig. 6-5A). The abovementioned model was applied to the resulting nonlinear regression parameters and revealed that altering temperature only had a significant effect on the polarity of the "slow" configuration (Fig. 6-5B). The distribution of probe was unchanged (linear regression: p=0.219). During TG-induced apoptosis, the polarity of the membrane was similarly altered (intuitive because of the change in Patman GP) but the largest change was in the distribution of the probe. Patman molecules shifted from residing primarily in the "slow" configuration into the "fast" configuration. This was interpreted to indicate a decrease in interlipid interactions that would anchor probe (and other lipid molecules) deep in the membrane making it easier for an individual molecule to protrude from the membrane . Because this parameter was unchanged with temperature manipulations, a condition in which

82

susceptibility is not induced, this redistribution of probe could be an important characteristic of the additional alteration caused by ionomycin.

To identify whether ionophore treatment significantly alters the distribution of Patman between configurations, and thus the anchoring of lipid molecules to the membrane, ionomycin was added midway through the probe's equilibration as shown in Fig. 6-6D. The addition of this drug caused a deviation from the original trajectory of Patman's emission intensity as it equilibrated with the membrane. As this makes determining exact, quantifiable changes in the above parameters difficult to obtain, a more qualitative approach was taken. This deviation was quantified by nonlinear regression as described in Materials and Methods to reveal a rate (constrained to be identical between 435 and 500 nm) and a scalar value for each wavelength. Computer simulations were performed to determine what these scalar values would be if different parameter values (polarity of the "slow" or "fast" configurations versus the distribution of probe among them) were altered. If only membrane polarity was changed (as it is when only temperature is varied), the scalars were always of opposite signs and equal magnitudes (Fig. 6-6B). Any other result only arose if the distribution of probe among configurations was altered (Fig. 6-6A and C). Therefore, if the sum of the normalized scalar values from 435 and 500 nm intensity profiles was always equal to zero, that would suggest a change in membrane polarity only. However, as reported in the Results section, the actual sum was a number significantly different from zero, which implicates that a redistribution of probe was caused by ionomycin treatment. Just as with TG-induced apoptosis , this suggests that calcium loading causes a reduction in the anchoring forces restricting phospholipids from migrating into the active site of sPLA$_2$, an effect absent when only temperature is varied.

To summarize to this point, ionomycin caused an additional alteration in membrane fluidity beyond that seen with increased temperature that was undetectable by absolute TMA-DPH anisotropy or Patman GP values. Patman equilibration kinetics analyses suggested that ionophore treatment reduces the anchoring of molecules deep in the membrane while temperature variation only alters the amount of water in the membrane. Because removal of actin filaments has been to shown to cause membrane softening (Lorenz et al., 2009), alterations in the actin cytoskeleton were investigated as a possible source of this discrepancy. A particle analysis of confocal images revealed that actin filaments are shorter (higher circularity index) after ionomycin treatment (Figs. 6-7 and 6-8), suggesting the network has been disrupted by some severing mechanism. While heating cells to 45 ºC increased the percentage of pixels in particles of higher circularity as well, the effect contributed less to the total variation than ionomycin and was less significant. The actin fragmentation at the high temperatures could also be due to the cells beginning to experience heat shock and initiate apoptotic cascades. Despite this small effect, ionomycin disrupts the actin network to a greater degree which would have a larger effect on membrane softness.

If actin disruption is the cause of weakened interactions among lipids leading to a redistribution of Patman after ionomycin treatment, the same should be true during TG-induced apoptosis. The experiments and analyses of Figs. 6-7 and 6-8 were repeated after varying lengths of incubations with TG. At a time of maximal membrane susceptibility to sPLA$_2$ (4 h with the drug), actin was severed compared to control samples. The percentage of pixels in particles of highest circularity was not as high as ionomycin images, presumably because ionomycin affects the entire population in a more synchronized manner than TG. Ionophore treatment induces 100% of the cell population into an "alive, yet susceptible" state (Bailey et al., 2007) while the

corresponding population in TG-induced apoptosis reaches a maximum just above 30% of the population .

Finally, the temporal onset of susceptibility to sPLA$_2$ during TG-induced apoptosis was overlaid with the onset of actin fragmentation for comparison (Fig. 6-9C). Although the 95% confidence intervals overlap, the data suggest that actin severing precedes or correlates with membrane alterations that cause cells to become vulnerable to cleavage. Future studies will use actin-severing drugs to isolate this effect and further validate the hypothesis that disruption of actin networks must occur for full susceptibility of plasma membranes to hydrolysis by sPLA$_2$.
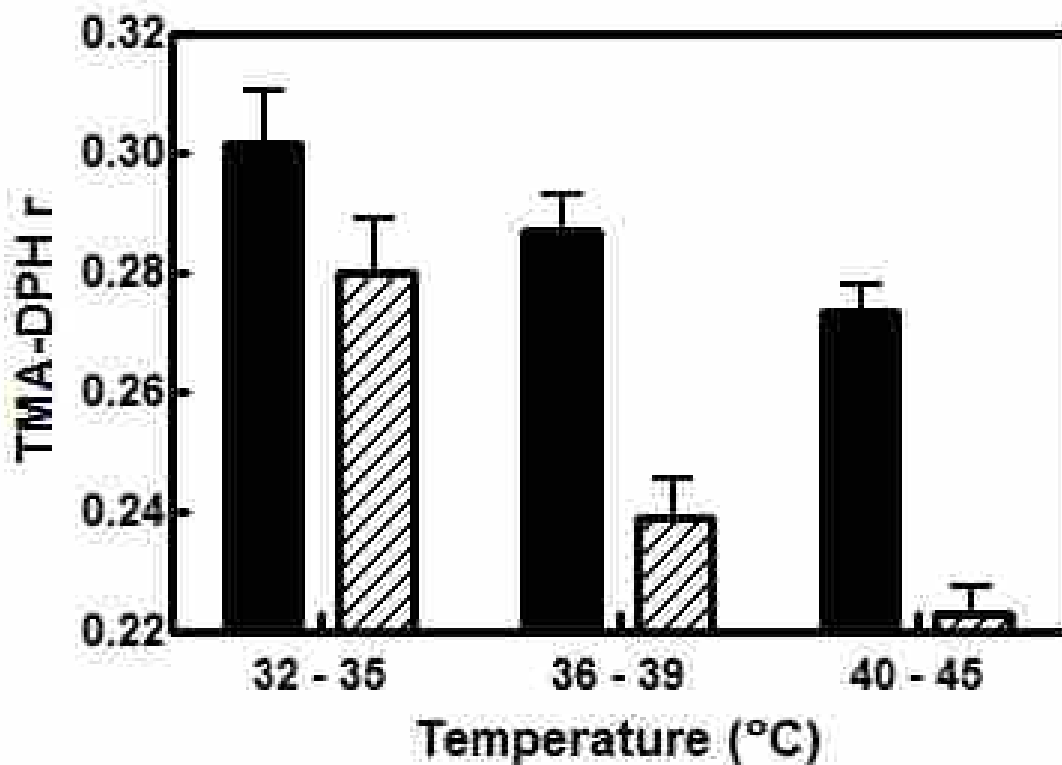
Figure 6-1: Effect of temperature and ionomycin on TMA-DPH anisotropy.
Cells were equilibrated at indicated temperature for 10 min before measurements made with TMA-DPH as described in Materials and Methods (before ionomycin; black bars). Ionomycin was then added and an additional measurement made after another 10 min (after ionomycin; striped bars). Two way analysis of variance showed that both ionomycin treatment and temperature were significant sources of variation (30.98%,$p<0.0001$ and 23.81%, $p<0.0001$ respectively) with interaction contributing to 3.35% of the total variation (p=0.0918) with n=9 – 12.
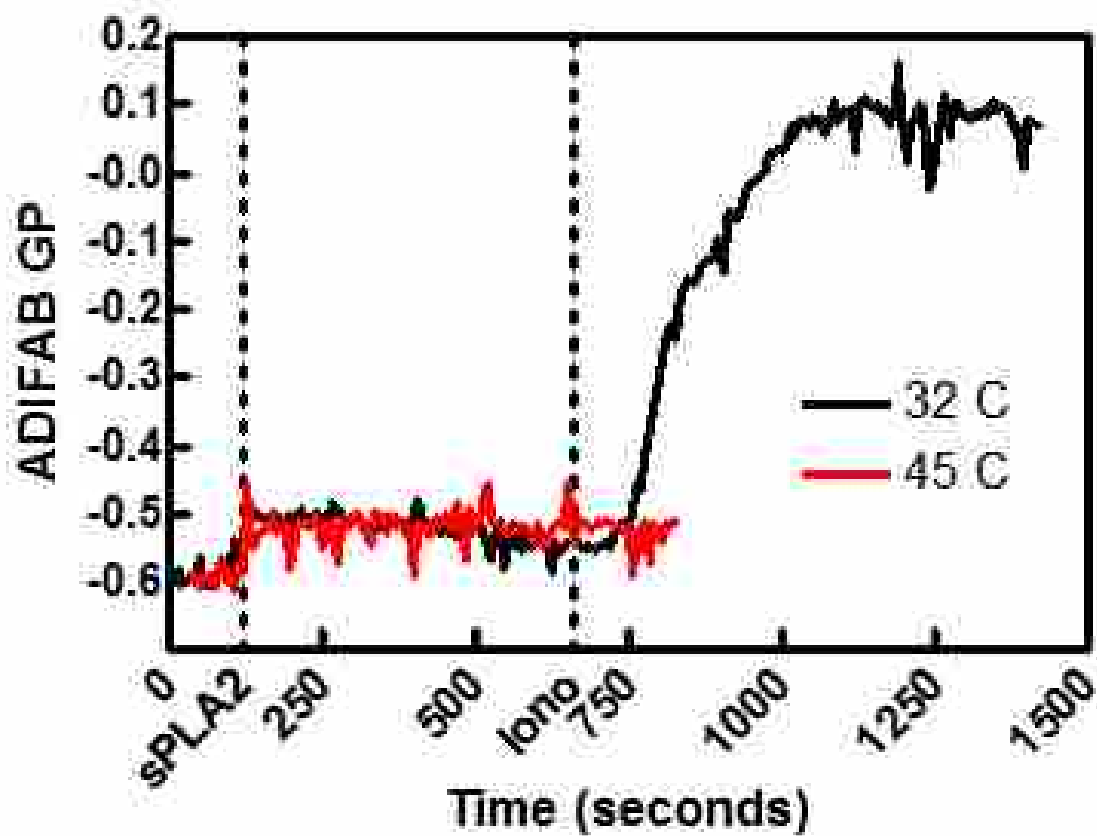
Figure 6-2: Example time profiles of ADIFAB GP after sPLA$_2$ addition at 32 and 45 °C.
Cells were incubated at either 32°C (black curve) or 45 °C (red curve) for 5 min prior to data acquisition. ADIFAB was added at t=0 with sPLA$_2$ and ionomycin (only for the 32 °C sample) added at the dotted lines as indicated. Emission intensity was collected at 432 and 505 nm and the GP calculated as described in Materials and Methods.
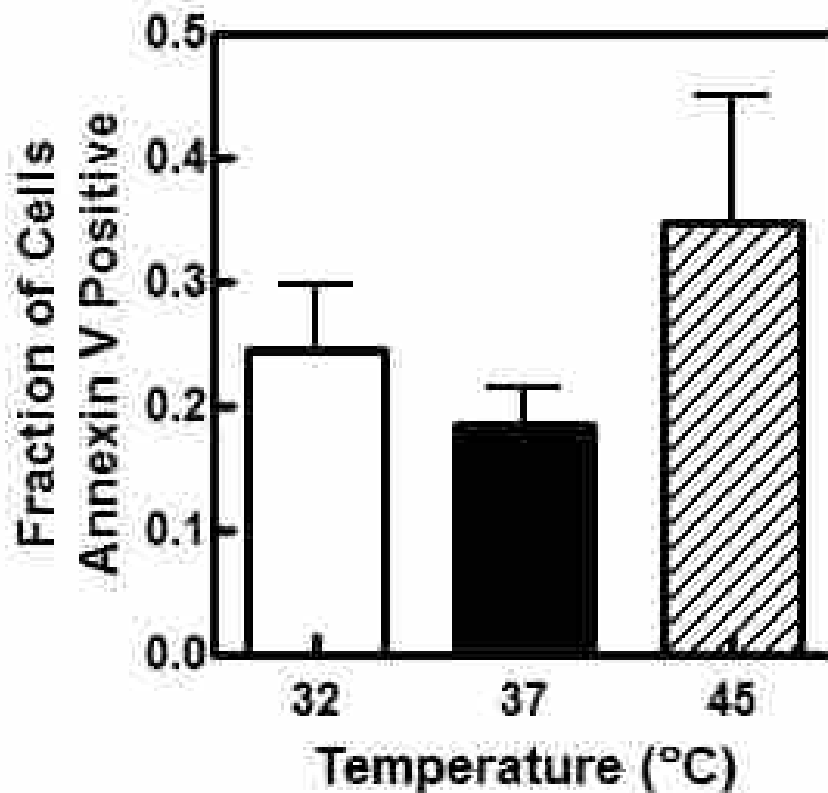
Figure 6-3: Annexin V binding at different temperatures assayed by flow cytometry.

Cells were incubated at indicated temperatures for 10 min prior to staining with fluorescent annexin V according to the manufacturer's protocol and as described in Materials and Methods. Resulting histograms of annexin V intensity were fit by nonlinear regression with a function composed of three Gaussian curves (low, medium, and high annexin V intensity). The means were constrained to be shared among the three temperatures for each experiment with the low population constrained to be centered at zero. The data are represented as the sum of the fraction of cells in the medium and high intensity populations. One way analysis of variance showed the means are not significantly different ($p = 0.5878$, $n = 3$). Bonferroni post test comparing all columns showed that none of the temperatures could be distinguished from each other ($p > 0.05$ in all cases).
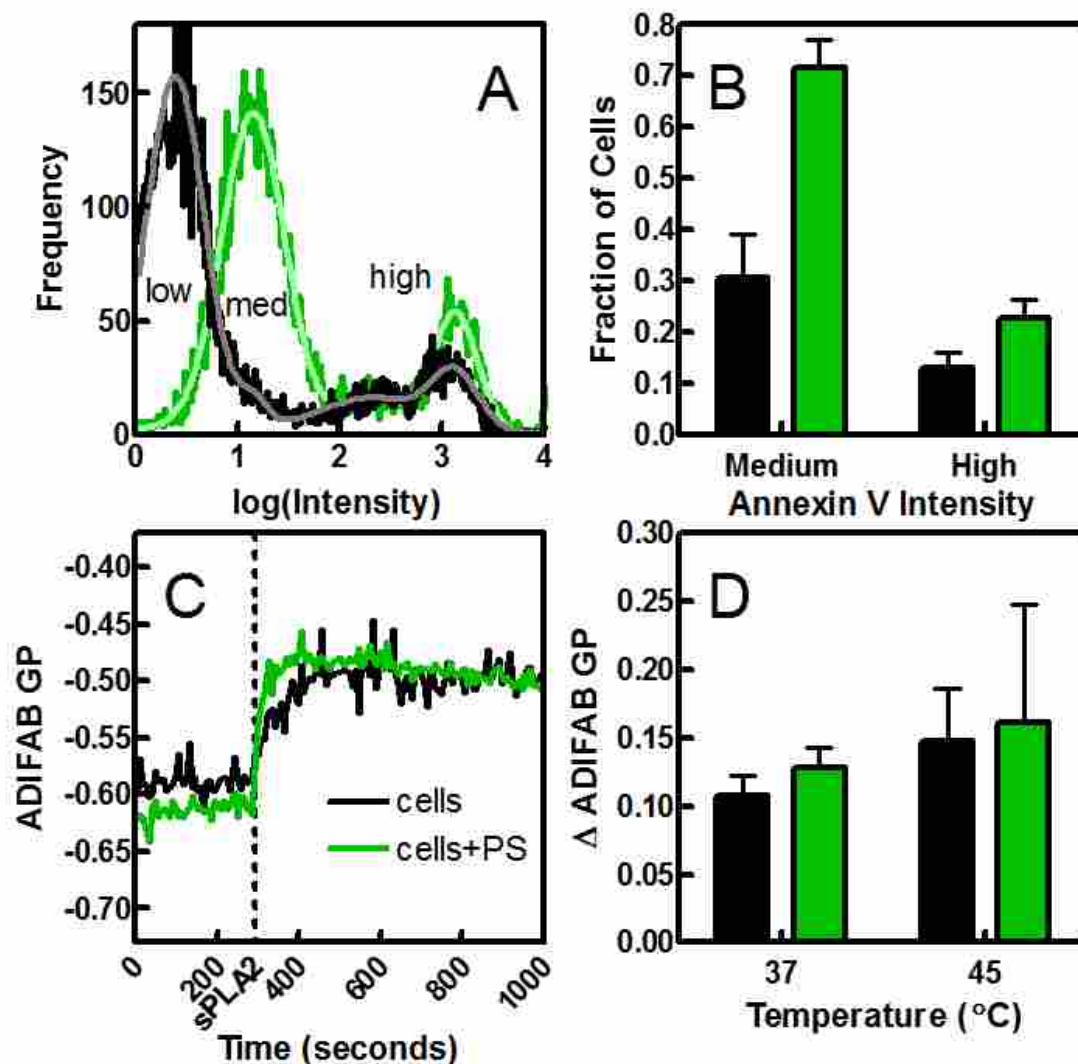
Figure 6-4: Susceptibility of cells loaded with exogenous PS.
Cells were incubated with vesicles containing exogenous PS for 30 min as described in Materials and Methods. Control cells are shown in black, cells with added PS in green. Panel A: Flow cytometry histograms of annexin V staining. Histograms were fit by nonlinear regression with a function composed of four Gaussian curves (low, medium, and high annexin V intensity as indicated with two Gaussian curves summed for the high population). The means were constrained to be shared among the control sample and the sample with added PS for each experiment. The percent of the cell population in each category was calculated using the area in each Gaussian curve. Panel B: Experiments were analyzed as shown in Panel A and the average percent of the cell population staining medium or high intensity are summarized here (n = 7). Two-way analysis of variance shows that the addition of vesicles contributed to 23.57% of the variation (p = 0.0001). Bonferroni's post test reported that loading the cells with PS statistically increased staining in the medium population (p < 0.001) but not the high intensity population (p > 0.05). Panel C: Example time profiles of ADIFAB GP (see Materials and Methods) with sPLA$_2$ added at the dotted line. Panel D: The maximum rise in ADIFAB GP of experiments such as those in Panel C was quantified and is summarized here (n = 3–9). Two-way analysis of variance reported that means are not statistically different (effect of temperature: p = 0.2549; effect of added PS: p = 0.5940; and interaction: p = 0.9226).
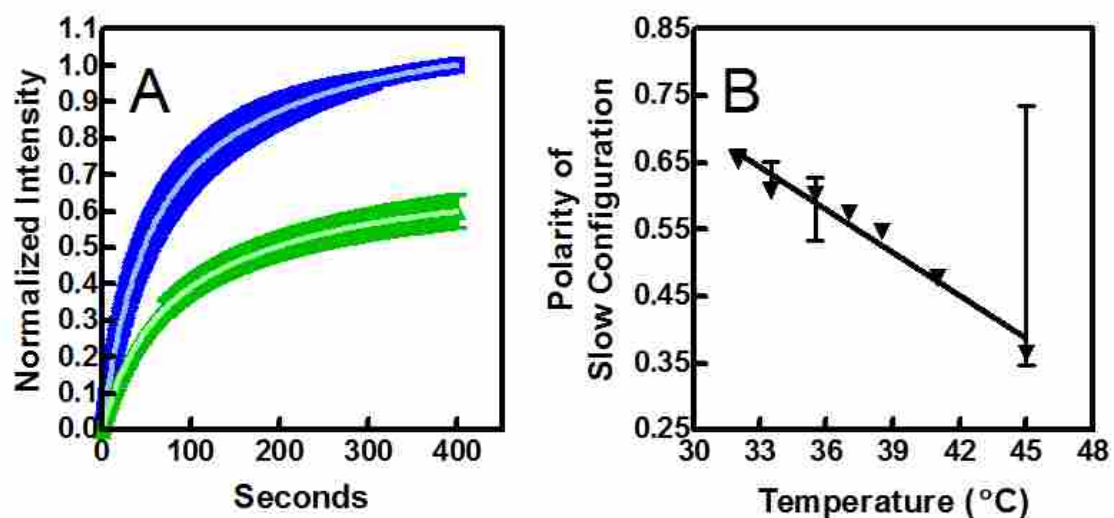
Figure 6-5: Patman equilibration analysis at different temperatures.
Patman emission was gathered at 435 and 500 nm over time after 10 min equilibration at indicated temperature as described in Materials and Methods. Experiments at the same temperature were aggregated by normalizing each set to the maximum intensity at 435 nm. Panel A is an example aggregate at 37 °C. These aggregates were fit by nonlinear regression and input into model equations as described in Materials and Methods. None of the model parameters correlated significantly with temperature except for the polarity of the slow configuration (Panel B; $n = 6 – 26$; $p = 0.0001$).
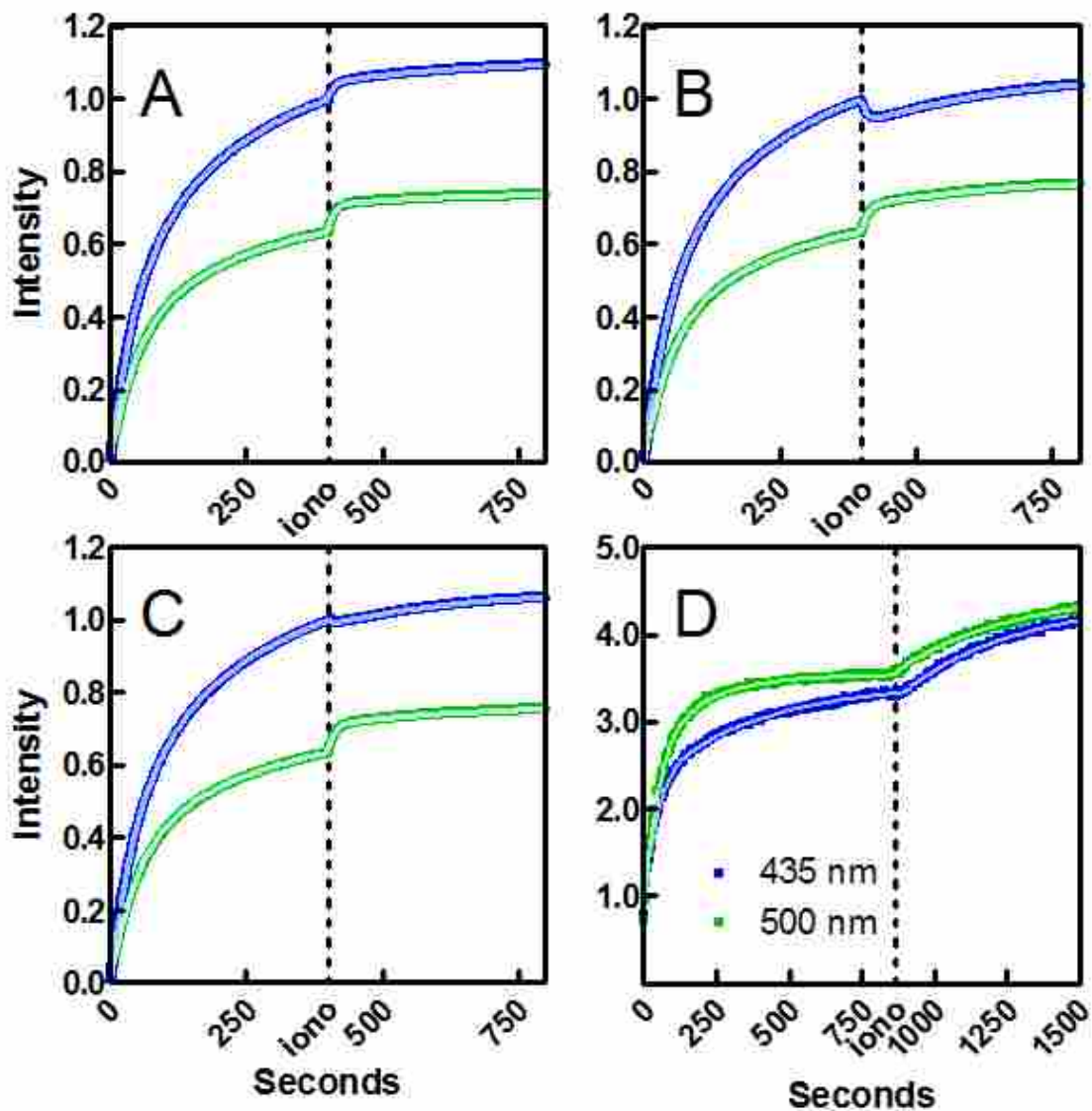
Figure 6-6: Effect of ionomycin on Patman equilibration based on computer simulations and experiments.

Panels A – C are example time courses from computer simulations in which ionomycin was added midway through Patman's equilibration. Panel A: Example simulation if ionomycin only alters the distribution of probe in the two configurations. Panel B: Example simulation if ionomycin only alters the polarity of one of the configurations. Panel C: Example simulation if both the distribution of the probe and the polarity of the environment are altered with ionomycin treatment. Panel D: An example of an actual time profile of Patman intensity. Data are fit by nonlinear regression as described in Materials and Methods.
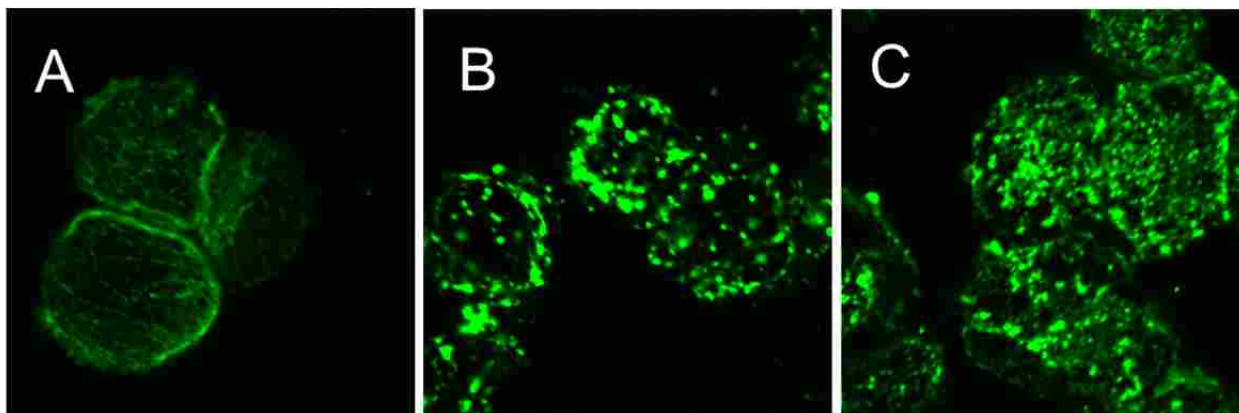
Figure 6-7: F-actin of control cells, ionomycin-treated cells, and cells incubated at 45 °C for 10 min visualized by phalloidin staining.

Cells were harvested and treated for 10 min (Panel A: control vehicle, Panel B: ionomycin, Panel C: 45 °C) before being mounted onto slides. They were then simultaneously fixed, permeablized, and stained with fluorescent phalloidin as described in Materials and Methods. These images were collected via confocal microscopy using a 60x objective with a 3x digital zoom.
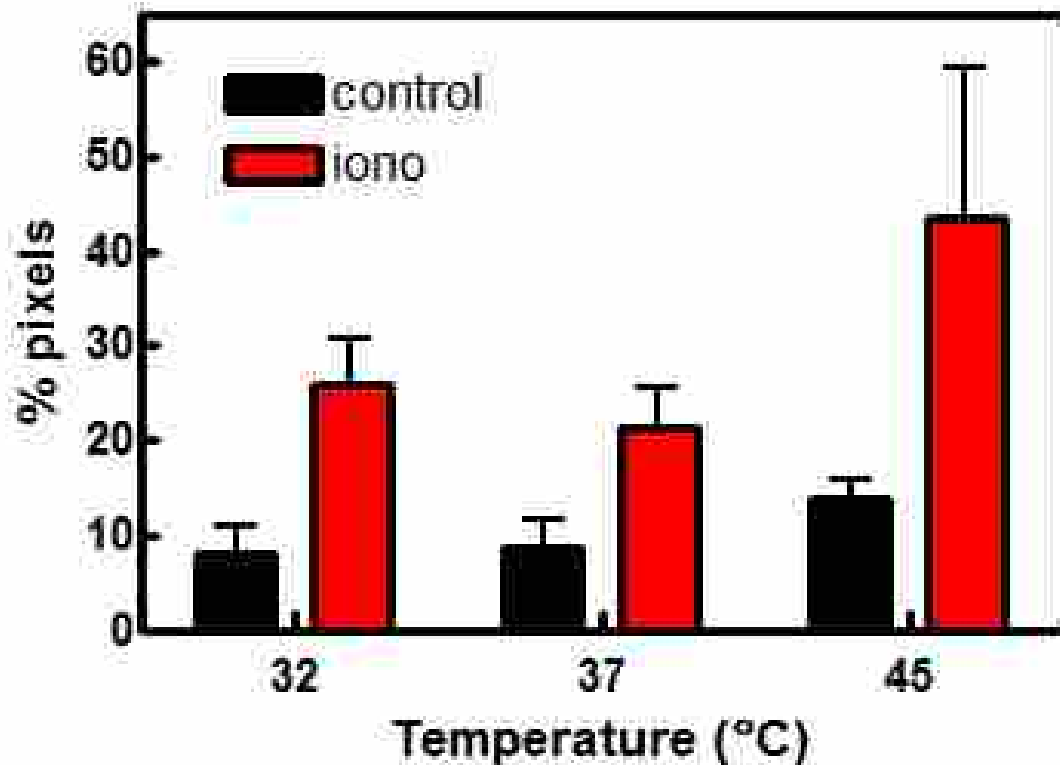
Figure 6-8: Effect of temperature and ionomycin on F-actin particle circularity.
Images such as those in Fig. 7 were analyzed using ImageJ as described in Materials and Methods. Cells were incubated for 10 min at the indicated temperature before simultaneous fixation, permeablization, and staining (black bars). Some samples were incubated for 10 min at temperature and then 10 more with ionomycin (red bars). Data are presented as the percentage of pixels in the image that are part of a particle of circularity index between 0.75 – 1.Two way analysis of varianceshowed that both temperature and ionomycin treatment were significant sources of variation ($p = 0.0315$ and $p < 0.0001$ respectively) with temperature comtributing to 14.29% of the total variation and ionomycin to 40.14%. The interaction between the two was insignificant.
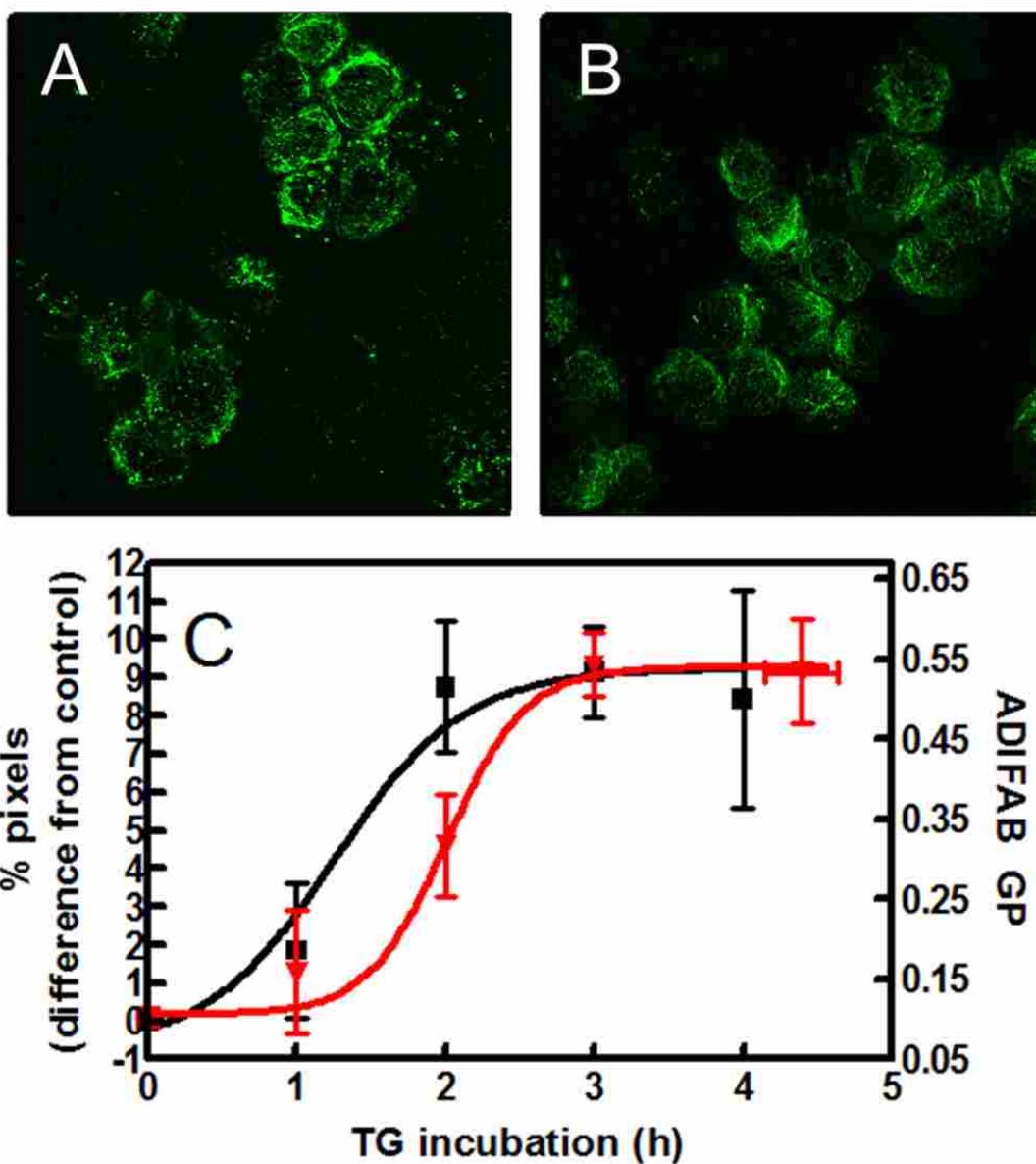
Figure 6-9: Actin fragmentation during TG-induced apoptosis.
Panels A and B are confocal images of phalloiding-stained F-actin after 4 h TG treatment (A) or 4 h control vehicle (B). Slides were prepared as in Fig. 7 and as described in Materials and Methods. Images were analyzed as in Fig. 8 and the percentage of pixels in particles of highest circularity $(0.75 - 1)$ are plotted in Panel C (black curve). The red curve overlaid in Panel C is the total change in ADIFAB GP after addition of sPLA$_2$ after different incubation times with TG (data from chapter 3).

CHAPTER 7: SUMMARY

Secretory PLA$_2$ has been an interesting topic in biophysical studies of membranes because it acts at a lipid-water interface and is regulated by the state of its substrate. The protein itself always exists in an active state, but not all bilayers are equally susceptible to hydrolytic attack. Furthermore, different isoforms of the enzyme exhibit differing levels of activity toward the same membranes. Originally, it was thought that negative charge on the membrane surface was the key factor in determining susceptibility of the bilayer to the enzyme's activity. More recently, this lab and others have emphasized the importance of the biophysical state of the membrane. In this dissertation, the molecular details of these physical properties were investigated.

Prior to this study, it was known that the plasma membrane undergoes changes in apoptosis detected by MC540, Laurdan, and DPH. An early increase in MC540 fluorescence indicates a decrease in lipid packing. This effect occurs in ionomycin-, DEX-, and TG-induced apoptosis, yet different isoforms respond differently to these treatments. Here it was found that a large enough increase in lipid packing caused increased membrane permeability to propidium iodide. Ionomycin treatment did not cause this increase in membrane permeability, and only the snake venom and hGX enzymes were able to attack these cells. Apoptotic cells, on the other hand, showed both the MC540 effect and the intermediate propidium iodide staining. These cells were attacked by the hGIIa and hGV isoforms. Understanding this physical change better, therefore, can explain some of the specificity of different human isozymes.

Lipid peroxidation was hypothesized as a possible mechanism for this increase in membrane permeability. This was tested by assaying membrane oxidation during apoptosis. The timing of reactive oxygen species appearing in the membrane correlated temporally with hGIIa

95

activity. Cells were then treated directly with oxidizing agents, resulting in fatty acid release after incubation with hGIIa sPLA$_2$.

Previous studies assaying Laurdan GP and DPH anisotropy during apoptosis suggested possible changes in membrane order and fluidity, but these were not always temporally associated with susceptibility. Here, charged analogs of these probes (Patman and TMA-DPH) were utilized to more confidently assay the plasma membrane rather than having data interpretation complicated by internal membrane staining. These studies revealed changes in membrane order and fluidity that matched the onset of membrane vulnerability to hydrolytic attack. These results combined with Patman equilibration results revealed that TG treatment caused enhanced phospholipid mobility, an increase in membrane polarity (mostly affecting deeper portions of the membrane), and a decrease in the forces that anchor lipids to the center of the bilayer. Using parallel vesicle studies with these same probes, the change in these forces was quantified in terms of energy and used to predict a 50–100 fold increase in the density of lipid protrusions into the active site of sPLA$_2$.

Next this physical change to the membrane and the effect of PS exposure were isolated to discover their individual influence on membrane susceptibility. Manipulating temperature caused alterations detected by Patman and TMA-DPH of sufficient magnitude to mimic ionomycin treatment, yet the plasma membrane remained resistant to sPLA$_2$. Phosphatidylserine was added exogenously to the membrane, but no fatty acid release resulted. These two effects were not sufficient (either on their own or in combination) to allow large amounts of hydrolysis as with ionomycin-treatment. Again, Patman equilibration kinetics analyses detected biophysical changes in ionomycin treatment that were absent in temperature experiments. Just as with TG treatment, ionophore treatment caused a decrease in lipid anchoring to the center of the bilayer.

Previously, no mechanism for this important physical change to the membrane had been proposed. Here it was shown that the severing and disrupting of the actin cytoskeleton was present in ionomycin-treated cells (susceptible) but not in cells incubated at high temperatures (resistant). Furthermore, the onset of actin severing during TG apoptosis preceded susceptibility to sPLA$_2$. Future experiments utilizing actin-disrupting drugs will be performed to provide further evidence that cytoskeletal alterations are responsible for membrane changes leading to susceptibility to hydrolytic enzymes.

Many biophysical membrane studies focus on artificial bilayers, but the end goal is to understand systems that are more physiologically relevant. This study was exciting in that it was successful in examining changes at such a molecular level in a system as complex as a living cell. It combined the classic use of fluorescent membrane probes with parallel data collected in artificial membranes as well as computer simulations and models to gain more details than previously possible. This is also the first attempt at suggesting mechanisms for the biophysical alterations discussed. A novel function of the intact cytoskeleton is also proposed: to protect the plasma membrane from hydrolytic damage.

REFERENCES

Ahn, H.J., Kim, Y.S., Kim, J.U., Han, S.M., Shin, J.W., and Yang, H.O. (2004). Mechanism of taxol-induced apoptosis in human SKOV3 ovarian carcinoma cells. Journal of Cellular Biochemistry *91*, 1043-1052.

Akiba, S., Nagatomo, R., Hayama, M., and Sato, T. (1997). Lipid peroxide overcomes the inability of platelet secretory phospholipase A(2) to hydrolyze membrane phospholipids in rabbit platelets. Journal of Biochemistry *122*, 859-864.

Alnemri, E.S., Livingston, D.J., Nicholson, D.W., Salvesen, G., Thornberry, N.A., Wong, W.W., and Yuan, J.Y. (1996). Human ICE/CED-3 protease nomenclature. Cell *87*, 171-171.

Andresen, T.L., Davidsen, J., Begtrup, M., Mouritsen, O.G., and Jorgensen, K. (2004). Enzymatic release of antitumor ether lipids by specific phospholipase A2 activation of liposome-forming prodrugs. Journal of Medicinal Chemistry *47*, 1694-1703.

Apellaniz, B., Nieva, J.L., Schwille, P., and Garcia-Saez, A.J. (2010). All-or-None versus Graded Single-Vesicle Analysis Reveals Lipid Composition Effects on Membrane Permeabilization. Biophysical Journal *99*, 3619-3628.

Ashman, R.F., Peckham, D., Alhasan, S., and Stunz, L.L. (1995). Membrane unpacking and the rapid disposal of apoptotic cells. Immunology Letters *48*, 159-166.

Atsumi, G., Murakami, M., Tajima, M., Shimbara, S., Hara, N., and Kudo, I. (1997). The perturbed membrane of cells undergoing apoptosis is susceptible to type II secretory phospholipase A(2) to liberate arachidonic acid. Biochimica Et Biophysica Acta-Lipids and Lipid Metabolism *1349*, 43-54.

Bailey, R.W., Nguyen, T., Robertson, L., Gibbons, E., Nelson, J., Christensen, R.E., Bell, J.P., Judd, A.M., and Bell, J.D. (2009). Sequence of Physical Changes to the Cell Membrane During Glucocorticoid-Induced Apoptosis in S49 Lymphoma Cells. Biophysical Journal *96*, 2709-2718.

Bailey, R.W., Olson, E.D., Vu, M.P., Brueseke, T.J., Robertson, L., Christensen, R.E., Parker, K.H., Judd, A.M., and Bell, J.D. (2007). Relationship between membrane physical properties and secretory phospholipase A2 hydrolysis kinetics in S49 cells during ionophore-induced apoptosis. Biophysical Journal *93*, 2350-2362.

Baker, S.F., Othman, R., and Wilton, D.C. (1998). Tryptophan-containing mutant of human (group IIa) secreted phospholipase A(2) has a dramatically increased ability to hydrolyze phosphatidylcholine vesicles and cell membranes. Biochemistry *37*, 13203-13211.

Basse, F., Stout, J.G., Sims, P.J., and Wiedmer, T. (1996). Isolation of an erythrocyte membrane protein that mediates Ca2+-dependent transbilayer movement of phospholipid. Journal of Biological Chemistry *271*, 17205-17210.

Beers, S.A., Buckland, A.G., Giles, N., Gelb, M.H., and Wilton, D.C. (2003). Effect of tryptophan insertions on the properties of the human group IIA phospholipase A(2): Mutagenesis produces an enzyme with characteristics similar to those of the human group V phospholipase A(2). Biochemistry *42*, 7326-7338.

Beers, S.A., Buckland, A.G., Koduri, R.S., Cho, W., Gelb, M.H., and Wilton, D.C. (2002). The antibacterial properties of secreted phospholipases A(2) - A major physiological role for the group IIA enzyme that depends on the very high pI of the enzyme to allow penetration of the bacterial cell wall. Journal of Biological Chemistry *277*, 1788-1793.

Belinsky, G.S., Rajan, T.V., Saria, E.A., Giardina, C., and Rosenberg, D.W. (2007). Expression of secretory phospholipase A2 in colon tumor cells potentiates tumor growth. Molecular Carcinogenesis *46*, 106-116.

Bell, J.D., Baker, M.L., Bent, E.D., Ashton, R.W., Hemming, D.J., and Hansen, L.D. (1995). Effects of temperature and glycerides on the enhancement of Agkistrodon piscivorus piscivorus phospholipase A2 activity by lysolecithin and palmitic acid. Biochemistry *34*, 11551-11560.

Bell, J.D., and Biltonen, R.L. (1989). The temporal sequence of events in the activation of phospholipase A2 by lipid vesicles. Studies with the monomeric enzyme from Agkistrodon piscivorus piscivorus. JBiolChem *264*, 12194-12200.

Bell, J.D., Burnside, M., Owen, J.A., Royall, M.L., and Baker, M.L. (1996). Relationships between bilayer structure and phospholipase A2 activity: interactions among temperature, diacylglycerol, lysolecithin, palmitic acid, and dipalmitoylphosphatidylcholine. Biochemistry *35*, 4945-4955.

Benz, P.M., Feller, S.M., Sickmann, A., Walter, U., and Renne, T. (2008). Prostaglandin-induced VASP phosphorylation controls alpha II-spectrin breakdown in apoptotic cells. International Immunopharmacology *8*, 319-324.

Berg, O.G., Gelb, M.H., Tsai, M.D., and Jain, M.K. (2001). Interfacial enzymology: the secreted phospholipase A(2)-paradigm. Chemical reviews *101*, 2613-2654.

Best, K.B., Ohran, A.J., Hawes, A.C., Hazlett, T.L., Gratton, E., Judd, A.M., and Bell, J.D. (2002). Relationship between erythrocyte membrane phase properties and susceptibility to secretory phospholipase A(2). Biochemistry *41*, 13982-13988.

Bevers, E.M., Comfurius, P., and Zwaal, R.F.A. (1983). CHANGES IN MEMBRANE PHOSPHOLIPID DISTRIBUTION DURING PLATELET ACTIVATION. Biochimica Et Biophysica Acta *736*, 57-66.

Bezzine, S., Bollinger, J.G., Singer, A.G., Veatch, S.L., Keller, S.L., and Gelb, M.H. (2002). On the binding preference of human groups IIA and X phospholipases A(2) for membranes with anionic phospholipids. Journal of Biological Chemistry *277*, 48523-48534.

Bian, X.P., Hughes, F.M., Huang, Y., Cidlowski, J.A., and Putney, J.W. (1997). Roles of cytoplasmic Ca2+ and intracellular Ca2+ stores in induction and suppression of apoptosis in S49 cells. American Journal of Physiology-Cell Physiology *41*, C1241-C1249.

Bidgood, M.J., Jamal, O.S., Cunningham, A.M., Brooks, P.M., and Scott, K.F. (2000). Type IIA secretory phospholipase A(2) up-regulates cyclooxygenase-2 and amplifies cytokine-mediated prostaglandin production in human rheumatoid synoviocytes. Journal of Immunology *165*, 2790-2797.

Birts, C.N., Barton, C.H., and Wilton, D.C. (2010). Catalytic and non-catalytic functions of human IIA phospholipase A2. Trends in Biochemical Sciences *35*, 28-35.

Boyanovsky, B.B., and Webb, N.R. (2009). Biology of Secretory Phospholipase A(2). Cardiovascular Drugs and Therapy *23*, 61-72.

Brill, A., Torchinsky, A., Carp, H., and Toder, V. (1999). The role of apoptosis in normal and abnormal embryonic development. Journal of Assisted Reproduction and Genetics *16*, 512-519.

Buckland, A.G., and Wilton, D.C. (1998). Inhibition of secreted phospholipases A(2) by annexin V. Competition for anionic phospholipid interfaces allows an assessment of the relative interfacial affinities of secreted phospholipases A(2). Biochimica Et Biophysica Acta-Lipids and Lipid Metabolism *1391*, 367-376.

Budtz, P.E., and Spies, I. (1989). EPIDERMAL TISSUE HOMEOSTASIS - APOPTOSIS AND CELL EMIGRATION AS MECHANISMS OF CONTROLLED CELL DELETION IN THE EPIDERMIS OF THE TOAD, BUFO-BUFO. Cell and Tissue Research *256*, 475-486.

Callahan, M.K., Williamson, P., and Schlegel, R.A. (2000). Surface expression of phosphatidylserine on macrophages is required for phagocytosis of apoptotic thymocytes. Cell Death and Differentiation *7*, 645-653.

Catala, A. (2012). Lipid peroxidation modifies the picture of membranes from the "Fluid Mosaic Model" to the "Lipid Whisker Model". Biochimie *94*, 101-109.

Chekeni, F.B., Elliott, M.R., Sandilos, J.K., Walk, S.F., Kinchen, J.M., Lazarowski, E.R., Armstrong, A.J., Penuela, S., Laird, D.W., Salvesen, G.S., *et al.* (2010). Pannexin 1 channels mediate 'find-me' signal release and membrane permeability during apoptosis. Nature *467*, 863-U136.

Chekeni, F.B., and Ravichandran, K.S. (2011). The role of nucleotides in apoptotic cell clearance: implications for disease pathogenesis. Journal of Molecular Medicine-Jmm *89*, 13-22.

Cho, W., Han, S.K., Lee, B.I., Snitko, Y., and Dua, R. (1999). Purification and assay of mammalian group I and group IIa secretory phospholipase A2. Methods in molecular biology (Clifton, NJ) *109*, 31-38.

Coleman, M.L., Sahai, E.A., Yeo, M., Bosch, M., Dewar, A., and Olson, M.F. (2001). Membrane blebbing during apoptosis results from caspase-mediated activation of ROCK I. Nature Cell Biology *3*, 339-345.

Cunningham, T.J., Yao, L., Oetinger, M., Cort, L., Blankenhorn, E.P., and Greenstein, J.I. (2006). Secreted phospholipase A2 activity in experimental autoimmune encephalomyelitis and multiple sclerosis. Journal of Neuroinflammation *3*.

Cuny, G.D., Degterev, A., and Yuan, J.Y. (2008). Necroptosis - a novel cell death mechanism. Drugs of the Future *33*, 225-233.

Dale, R.E., Chen, L.A., and Brand, L. (1977). Rotational relaxation of the "microviscosity" probe diphenylhexatriene in paraffin oil and egg lecithin vesicles. JBiolChem *252*, 7500-7510.

Daleke, D.L. (2003). Regulation of transbilayer plasma membrane phospholipid asymmetry. Journal of Lipid Research *44*, 233-242.

Darzynkiewicz, Z., Juan, G., Li, X., Gorczyca, W., Murakami, T., and Traganos, F. (1997). Cytometry in cell necrobiology: Analysis of apoptosis and accidental cell death (necrosis). Cytometry *27*, 1-20.

Deamer, D.W., and Bramhall, J. (1986). PERMEABILITY OF LIPID BILAYERS TO WATER AND IONIC SOLUTES. Chemistry and Physics of Lipids *40*, 167-188.

Dekkers, D.W.C., Comfurius, P., Schroit, A.J., Bevers, E.M., and Zwaal, R.F.A. (1998). Transbilayer movement of NBD-labeled phospholipids in red blood cell membranes: Outward-directed transport by the multidrug resistance protein 1 (MRP1). Biochemistry *37*, 14833-14837.

Devaux, P.F., Herrmann, A., Ohlwein, N., and Koziov, M.M. (2008). How lipid flippases can modulate membrane structure. Biochimica Et Biophysica Acta-Biomembranes *1778*, 1591-1600.

Diamantis, A., Magiorkinis, E., Sakorafas, G.H., and Androutsos, G. (2008). A Brief History of Apoptosis: From Ancient to Modern Times. Onkologie *31*, 702-706.

Diaz, C., Lee, A.T., McConkey, D.J., and Schroit, A.J. (1999). Phosphatidylserine externalization during differentiation-triggered apoptosis of erythroleukemic cells. Cell Death and Differentiation *6*, 218-226.

Diraviyam, K., and Murray, D. (2006). Computational analysis of the membrane association of group IIA secreted phospholipases A2: a differential role for electrostatics. Biochemistry *45*, 2584-2598.

Dong, Z., Liu, Y., Scott, K.F., Levin, L., Gaitonde, K., Bracken, R.B., Burke, B., Zhai, Q.J., Wang, J., Oleksowicz, L.*, et al.* (2010). Secretory phospholipase A2-IIa is involved in prostate cancer progression and may potentially serve as a biomarker for prostate cancer. Carcinogenesis *31*, 1948-1955.

Drummen, G.P., van Liebergen, L.C., Op den Kamp, J.A., and Post, J.A. (2002). C11-BODIPY(581/591), an oxidation-sensitive fluorescent lipid peroxidation probe: (micro)spectroscopic characterization and validation of methodology. Free radical biology & medicine *33*, 473-490.

Eguchi, K. (2001). Apoptosis in autoimmune diseases. Internal Medicine *40*, 275-284.

Eizirik, D.L., and Mandrup-Poulsen, T. (2001). A choice of death - the signal-transduction of immune-mediated beta-cell apoptosis. Diabetologia *44*, 2115-2133.

Elmore, S. (2007). Apoptosis: A review of programmed cell death. Toxicologic Pathology *35*, 495-516.

Fabisiak, J.P., Tyurina, Y.Y., Tyurin, V.A., Lazo, J.S., and Kagan, V.E. (1998). Random versus selective membrane phospholipid oxidation in apoptosis: role of phosphatidylserine. Biochemistry *37*, 13781-13790.

Fadeel, B. (2004). Plasma membrane alterations during apoptosis: Role in corpse clearance. Antioxidants & Redox Signaling *6*, 269-275.

Fadeel, B., and Orrenius, S. (2005). Apoptosis: a basic biological phenomenon with wide-ranging implications in human disease. Journal of Internal Medicine *258*, 479-517.

Fadeel, B., Xue, D., and Kagan, V. (2010). Programmed cell clearance: Molecular regulation of the elimination of apoptotic cell corpses and its role in the resolution of inflammation. Biochemical and Biophysical Research Communications *396*, 7-10.

Fadok, V.A., Bratton, D.L., Frasch, S.C., Warner, M.L., and Henson, P.M. (1998). The role of phosphatidylserine in recognition of apoptotic cells by phagocytes. Cell Death and Differentiation *5*, 551-562.

Fadok, V.A., Bratton, D.L., Rose, D.M., Pearson, A., Ezekewitz, R.A.B., and Henson, P.M. (2000). A receptor for phosphatidylserine-specific clearance of apoptotic cells. Nature *405*, 85-90.

Fadok, V.A., Voelker, D.R., Campbell, P.A., Cohen, J.J., Bratton, D.L., and Henson, P.M. (1992). EXPOSURE OF PHOSPHATIDYLSERINE ON THE SURFACE OF APOPTOTIC LYMPHOCYTES TRIGGERS SPECIFIC RECOGNITION AND REMOVAL BY MACROPHAGES. Journal of Immunology *148*, 2207-2216.

Feng, X.Q., You, Y., Xiao, J., and Zou, P. (2006). Thapsigargin-induced apoptosis of K562 cells and its mechanism. Zhongguo Shi YanXueYeXueZa Zhi *14*, 25-30.

Fiorini, R., Littarru, G.P., Coppa, G.V., and Kantar, A. (2000). Plasma membrane polarity of polymorphonuclear leucocytes from children with primary ciliary dyskinesia. European Journal of Clinical Investigation *30*, 519-525.

Franchino, H., Stevens, E., Nelson, J., Bell, T.A., and Bell, J.D. (2013). Wavelength dependence of patman equilibration dynamics in phosphatidylcholine bilayers. Biochimica et biophysica acta *1828*.

Franklin-Tong, V.E., and Gourlay, C.W. (2008). A role for actin in regulating apoptosis/programmed cell death: evidence spanning yeast, plants and animals. Biochemical Journal *413*, 389-404.

Freire, E., and Biltonen, R. (1978). ESTIMATION OF MOLECULAR AVERAGES AND EQUILIBRIUM FLUCTUATIONS IN LIPID BILAYER SYSTEMS FROM EXCESS HEAT-CAPACITY FUNCTION. Biochimica Et Biophysica Acta *514*, 54-68.

Galluzzi, L., Kepp, O., and Kroemer, G. (2009). RIP Kinases Initiate Programmed Necrosis. Journal of Molecular Cell Biology *1*, 8-10.

Gaus, K., Chklovskaia, E., Fazekas de St Groth, B., Jessup, W., and Harder, T. (2005). Condensation of the plasma membrane at the site of T lymphocyte activation. Journal of Cell Biology *171*, 121-131.

Gaus, K., Le Lay, S., Balasubramanian, N., and Schwartz, M.A. (2006). Integrin-mediated adhesion regulates membrane order. Journal of Cell Biology *174*, 725-734.

Gourlay, C.W., and Ayscough, K.R. (2005). The actin cytoskeleton: a key regulator of apoptosis and ageing? Nature Reviews Molecular Cell Biology *6*, 583-U585.

Greenberg, M.E., Li, X.-M., Gugiu, B.G., Gu, X., Qin, J., Salomon, R.G., and Hazen, S.L. (2008). The lipid whisker model of the structure of oxidized cell membranes. Journal of Biological Chemistry *283*, 2385-2396.

Greenberg, M.E., Sun, M.J., Zhang, R.L., Febbraio, M., Silverstein, R., and Hazen, S.L. (2006). Oxidized phosphatidylserine-CD36 interactions play an essential role in macrophage-dependent phagocytosis of apoptotic cells. J Exp Med *203*, 2613-2625.

Gressner, A.M. (2001). The up-and-down of hepatic stellate cells in tissue injury: Apoptosis restore's cellular homeostasis. Gastroenterology *120*, 1285-1288.

Griffith, T.S., Brunner, T., Fletcher, S.M., Green, D.R., and Ferguson, T.A. (1995). FAS LIGAND-INDUCED APOPTOSIS AS A MECHANISM OF IMMUNE PRIVILEGE. Science *270*, 1189-1192.

Grossmann, J. (2002). Molecular mechanisms of "detachment-induced apoptosis-Anoikis". Apoptosis *7*, 247-260.

Halperin, A., and Mouritsen, O.G. (2005). Role of lipid protrusions in the function of interfacial enzymes. European Biophysics Journal with Biophysics Letters *34*, 967-971.

Han, S.K., Kim, K.P., Koduri, R., Bittova, L., Munoz, N.M., Leff, A.R., Wilton, D.C., Gelb, M.H., and Cho, W. (1999). Roles of Trp31 in high membrane binding and proinflammatory activity of human group V phospholipase A2. JBiolChem *274*, 11881-11888.

Hanahan, D., and Weinberg, R.A. (2000). The hallmarks of cancer. Cell *100*, 57-70.

Harris, F.M., Best, K.B., and Bell, J.D. (2002). Use of laurdan fluorescence intensity and polarization to distinguish between changes in membrane fluidity and phospholipid order. BiochimBiophysActa *1565*, 123-128.

Harris, F.M., Smith, S.K., and Bell, J.D. (2001). Physical properties of erythrocyte ghosts that determine susceptibility to secretory phospholipase A(2). Journal of Biological Chemistry *276*, 22722-22731.

Hazen, S.L. (2008). Oxidized phospholipids as endogenous pattern recognition ligands in innate immunity. J Biol Chem *283*, 15527-15531.

Heiner, A.L., Gibbons, E., Fairbourn, J.L., Gonzalez, L.J., McLemore, C.O., Brueseke, T.J., Judd, A.M., and Bell, J.D. (2008). Effects of cholesterol on physical properties of human

erythrocyte membranes: Impact on susceptibility to hydrolysis by secretory phospholipase A(2). Biophysical Journal *94*, 3084-3093.

Hengartner, M.O. (2000). The biochemistry of apoptosis. Nature *407*, 770-776.

Henshaw, J.B., Olsen, C.A., Farnbach, A.R., Nielson, K.H., and Bell, J.D. (1998). Definition of the specific roles of lysolecithin and palmitic acid in altering the susceptibility of dipalmitoylphosphatidylcholine bilayers to phospholipase A(2). Biochemistry *37*, 10709-10721.

Hitomi, J., Katayama, T., Eguchi, Y., Kudo, T., Taniguchi, M., Koyama, Y., Manabe, T., Yamagishi, S., Bando, Y., Imaizumi, K.*, et al.* (2004). Involvement of caspase-4 in endoplasmic reticulum stress-induced apoptosis and A beta-induced cell death. Journal of Cell Biology *165*, 347-356.

Honger, T., Jorgensen, K., Biltonen, R.L., and Mouritsen, O.G. (1996). Systematic relationship between phospholipase A(2) activity and dynamic lipid bilayer microheterogeneity. Biochemistry *35*, 9003-9006.

Howland, M.C., and Parikh, A.N. (2010). Model Studies of Membrane Disruption by Photogenerated Oxidative Assault. Journal of Physical Chemistry B *114*, 6377-6385.

Hoyrup, P., Callisen, T.H., Jensen, M.O., Halperin, A., and Mouritsen, O.G. (2004). Lipid protrusions, membrane softness, and enzymatic activity. Physical Chemistry Chemical Physics *6*, 1608-1615.

Huotari, V., Vaaraniemi, J., Lehto, V.P., and Eskelinen, S. (1996). Regulation of the disassembly assembly of the membrane skeleton in Madin-Darby canine kidney cells. Journal of Cellular Physiology *167*, 121-130.

Hurt-Camejo, E., Paredes, S., Masana, L., Camejo, G., Sartipy, P., Rosengren, B., Pedreno, J., Vallve, J.C., Benito, P., and Wiklund, O. (2001). Elevated levels of small, low-density lipoprotein with high affinity for arterial matrix components in patients with rheumatoid arthritis - Possible contribution of phospholipase A(2) to this atherogenic profile. Arthritis and Rheumatism *44*, 2761-2767.

Ivandic, B., Castellani, L.W., Wang, X.P., Qiao, J.H., Mehrabian, M., Navab, M., Fogelman, A.M., Grass, D.S., Swanson, M.E., de Beer, M.C.*, et al.* (1999). Role of group II secretory phospholipase A(2) in atherosclerosis - 1. Increased atherogenesis and altered lipoproteins in transgenic mice expressing group IIa phospholipase A(2). Arteriosclerosis Thrombosis and Vascular Biology *19*, 1284-1290.

Jaattela, M., and Tschopp, J. (2003). Caspase-independent cell death in T lymphocytes. Nature Immunology *4*, 416-423.

Jain, M.K., Yu, B.Z., and Kozubek, A. (1989). Binding of phospholipase A2 to zwitterionic bilayers is promoted by lateral segregation of anionic amphiphiles. BiochimBiophysActa *980*, 23-32.

Janicke, R.U., Sprengart, M.L., Wati, M.R., and Porter, A.G. (1998). Caspase-3 is required for DNA fragmentation and morphological changes associated with apoptosis. Journal of Biological Chemistry *273*, 9357-9360.

Jensen, L.B., Burgess, N.K., Gonda, D.D., Spencer, E., Wilson-Ashworth, H.A., Driscoll, E., Vu, M.P., Fairbourn, J.L., Judd, A.M., and Bell, J.D. (2005). Mechanisms governing the level of susceptibility of erythrocyte membranes to secretory phospholipase A(2). Biophysical Journal *88*, 2692-2705.

Jiang, J., Kini, V., Belikova, N., Serinkan, B.F., Borisenko, G.G., Tyurina, Y.Y., Tyurin, V.A., and Kagan, V.E. (2004). Cytochrome c release is required for phosphatidylserine peroxidation during Fas-triggered apoptosis in lung epithelial A549 cells. Lipids *39*, 1133-1142.

Jones, S.C., Thomas, T.H., and Marshall, S.M. (1998). Abnormal regulation of cell membrane fluidity in diabetic nephropathy. Diabetologia *41*, 337-342.

Jurkiewicz, P., Olzynska, A., Langner, M., and Hof, M. (2006). Headgroup hydration and mobility of DOTAP/DOPC bilayers: a fluorescence solvent relaxation study. Langmuir *22*, 8741-8749.

Kagan, V.E., Gleiss, B., Tyurina, Y.Y., Tyurin, V.A., Elenstrom-Magnusson, C., Liu, S.X., Serinkan, F.B., Arroyo, A., Chandra, J., Orrenius, S.*, et al.* (2002). A role for oxidative stress in apoptosis: oxidation and externalization of phosphatidylserine is required for macrophage clearance of cells undergoing Fas-mediated apoptosis. JImmunol *169*, 487-499.

Kass, G.E.N., and Orrenius, S. (1999). Calcium signaling and cytotoxicity. Environmental Health Perspectives *107*, 25-35.

Khandelia, H., and Mouritsen, O.G. (2009). Lipid Gymnastics: Evidence of Complete Acyl Chain Reversal in Oxidized Phospholipids from Molecular Simulations. BiophysJ *96*, 2734-2743.

Kinkaid, A.R., and Wilton, D.C. (1995). The effect of anions on interfacial binding and activation of secretory phospholipase A2. BiochemSocTrans *23*, 556S.

Koduri, R.S., Baker, S.F., Snitko, Y., Han, S.K., Cho, W., Wilton, D.C., and Gelb, M.H. (1998). Action of human group IIa secreted phospholipase A2 on cell membranes. Vesicle but not heparinoid binding determines rate of fatty acid release by exogenously added enzyme. JBiolChem *273*, 32142-32153.

Korotaeva, A.A., Samoilova, E.V., Piksina, G.F., and Prokazova, N.V. (2010). Oxidized phosphatidylcholine stimulates activity of secretory phospholipase A2 group IIA and abolishes sphingomyelin-induced inhibition of the enzyme. Prostaglandins & Other Lipid Mediators *91*, 38-41.

Korotaeva, A.A., Samoilova, E.V., Pirkova, A.A., Ameliushkina, V.A., Prokazova, N.V., Tkachuk, V.A., and Chazov, E.I. (2009a). Opposite effects of native and oxidized lipoproteins on the activity of secretory phospholipase A(2) group IIA. Prostaglandins Other Lipid Mediat *90*, 37-41.

Korotaeva, A.A., Samoilova, E.V., Pirkova, A.A., and Prokazova, N.V. (2009b). The effect of LDL on the activity of proinflammatory secretory phospholipase A2 (IIA) depends on the degree of their oxidation. Rossiiskii fiziologicheskii zhurnal imeni IM Sechenova / Rossiiskaia akademiia nauk *95*, 476-483.

Koynova, R., and Caffrey, M. (1993). LIPIDAT - A DATABASE OF LIPID PHASE-TRANSITION TYPES, TEMPERATURES AND ENTHALPY CHANGES - AN UPDATE. Biophysical Journal *64*, A273-A273.

Krahling, S., Callahan, M.K., Williamson, P., and Schlegel, R.A. (1999). Exposure of phosphatidylserine is a general feature in the phagocytosis of apoptotic lymphocytes by macrophages. Cell Death and Differentiation *6*, 183-189.

Kuhry, J.G., Fonteneau, P., Duportail, G., Maechling, C., and Laustriat, G. (1983). TMA-DPH: a suitable fluorescence polarization probe for specific plasma membrane fluidity studies in intact living cells. Cell Biophys *5*, 129-140.

Kupert, E., Anderson, M., Liu, Y., Succop, P., Levin, L., Wang, J., Wikenheiser-brokamp, K., Chen, P., Pinney, S.M., Macdonald, T.*, et al.* (2011). Plasma secretory phospholipase A2-IIa as a potential biomarker for lung cancer in patients with solitary pulmonary nodules. Bmc Cancer *11*.

Lakowicz, J.R., Bevan, D.R., Maliwal, B.P., Cherek, H., and Balter, A. (1983). Synthesis and characterization of a fluorescence probe of the phase transition and dynamic properties of membranes. Biochemistry *22*, 5714-5722.

Lauber, K., Bohn, E., Krober, S.M., Xiao, Y.J., Blumenthal, S.G., Lindemann, R.K., Marini, P., Wiedig, C., Zobywalski, A., Baksh, S.*, et al.* (2003). Apoptotic cells induce migration of phagocytes via caspase-3-mediated release of a lipid attraction signal. Cell *113*, 717-730.

Leadsham, J.E., Kotiadis, V.N., Tarrant, D.J., and Gourlay, C.W. (2010). Apoptosis and the yeast actin cytoskeleton. Cell Death and Differentiation *17*, 754-762.

Lee, J.C.M., Simonyi, A., Sun, A.Y., and Sun, G.Y. (2011). Phospholipases A(2) and neural membrane dynamics: implications for Alzheimer's disease. Journal of neurochemistry *116*, 813-819.

Leist, M., and Jaattela, M. (2001). Four deaths and a funeral: From caspases to alternative mechanisms. Nature Reviews Molecular Cell Biology *2*, 589-598.

Leitinger, N., Watson, A.D., Hama, S.Y., Ivandic, B., Qiao, J.H., Huber, J., Faull, K.F., Grass, D.S., Navab, M., Fogelman, A.M.*, et al.* (1999). Role of group II secretory phospholipase A2 in atherosclerosis: 2. Potential involvement of biologically active oxidized phospholipids. ArteriosclerThrombVascBiol *19*, 1291-1298.

Lenardo, M., Chan, F.K.M., Hornung, F., McFarland, H., Siegel, R., Wang, J., and Zheng, L.X. (1999). Mature T lymphocyte apoptosis - Immune regulation in a dynamic and unpredictable antigenic environment. Annual Review of Immunology *17*, 221-253.

Lichtenberg, D., Romero, G., Menashe, M., and Biltonen, R.L. (1986). Hydrolysis of dipalmitoylphosphatidylcholine large unilamellar vesicles by porcine pancreatic phospholipase A2. JBiolChem *261*, 5334-5340.

Liu, F., and Chong, P.L.G. (1999). Evidence for a regulatory role of cholesterol superlattices in the hydrolytic activity of secretory phospholipase A2 in lipid membranes. Biochemistry *38*, 3867-3873.

Lorenz, B., Mey, I., Steltenkamp, S., Fine, T., Rommel, C., Mueller, M.M., Maiwald, A., Wegener, J., Steinem, C., and Janshoff, A. (2009). Elasticity Mapping of Pore-Suspending Native Cell Membranes. Small *5*, 832-838.

Maraganore, J.M., Merutka, G., Cho, W., Welches, W., Kezdy, F.J., and Heinrikson, R.L. (1984). A NEW CLASS OF PHOSPHOLIPASES-A2 WITH LYSINE IN PLACE OF ASPARTATE-49 - FUNCTIONAL CONSEQUENCES FOR CALCIUM AND SUBSTRATE BINDING. Journal of Biological Chemistry *259*, 3839-3843.

Markova, M., Koratkar, R.A., Silverman, K.A., Sollars, V.E., Mac-Phee-Pellini, M., Walters, R., Palazzo, J.P., Buchberg, A.M., Siracusa, L.D., and Farber, S.A. (2005). Diversity in secreted PLA(2)-IIA activity among inbred mouse strains that are resistant or susceptible to Apc(Min/+) tumorigenesis. Oncogene *24*, 6450-6458.

Marsh, D., Watts, A., and Knowles, P.F. (1976). EVIDENCE FOR PHASE BOUNDARY LIPID - PERMEABILITY OF TEMPO-CHOLINE INTO DIMYRISTOYLPHOSPHATIDYLCHOLINE VESICLES AT PHASE-TRANSITION. Biochemistry *15*, 3570-3578.

Martin, S.J., Reutelingsperger, C.P.M., McGahon, A.J., Rader, J.A., Vanschie, R., Laface, D.M., and Green, D.R. (1995). EARLY REDISTRIBUTION OF PLASMA-MEMBRANE PHOSPHATIDYLSERINE IS A GENERAL FEATURE OF APOPTOSIS REGARDLESS OF THE INITIATING STIMULUS - INHIBITION BY OVEREXPRESSION OF BCL-2 AND ABL. Journal of Experimental Medicine *182*, 1545-1556.

Mazur, A.J., Nowak, D., Mannherz, H.G., and Malicka-Blaszkiewicz, M. (2009). Methotrexate induces apoptosis in CaSki and NRK cells and influences the organization of their actin cytoskeleton. European Journal of Pharmacology *613*, 24-33.

McLean, L.R., Hagaman, K.A., and Davidson, W.S. (1993). Role of lipid structure in the activation of phospholipase A2 by peroxidized phospholipids. Lipids *28*, 505-509.

Menashe, M., Lichtenberg, D., Gutierrez-Merino, C., and Biltonen, R.L. (1981). Relationship between the activity of pancreatic phospholipase A2 and the physical state of the phospholipid substrate. JBiolChem *256*, 4541-4543.

Metzstein, M.M., Stanfield, G.M., and Horvitz, H.R. (1998). Genetics of programmed cell death in C-elegans: past, present and future. Trends in Genetics *14*, 410-416.

Mitran, S., and Young, J. (2011). Multiscale Computation of Cytoskeletal Mechanics During Blebbing. In Cellular and Biomolecular Mechancis and Mechanobiology, A. Gefen, ed. (New York: Springer), pp. 345-371.

Mock, J.N., Costyn, L.J., Wilding, S.L., Arnoldz, R.D., and Cummings, B.S. (2013). Evidence for distinct mechanisms of uptake and antitumor activity of secretory phospholipase A(2) responsive liposome in prostate cancer. Integrative Biology *5*, 172-182.

Morishima, N., Nakanishi, K., Takenouchi, H., Shibata, T., and Yasuhiko, Y. (2002). An endoplasmic reticulum stress-specific caspase cascade in apoptosis - Cytochrome c-independent activation of caspase-9 by caspase-12. Journal of Biological Chemistry *277*, 34287-34294.

Mower, D.A., Peckham, D.W., Illera, V.A., Fishbaugh, J.K., Stunz, L.L., and Ashman, R.F. (1994). DECREASED MEMBRANE PHOSPHOLIPID PACKING AND DECREASED CELL-SIZE PRECEDE DNA CLEAVAGE IN MATURE MOUSE B-CELL APOPTOSIS. Journal of Immunology *152*, 4832-4842.

Mueller, R.B., Sheriff, A., Gaipl, U.S., Wesselborg, S., and Lauber, K. (2007). Attraction of phagocytes by apoptotic cells is mediated by lysophosphatidylcholine. Autoimmunity *40*, 342-344.

Murakami, M., Kambe, T., Shimbara, S., Higashino, K., Hanasaki, K., Arita, H., Horiguchi, M., Arita, M., Arai, H., Inoue, K.*, et al.* (1999). Different functional aspects of the group II

subfamily (Types IIA and V) and type X secretory phospholipase A(2)s in regulating arachidonic acid release and prostaglandin generation. Implications of cyclooxygenase-2 induction and phospholipid scramblase-mediated cellular membrane perturbation. JBiolChem *274*, 31435-31444.

Nagata, S. (2010). Apoptosis and autoimmune diseases. Clearance of Dying Cells in Healthy and Diseased Immune Systems *1209*, 10-16.

Nakagawa, T., and Yuan, J.Y. (2000). Cross-talk between two cysteine protease families: Activation of caspase-12 by calpain in apoptosis. Journal of Cell Biology *150*, 887-894.

Nakagawa, T., Zhu, H., Morishima, N., Li, E., Xu, J., Yankner, B.A., and Yuan, J.Y. (2000). Caspase-12 mediates endoplasmic-reticulum-specific apoptosis and cytotoxicity by amyloid-beta. Nature *403*, 98-103.

Narula, J., Haider, N., Arbustini, E., and Chandrashekhar, Y. (2006). Mechanisms of disease: apoptosis in heart failure - seeing hope in death. Nature Clinical Practice Cardiovascular Medicine *3*, 681-688.

Nelson, J., Gibbons, E., Pickett, K.R., Streeter, M., Warcup, A.O., Yeung, C.H.Y., Judd, A.M., and Bell, J.D. (2011). Relationship between membrane permeability and specificity of human secretory phospholipase A(2) isoforms during cell death. Biochimica Et Biophysica Acta-Biomembranes *1808*, 1913-1920.

Nielson, K.H., Olsen, C.A., Allred, D.V., O'Neill, K.L., Burton, G.F., and Bell, J.D. (2000). Susceptibility of S49 lymphoma cell membranes to hydrolysis by secretory phospholipase A(2) during early phase of apoptosis. Biochimica Et Biophysica Acta-Molecular and Cell Biology of Lipids *1484*, 163-174.

Nunez, R., Sancho-Martinez, S.M., Novoa, J.M.L., and Lopez-Hernandez, F.J. (2010). Apoptotic volume decrease as a geometric determinant for cell dismantling into apoptotic bodies. Cell Death and Differentiation *17*, 1665-1671.

Okouchi, M., Ekshyyan, O., Maracine, M., Aw, T.Y., Calabrese, V., Ciriolo, M., Keller, J., and Maher, P. (2007). Neuronal apoptosis in neurodegeneration. Antioxidants & Redox Signaling *9*, 1059-1096.

Olson, E.D., Nelson, J., Griffith, K., Nguyen, T., Streeter, M., Wilson-Ashworth, H.A., Gelb, M.H., Judd, A.M., and Bell, J.D. (2010). Kinetic Evaluation of Cell Membrane Hydrolysis during Apoptosis by Human Isoforms of Secretory Phospholipase A(2). Journal of Biological Chemistry *285*, 10993-11002.

Pan, Y.H., Yu, B.Z., Singer, A.G., Ghomashchi, F., Lambeau, G., Gelb, M.H., Jain, M.K., and Bahnson, B.J. (2002). Crystal structure of human group X secreted phospholipase A(2) - Electrostatically neutral interfacial binding surface targets zwitterionic membranes. Journal of Biological Chemistry *277*, 29086-29093.

Parasassi, T., De Stasio, G., Ravagnan, G., Rusch, R.M., and Gratton, E. (1991). Quantitation of lipid phases in phospholipid vesicles by the generalized polarization of Laurdan fluorescence. BiophysJ *60*, 179-189.

Parisio, G., Marini, A., Biancardi, A., Ferrarini, A., and Mennucci, B. (2011). Polarity-sensitive fluorescent probes in lipid bilayers: bridging spectroscopic behavior and microenvironment properties. JPhysChemB *115*, 9980-9989.

Pato, C., Stetzkowski-Marden, F., Gaus, K., Recouvreur, M., Cartaud, A., and Cartaud, J. (2008). Role of lipid rafts in agrin-elicited acetylcholine receptor clustering. Chemico-Biological Interactions *175*, 64-67.

Peter, C., Waibel, M., Radu, C.G., Yang, L.V., Witte, O.N., Schulze-Osthoff, K., Wesselborg, S., and Lauber, K. (2008). Migration to apoptotic "Find-me" signals is mediated via the phagocyte receptor G2A. Journal of Biological Chemistry *283*, 5296-5305.

Peter, C., Wesselborg, S., Herrmann, M., and Lauber, K. (2010a). Dangerous attraction: phagocyte recruitment and danger signals of apoptotic and necrotic cells. Apoptosis *15*, 1007-1028.

Peter, C., Wesselborg, S., and Lauber, K. (2010b). Apoptosis: Opening PANdora's BoX. Current Biology *20*, R940-R942.

Peter, C., Wesselborg, S., and Lauber, K. (2010c). Molecular Suicide Notes: Last Call from Apoptosing Cells. Journal of Molecular Cell Biology *2*, 78-80.

Piga, R., Saito, Y., Yoshida, Y., and Niki, E. (2007). Cytotoxic effects of various stressors on PC12 cells: Involvement of oxidative stress and effect of antioxidants. NeuroToxicology *28*, 67-75.

Pinto, F., Brenner, T., Dan, P., Krimsky, M., and Yedgar, S. (2003). Extracellular phospholipase A(2) inhibitors suppress central nervous system inflammation. Glia *44*, 275-282.

Pozarowski, P., Huang, X., Halicka, D.H., Lee, B., Johnson, G., and Darzynkiewicz, Z. (2003). Interactions of fluorochrome-labeled caspase inhibitors with apoptotic cells: a caution in data interpretation. Cytometry A *55*, 50-60.

Pruzanski, W., Stefanski, E., de Beer, F.C., de Beer, M.C., Vadas, P., Ravandi, A., and Kuksis, A. (1998). Lipoproteins are substrates for human secretory group IIA phospholipase A2: preferential hydrolysis of acute phase HDL. JLipid Res *39*, 2150-2160.

Raggers, R.J., Pomorski, T., Holthuis, J.C.M., Kalin, N., and van Meer, G. (2000). Lipid traffic: The ABC of transbilayer movement. Traffic *1*, 226-234.

Rajendran, L., Beckmann, J., Magenau, A., Boneberg, E.-M., Gaus, K., Viola, A., Giebel, B., and Illges, H. (2009). Flotillins Are Involved in the Polarization of Primitive and Mature Hematopoietic Cells. PLoS One *4*, Article No.: e8290.

Rao, R.V., Castro-Obregon, S., Frankowski, H., Schuler, M., Stoka, V., del Rio, G., Bredesen, D.E., and Ellerby, H.M. (2002). Coupling endoplasmic reticulum stress to the cell death program - An Apaf-1-independent intrinsic pathway. Journal of Biological Chemistry *277*, 21836-21842.

Rao, R.V., Hermel, E., Castro-Obregon, S., del Rio, G., Ellerby, L.M., Ellerby, H.M., and Bredesen, D.E. (2001). Coupling endoplasmic reticulum stress to the cell death program - Mechanism of caspase activation. Journal of Biological Chemistry *276*, 33869-33874.

Riccardi, C., and Nicoletti, I. (2006). Analysis of apoptosis by propidium iodide staining and flow cytometry. Nature Protocols *1*, 1458-1461.

Richieri, G.V., and Kleinfeld, A.M. (1995). Continuous measurement of phospholipase A2 activity using the fluorescent probe ADIFAB. AnalBiochem *229*, 256-263.

Santoro, N., Lisi, A., Pozzi, D., Pasquali, E., Serafino, A., and Grimaldi, S. (1997). Effect of extremely low frequency (ELF) magnetic field exposure on morphological and biophysical properties of human lymphoid cell line (Raji). Biochimica Et Biophysica Acta-Molecular Cell Research *1357*, 281-290.

Sardao, V.A., Oliveira, P.J., Holy, J., Oliveira, C.R., and Wallace, K.B. (2007). Vital imaging of H9c2 myoblasts exposed to tert-butylhydroperoxide - characterization of morphological features of cell death. Bmc Cell Biol *8*.

Schneider, C.A., Rasband, W.S., and Eliceiri, K.W. (2012). NIH Image to ImageJ: 25 years of image analysis. Nature Methods *9*, 671-675.

Scott, D.L., and Sigler, P.B. (1994). STRUCTURE AND CATALYTIC MECHANISM OF SECRETORY PHOSPHOLIPASES A(2). Advances in Protein Chemistry, Vol 45 *45*, 53-88.

Scott, D.L., White, S.P., Otwinowski, Z., Yuan, W., Gelb, M.H., and Sigler, P.B. (1990). Interfacial catalysis: the mechanism of phospholipase A2. Science *250*, 1541-1546.

Seigneuret, M., and Devaux, P.F. (1984). ATP-DEPENDENT ASYMMETRIC DISTRIBUTION OF SPIN-LABELED PHOSPHOLIPIDS IN THE ERYTHROCYTE-MEMBRANE - RELATION TO SHAPE CHANGES. Proceedings of the National Academy of Sciences of the United States of America-Biological Sciences *81*, 3751-3755.

Serra, M.V., Kamp, D., and Haest, C.W.M. (1996). Pathways for flip-flop of mono- and di-anionic phospholipids in the erythrocyte membrane. Biochimica Et Biophysica Acta-Biomembranes *1282*, 263-273.

Singer, A.G., Ghomashchi, F., Le Calvez, C., Bollinger, J., Bezzine, S., Rouault, M., Sadilek, M., Nguyen, E., Lazdunski, M., Lambeau, G*., et al.* (2002). Interfacial kinetic and binding properties of the complete set of human and mouse groups I, II, V, X, and XII secreted phospholipases A(2). Journal of Biological Chemistry *277*, 48535-48549.

Smith, H.L., Howland, M.C., Szmodis, A.W., Li, Q., Daemen, L.L., Parikh, A.N., and Majewski, J. (2009). Early Stages of Oxidative Stress-Induced Membrane Permeabilization: A Neutron Reflectometry Study. Journal of the American Chemical Society *131*, 3631-3638.

Smith, S.K., Farnbach, A.R., Harris, F.M., Hawes, A.C., Jackson, L.R., Judd, A.M., Vest, R.S., Sanchez, S., and Bell, J.D. (2001). Mechanisms by which intracellular calcium induces susceptibility to secretory phospholipase A(2) in human erythrocytes. Journal of Biological Chemistry *276*, 22732-22741.

Snitko, Y., Koduri, R.S., Han, S.K., Othman, R., Baker, S.F., Molini, B.J., Wilton, D.C., Gelb, M.H., and Cho, W. (1997). Mapping the interfacial binding surface of human secretory group IIa phospholipase A2. Biochemistry *36*, 14325-14333.

Squier, M.K.T., Miller, A.C.K., Malkinson, A.M., and Cohen, J.J. (1994). CALPAIN ACTIVATION IN APOPTOSIS. Journal of Cellular Physiology *159*, 229-237.

Stillwell, W., Wassall, S.R., Dumaual, A.C., Ehringer, W.D., Browning, C.W., and Jenski, L.J. (1993). Use of merocyanine (MC540) in quantifying lipid domains and packing in phospholipid vesicles and tumor cells. BiochimBiophysActa *1146*, 136-144.

Stott, B.M., Vu, M.P., McLemore, C.O., Lund, M.S., Gibbons, E., Brueseke, T.J., Wilson-Ashworth, H.A., and Bell, J.D. (2008). Use of fluorescence to determine the effects of cholesterol on lipid behavior in sphingomyelin liposomes and erythrocyte membranes. Journal of Lipid Research *49*, 1202-1215.

Sun, G.Y., Xu, J., Jensen, M.D., Yu, S., Wood, W.G., Gonzalez, F.A., Simonyi, A., Sun, A.Y., and Weisman, G.A. (2005). Phospholipase A2 in astrocytes: responses to oxidative stress, inflammation, and G protein-coupled receptor agonists. MolNeurobiol *31*, 27-41.

Triggiani, M., Granata, F., Frattini, A., and Marone, G. (2006). Activation of human inflammatory cells by secreted phospholipases A(2). Biochimica Et Biophysica Acta-Molecular and Cell Biology of Lipids *1761*, 1289-1300.

Triggiani, M., Granata, F., Giannattasio, G., and Marone, G. (2005). Secretory phospholipases A(2) in inflammatory and allergic diseases: Not just enzymes. Journal of Allergy and Clinical Immunology *116*, 1000-1006.

Tyurin, V.A., Tyurina, Y., Jung, M.Y., Tungekar, M.A., Wasserloos, K.J., Bayir, H., Greenberger, J.S., Kochanek, P.M., Shvedova, A.A., Pitt, B.*, et al.* (2009). Mass-spectrometric analysis of hydroperoxy- and hydroxy-derivatives of cardiolipin and phosphatidylserine in cells and tissues induced by pro-apoptotic and pro-inflammatory stimuli. Journal of Chromatography B-Analytical Technologies in the Biomedical and Life Sciences *877*, 2863-2872.

Tyurin, V.A., Tyurina, Y.Y., Feng, W., Mnuskin, A., Jiang, J., Tang, M., Zhang, X., Zhao, Q., Kochanek, P.M., Clark, R.S.*, et al.* (2008a). Mass-spectrometric characterization of phospholipids and their primary peroxidation products in rat cortical neurons during staurosporine-induced apoptosis. JNeurochem *107*, 1614-1633.

Tyurin, V.A., Tyurina, Y.Y., Kochanek, P.M., Hamilton, R., DeKosky, S.T., Greenberger, J.S., Bayir, H., and Kagan, V.E. (2008b). Oxidative lipidomics of programmed cell death. Programmed Cell Death, General Principles for Studying Cell Death, Pt A *442*, 375-393.

Tyurina, Y.Y., Shvedova, A.A., Kawai, K., Tyurin, V.A., Kommineni, C., Quinn, P.J., Schor, N.F., Fabisiak, J.P., and Kagan, V.E. (2000). Phospholipid signaling in apoptosis: peroxidation and externalization of phosphatidylserine. Toxicology *148*, 93-101.

Tyurina, Y.Y., Tyurin, V.A., Zhao, Q., Djukic, M., Quinn, P.J., Pitt, B.R., and Kagan, V.E. (2004). Oxidation of phosphatidylserine: a mechanism for plasma membrane phospholipid scrambling during apoptosis? Biochemical and Biophysical Research Communications *324*, 1059-1064.

Vaculova, A., and Zhivotovsky, B. (2008). Caspases: Determination of their activities in apoptotic cells. In Programmed Cell Death, General Principles for Studying Cell Death, Pt A, pp. 157-181.

Veatch, W.R., and Stryer, L. (1977). Effect of cholesterol on the rotational mobility of diphenylhexatriene in liposomes: a nanosecond fluorescence anisotrophy study. JMolBiol *117*, 1109-1113.

Verhoven, B., Schlegel, R.A., and Williamson, P. (1995). MECHANISMS OF PHOSPHATIDYLSERINE EXPOSURE, A PHAGOCYTE RECOGNITION SIGNAL, ON APOPTOTIC T-LYMPHOCYTES. Journal of Experimental Medicine *182*, 1597-1601.

Verkleij, A.J., and Post, J.A. (2000). Membrane phospholipid asymmetry and signal transduction. Journal of Membrane Biology *178*, 1-10.

Vitale, M., Zamai, L., Mazzotti, G., Cataldi, A., and Falcieri, E. (1993). DIFFERENTIAL KINETICS OF PROPIDIUM IODIDE UPTAKE IN APOPTOTIC AND NECROTIC THYMOCYTES. Histochemistry *100*, 223-229.

Volinsky, R., Cwiklik, L., Jurkiewicz, P., Hof, M., Jungwirth, P., and Kinnunen, P.K.J. (2011). Oxidized Phosphatidylcholines Facilitate Phospholipid Flip-Flop in Liposomes. BiophysJ *101* 1376-1384.

Wang, K.K.W. (2000). Calpain and caspase: can you tell the difference? Trends in Neurosciences *23*, 20-26.

Williams, R.M., and Webb, W.W. (2000). Single granule pH cycling in antigen-induced mast cell secretion. Journal of cell science *113 Pt 21*, 3839-3850.

Williamson, P., Mattocks, K., and Schlegel, R.A. (1983). Merocyanine 540, a fluorescent probe sensitive to lipid packing. BiochimBiophysActa *732*, 387-393.

Wilson, H.A., Huang, W.H., Waldrip, J.B., Judd, A.M., Vernon, L.P., and Bell, J.D. (1997). Mechanisms by which thionin induces susceptibility of S49 cell membranes to extracellular phospholipase A(2). Biochimica Et Biophysica Acta-Lipids and Lipid Metabolism *1349*, 142-156.

Wilson, H.A., Waldrip, J.B., Nielson, K.H., Judd, A.M., Han, S.K., Cho, W.W., Sims, P.J., and Bell, J.D. (1999). Mechanisms by which elevated intracellular calcium induces S49 cell membranes to become susceptible to the action of secretory phospholipase A(2). Journal of Biological Chemistry *274*, 11494-11504.

Wilson-Ashworth, H.A., Bahm, Q., Erickson, J., Shinkle, A., Vu, M.P., Woodbury, D., and Bell, J.D. (2006). Differential detection of phospholipid fluidity, order, and spacing by fluorescence spectroscopy of bis-pyrene, prodan, nystatin, and merocyanine 540. Biophysical Journal *91*, 4091-4101.

Wilson-Ashworth, H.A., Judd, A.M., Law, R.M., Freestone, B.D., Taylor, S., Mizukawa, M.K., Cromar, K.R., Sudweeks, S., and Bell, J.D. (2004). Formation of transient non-protein calcium pores by lysophospholipids in S49 lymphoma cells. Journal of Membrane Biology *200*, 25-33.

Witasp, E., Kagan, V., and Fadeel, B. (2008). Programmed cell clearance: Molecular mechanisms and role in autoimmune disease, chronic inflammation, and anti-cancer immune responses. Current Immunology Reviews *4*, 53-69.

Wolkers, W.F., Looper, S.A., Fontanilla, R.A., Tsvetkova, N.M., Tablin, F., and Crowe, J.H. (2003). Temperature dependence of fluid phase endocytosis coincides with membrane properties of pig platelets. Biochimica Et Biophysica Acta-Biomembranes *1612*, 154-163.

Yajima, D., Motani, H., Hayakawa, M., Sato, Y., Sato, K., and Iwase, H. (2009). The relationship between cell membrane damage and lipid peroxidation under the condition of hypoxia-reoxygenation: analysis of the mechanism using antioxidants and electron transport inhibitors. Cell Biochemistry and Function *27*, 338-343.

Yoshida, I., Monji, A., Tashiroa, K., Nakamura, K., Inoue, R., and Kanba, S. (2006). Depletion of intracellular Ca2+ store itself may be a major factor in thapsigargin-induced ER stress and apoptosis in PC12 cells. Neurochemistry International *48*, 696-702.

Yu, B.Z., Poi, M.J., Ramagopal, U.A., Jain, R., Ramakumar, S., Berg, O.G., Tsai, M.D., Sekar, K., and Jain, M.K. (2000). Structural basis of the anionic interface preference and k*(cat) activation of pancreatic phospholipase A(2). Biochemistry *39*, 12312-12323.

Zachowski, A., Favre, E., Cribier, S., Herve, P., and Devaux, P.F. (1986). OUTSIDE INSIDE TRANSLOCATION OF AMINOPHOSPHOLIPIDS IN THE HUMAN-ERYTHROCYTE MEMBRANE IS MEDIATED BY A SPECIFIC ENZYME. Biochemistry *25*, 2585-2590.

Zamai, L., Falcieri, E., Marhefka, G., and Vitale, M. (1996). Supravital exposure to propidium iodide identifies apoptotic cells in the absence of nucleosomal DNA fragmentation. Cytometry *23*, 303-311.

Zhou, Q.S., Zhao, J., Stout, J.G., Luhm, R.A., Wiedmer, T., and Sims, P.J. (1997). Molecular cloning of human plasma membrane phospholipid scramblase - A protein mediating transbilayer movement of plasma membrane phospholipids. Journal of Biological Chemistry *272*, 18240-18244.

Zhu, D.H., Tan, K.S., Zhang, X.L., Sun, A.Y., Sun, G.Y., and Lee, J.C.M. (2005). Hydrogen peroxide alters membrane and cytoskeleton properties and increases intercellular connections in astrocytes. Journal of Cell Science *118*, 3695-3703.

Zipfel, W.R., Williams, R.M., and Webb, W.W. (2003). Nonlinear magic: multiphoton microscopy in the biosciences. NatBiotechnol *21*, 1369-1377.

CURRICULUM VITAE

ELIZABETH GIBBONS

1367 S 1400 E, Provo, UT 84606| 801-867-0230 | liz.gibbons7@gmail.com

EDUCATION

Brigham Young University
Ph.D. in Physiology and Developmental Biology   **2013**
Dissertation: "Susceptibility of Apoptotic Cells to Hydrolysis by $sPLA_2$:
Molecular Basis and Mechanisms Defined"

Brigham Young University
B.S. in Biophysics   **2008**
Magna Cum Laude

TEACHING EXPERIENCE

Assistant Instructor – PDBio 120 "Science of Biology"   **2012**
For a section of 224 students: taught lectures, assisted in creating and
administering weekly assessments, taught weekly help sessions.

Teaching Assistant – PDBio 363 "Advanced Physiology Lab"   **2012**
Provided weekly instruction and lab assistance, held reviews, and corrected
lab reports.

Teaching Assistant – PDBio 120 "Science of Biology"   **2011**
Attended class to explain concepts and answer questions, held weekly
office hours.

Tutor – Life Sciences Learning Center   **2007–2008**
Provided tutoring to undergraduate students in all core Biology courses.

MEMBERSHIPS

Biophysical Society   **2008–Present**

AWARDS

Full Tuition Award, *PDBio Department, Brigham Young University*   **2011–2013**

Research Assistantship, *PDBio Department, Brigham Young University*   **2011, 2013**

Teaching Assistantship, *PDBio Department, Brigham Young University*   **2011–2012**

Cancer Research Center Summer Research Fellowships, *Brigham Young University*   **2011, 2012**

Half Tuition Award, *PDBio Department, Brigham Young University*   **2008–2009**

Research Assistantship*, Brigham Young University*   **2008–2009**

Phi Kappa Phi Honor Society, *Brigham Young University Chapter*   **2008**

Office of Research and Creative Activities Grant, *Brigham Young University*   **2008**

JOURNAL ARTICLES

Gibbons E, Nelson J, Anderson L, Brewer K, Melchor S, Judd AM, Bell JD. Role of membrane oxidation in controlling the activity of human group IIa secretory phospholipase A(2) toward apoptotic lymphoma cells. BBA-Biomembranes 2013;1828(2):670-676.

Gibbons E, Pickett KR, Streeter MC, Warcup AO, Nelson J, Judd AM, Bell JD. Molecular details of membrane fluidity changes during apoptosis and relationship to phospholipase A(2) activity. BBA-Biomembranes 2013;1828(2):887-895.

Nelson J, Gibbons E, Pickett KR, Streeter M, Warcup AO, Yeung CHY, Judd AM, Bell JD. Relationship between membrane permeability and specificity of human secretory phospholipase A(2) isoforms during cell death. BBA-Biomembranes 2011;1808(7):1913-1920.

Bailey RW, Nguyen T, Robertson L, Gibbons E, Nelson J, Christensen RE, Bell JP, Judd AM, Bell JD. Sequence of Physical Changes to the Cell Membrane During Glucocorticoid-Induced Apoptosis in S49 Lymphoma Cells. Biophys J 2009;96(7):2709-2718.

Gonzalez L, Gibbons E, Bailey R, Fairbourn J, Nguyen T, Smith S, Best K, Nelson J, Judd A, Bell J. The influence of membrane physical properties on microvesicle release in human erythrocytes. PMC Biophysics 2009;2:7.

Heiner AL, Gibbons E, Fairbourn JL, Gonzalez LJ, McLemore CO, Brueseke TJ, Judd AM, Bell JD. Effects of cholesterol on physical properties of human erythrocyte membranes: Impact on susceptibility to hydrolysis by secretory phospholipase A2. Biophys J 2008;94(8):3084-3093.

Stott BM, Vu MP, McLemore CO, Lund MS, Gibbons E, Brueseke TJ, Wilson-Ashworth HA, Bell JD. Use of fluorescence to determine the effects of cholesterol on lipid behavior in sphingomyelin liposomes and erythrocyte membranes. J Lipid Res 2008;49(6):1202-1215.

MEETING ABSTRACTS

Bell JD, Wiberg H, Gibbons E, Nelson J. Using Creative Grading Schemes to Enhance Student Learning through Weekly Formative Assessments. 2013. *SABER National Meeting.*

Gibbons E, Pickett KR, Streeter MC, Warcup AO, Nelson J, Judd AM, Bell JD. Relationship between Membrane Fluidity Changes, Phospholipid Protrusion Probability and Phospholipase A2 Activity during Thapsigargin-induced Apoptosis. 2013. *Biophys J.*

Gibbons E, Anderson L, Damm K, Melchor S, Nelson J, Judd AM, Bell JD. Role of membrane oxidation in controlling the activity of secretory phospholipase A$_2$ toward apoptotic lymphoma cells. 2012. *Biophys J* 102(suppl), (#3190)

Gonzalez LJ, Gibbons E, Bailey RW, Fairbourn J, Nguyen T, Smith SK, Best KB, Nelson J, Judd AM, Bell JD. The influence of membrane physical properties on microvesicle release in human erythrocytes. 2011. *Biophys J* 100 (suppl), (#202).

Gibbons E, Askew CE, Griffith KR, Streeter MC, Warcup AO, Yeung C, Judd AM, Bell JD. Membrane changes during apoptosis: part of the process or characteristics of the corpse?. 2009. *Biophys J* 96 (suppl), (#2191).

Bailey RW, Gibbons E, Robertson L, Nguyen TT, Nelson J, Judd AM, Bell JD. Biophysical changes in the plasma membrane during glucocorticoid-stimulated apoptosis promote hydrolysis by secretory phospholipase A$_2$. 2008. *Biophys J* 94 (suppl), (#2841).

COMMUNITY SERVICE

Guest Science Instructor – *Freedom Academy; Provo, UT* **2013**
Visited 1st grade classrooms to do demonstrations and hands-on science experiments.

Guest Science Instructor – *Nebo School District* **2012–2013**
Visited 6th grade classrooms to do hands-on activities, help with science projects, judge science fairs.

Volunteer Assistant Soccer Coach – *Provo City Soccer League* **2012–2013**
Managed soccer teams of elementary school-aged girls.

Full-Time Missionary, *The Church of Jesus Christ of Latter-Day Saints* **2009–2010**
 Strengthened local congregations, taught and served weekly in the community.

Tutor, *Tutor Outreach Provo Schools* **2006**
Assisted in a kindergarten classroom once a week.